

Endogenous Stress Signaling within Human Multicellular Aggregates (Spheroids)

Graham D. Jack

Dissertation submitted to the faculty of Virginia Polytechnic Institute and State
University in fulfillment of the requirements for the degree of

Doctorate of Philosophy
in
Biochemistry

Rich Helm, Chair
Malcolm Potts
John Hess
David Bevan
John McDowell
T.M. Murali

July 10th 2006
Blacksburg Va

Keyword: Multicellular aggregates, human cells, survival, NF-kB, JNK

Endogenous Stress Signaling within Human Multicellular Aggregates (Spheroids)

Graham Jack

Dissertation Summary

A wide variety of adherent mammalian cells can be induced into a reversible state of metabolic arrest (quiescence) by conversion to non-adherent multicellular aggregates. These “spheroids” can be maintained at room temperature under oxygen- and nutrient-deprived conditions for extended periods of time (weeks) as well as converted back to viable proliferating monolayers. Herein it is shown that HEK293 spheroid arrest and recovery requires the co-activation of both NF- κ B and JNK, and chemical inhibition of either NF- κ B nuclear translocation or JNK phosphorylation leads to cell death. Cytokine profiling within the aggregates during the arrest and recovery process is suggestive that a cyclical cascade was in operation, leading to endogenous cytokine production of TNF- α , IL-1 β , and IL-8, thereby propagating the cellular stress signal within cells as well as throughout the aggregate.

Cytokines exist *in vivo* as mixtures, yet tissue culture studies delineating how cells respond to these molecules are often performed using individual effectors added exogenously. Are the results obtained in these studies true representations of physiological responses? As HEK293 multicellular aggregates (spheroids) survive long term arrest by endogenous cytokine (TNF- α and IL-1 β) and chemokine (IL-8) signaling, adherent monolayer cells were evaluated for their ability to provide a “spheroid signal response” when exposed to TNF- α , IL-1 β and IL-8 individually, and in combination, at concentrations observed in the aggregates. The spheroid signal transduction response

was only observed when all three cytokines were present, demonstrating that signal transduction cascade mechanisms are cytokine-profile dependent.

To determine if similar processes were involved in the arrest and recovery of multicellular aggregates derived from other cell types, the responses of primary human foreskin fibroblasts (HFF-2) and a glioblastoma cell line (T98G) were characterized, utilizing the procedures developed in the HEK293 study. Both the T98G and HFF-2 cell lines entered and exited from the long term arrest utilizing an autocrine response. However, while the carcinoma cell line was dependent upon NF- κ B for survival, its signaling partner was Gadd45 α and signaling occurred through the p38 pathway. Primary fibroblast arrest and recovery proceeded through the p38 pathway as well, but was independent of NF- κ B. Thus, three different cell types and transformation states (HEK293, HFF-2, and T98G) provided three different routes to survival, all with cyclical cytokine production and signaling. These routes cannot be measured or modulated effectively in adherent monolayers. Multicellular aggregates provide higher ordered systems that can be used to describe signaling pathways within a cell, highlighting the role of autocrine responses and the synergistic relationships between cytokines and neighboring cells.

Acknowledgements

For their contributions to my education, scientific understanding, and scientific career, I would like to acknowledge the following people:

Dr. Peter Chidiac, for helping to start my scientific career, for his advice during a few tough decisions, and finally for my initiation to cell signaling which became one of my passions.

Dr. Brian Storrie, for my start at Virginia Tech and his appreciation of my work.

Dr. Rich Helm, my supervisor, for putting up with my antics and flaws, having my back when I needed it, leaving his door open for help with my project and advice, and most importantly giving me this opportunity.

Dr. Malcolm Potts, my co-supervisor, for his advice during my stay here, and also for this opportunity.

My thesis committee, John Hess, David Bevan, John McDowell, and T.M. Murali for their time, questions and comments which helped form part of my research.

M. Carla Cabrera, a great undergraduate assistant and closest friend, for her support in and out of the lab. Thank you for your help in keeping my sanity in check and my writing understandable for the last 3 years.

Steve Slaughter, for dealing with my computer incompetence and all his help on my project.

Jamie Garst, a.k.a. Mr. Muffin, for his help on my project, making me laugh at work, and almost getting my truck out of the mud.

Mike Manning, for keeping a steady hand pipetting, even while being yelled at (Sorry).

Debbie Wright, Tara Pilonero, and Jody Jervis for their assistance and friendly banter.

Ken Hurley, a great friend, for keeping a roof over my head, my truck on the road and a smile on my face.

Finally, I would like to thank my family, in Canada for their support, and especially my brother Greg (Coach) Jack for keeping food and drink in my stomach.

Table of Contents

Dissertation Summary	ii
Acknowledgements	iv
Table of Contents	v
Figures	vii
Tables	ix
Chapter 1	1
Background	2
Rational and Significance	4
Overview of Thesis	8
References	13
Chapter 2	15
Abstract	16
Introduction	17
Materials and Methods	19
Results	25
Discussion	37
References	42
Supplemental Information	45

Chapter 3	52
Abstract	53
Introduction	54
Material and Methods	55
Results and Discussion	57
References	68
Supplemental Information	70
Chapter 4	75
Abstract	76
Introduction	77
Materials and Methods	79
Results	83
Discussion	98
References	106
Supplemental Information	111
Chapter 5	123
Concluding Remarks	124
Future Directions	125
Curriculum Vitae	127

Figures

Chapter 1

Fig.1.1 Schematic representation of TNF- α induced pathways	7
Fig.1.2 Schematic representation of identified signaling pathways	12

Chapter 2

Fig. 2.1 HEK293 cells can be stored for extended periods of time as aggregates	27
Fig. 2.2 Transcriptional profiling of HEK293 aggregates	29
Fig. 2.3 Quiescence and recovery involves NF- κ B and JNK signaling	34
Fig. 2.4 Selected cytokine profiling in HEK293 cells	36
Fig. 2.S1 Graphical depiction of highest up and down regulated genes	50
Fig. 2.S2 Cytokine profile data in HEK293 cells	51

Chapter 3

Fig. 3.1 Changes in HEK293 cellular morphology due to cytokine treatments	59
Fig. 3.2 Effects of cytokine treatments on HEK293 cell viability	60
Fig. 3.3 Cytokine/chemokine concentrations in media	62
Fig. 3.4 Differential activation of intracellular signaling pathways	64
Fig. 3.S1 Light micrographs of HEK293 cells expose to cytokine treatments	72
Fig. 3.S2 Differential activation of intracellular signaling pathways	73
Fig. 3.S3 Protein identification by mass spectrometry	74

Chapter 4

Fig. 4.1 HFF-2 and T98G cells can undergo arrest and recovery	85
---	----

Fig. 4.2 HFF-2 and T98G cells respond differently to NF- κ B inhibition	89
Fig. 4.3 HFF-2 and T98G cytokine signaling profiles	94
Fig. 4.4 HFF-2 and T98G gene expression profiles	97
Fig. 4.5 Activated pathways within HEK293, HFF-2 and T98G cells	100
Fig. 4.S1 Graphical depiction of gene expression changes in HFF-2 cells	113
Fig. 4.S2 Graphical depiction of gene expression changes in HFF-2 cells	114
Fig. 4.S3 HFF-2 and T98G cytokine signaling profiles	115

Tables

Chapter 2

Table 2.1 Transcriptional fold changes in <i>Gadd45</i> genes	30
Table 2.S1 HEK293 microarray master key	45
Table 2.S2 HEK293 probe gene sets	46
Table 2.S3. HEK293 fluorescence intensities	48

Chapter 3

Table 3.1 HEK293 identified proteins by mass spectrometry	66
---	----

Chapter 4

Table 4.1 Viability analysis for HFF-2 and T98G cells	91
Table 4.S1 10 fold gene expression changes for HFF-2 cells	117
Table 4.S2 10 fold gene expression changes for HFF-2 cells	119
Table 4.S3 Microarray master key	121
Table 4.S4 Transcriptional fold changes in <i>Gadd45</i> genes	122

Chapter 1

Dissertation Introduction

Background

Logistical problems and costs associated with the preservation, storage and distribution of cell lines and biomedical products at ultra-low temperature, as well as the potential utility of robust cell-based biosensors (Rider *et al.*, 2003), have prompted speculation whether air-drying may offer a means to induce quiescence of mammalian cells. The capacity and the basis for reversible, metabolic arrest have considerable implications for many areas of cell biology. Growing interest in the mechanistic basis for quiescence of mammalian cells derives from the conclusion that such an understanding has the potential to enable development of novel immuno-suppressants and anticancer therapies, and to provide insights into the molecular basis for such diverse processes as aging and neurodegenerative diseases (Gray *et al.*, 2004; Collier *et al.*, 2006).

There are limited studies that deal with the growth responses of mammalian cells to air-drying, and there is a paucity of data on the signaling pathways or the physiological and molecular mechanisms that may be involved in the sensitivity, or tolerance, of such stress. Recent attempts to dry and revive nucleated mammalian cells employed the non-reducing disaccharide trehalose, either as an additive or, through its endogenous de novo synthesis following cell transformation with *otsAB* genes (de Castro and Tunnacliffe, 2000; Guo *et al.*, 2000; Huang and Tunnacliffe, 2004; Matsuo, 2001; Puhlev *et al.*, 2001). Trehalose often accumulates to high concentrations in desiccation-tolerant (anhydrobiotic) cells and it has unique properties that can convey protection on sensitive cells (Crowe and Crowe, 2000). In another study, the structural integrity of human 293 kidney (HEK293) cells was maintained when they were air-dried in the presence of an extracellular polysaccharide (glycan) that constitutes the extracellular matrix of the

desiccation tolerant cyanobacterium *Nostoc commune* (Bloom *et al.*, 2001). These different approaches, however, achieved limited success with variable cell viability for only very short periods of dry storage.

A common feature of the experimental design for these studies was the use of cells grown in two-dimensional (monolayer) culture. While understood by tumor biologists for some time, only recently has it become widely known that the function and behavior of mammalian cells in two-dimensional (2-D) and three-dimensional (3-D) culture can be radically different (Jacks and Weinberg, 2002; Schmeichel and Bissell, 2003; Sutherland, 1988). 3-D multicellular aggregates of cells, called spheroids, mimic avascular tumor stages or micrometastases in many aspects and have been studied intensively as an experimental model reflecting an *in vivo*-like micromilieu with 3D metabolic gradients (Walenta *et al.*, 2000). A susceptibility to air-drying may reflect the inherent properties of nucleated mammalian cells, as well as a poor understanding of how experimental variables, such as 2-D or 3-D culture may affect viability. Previous work from our lab has shown that monolayer cultures of mammalian cells (HEK293) cannot withstand desiccation, whereas partially-dried 3-D multicellular spheroids maintain viability during long-term (at least 6 weeks) storage in air, at room temperature (Jack *et al.*, 2006). These initial studies with the HEK293 aggregate model system were used as the starting point of the research reported herein. The goal of this research is to elucidate the roles of activated signaling pathways utilized by these mammalian cells in 3-D culture to maintain viability (survival) during forced metabolic arrest.

Rationale and Significance

Multiple signaling pathways have been implicated as playing essential roles in cellular apoptosis and/or quiescence in human cells. The experimental approaches taken to understand these pathways typically involve genetic engineering (knockouts and over-expression) and/or the addition of exogenous chemokines and/or cytokines to monolayer cell cultures which can result in “wide open” or “fully gated” responses. While this allows for easier detection of the signal transduction response changes, the amount of targeted protein present as well as the concentration of exogenous effector added may be at levels that are typically not encountered by normally functioning cells. Thus any response observed when employing these experimental techniques and/or conditions may not be applicable to cells responding to a realistic physiological stress. The use of these approaches as well as the cell line or cellular transformation state used (*i.e.* primary, carcinoma, virally-infected) may explain the areas of discrepancy and/or controversy in the published literature relating to the stress response signaling relationship of parallel and interacting pathways in both survival and apoptosis. The alternative approach utilized by our group to understanding the relationship between such pathways is to provide an external stress to multicellular aggregates. This morphology permits facile diffusion and uptake of cytokines. Observing the inherent signal transduction cascades permits a more realistic physiological response.

Further complicating this area of signal transduction is the reported roles of JNK MAPKinase signaling and activation in cell survival versus apoptosis. JNK activation has been suggested to be critical in both apoptosis (De Smaele *et al.*, 2001) and cell survival (Davis, 2000), with correlative studies indicating that JNK activation participates in both

apoptotic and/or antiapoptotic responses mediated from exogenous TNF- α cytokine signaling (Lamb *et al.*, 2003). These opposing results suggest that a more complex cascade or mechanism is required for the operation of this signaling pathway. Previous studies using cells in which NF- κ B signaling is impaired have suggested that NF- κ B activation acts antagonistically by increasing transcription of multiple genes (*xiap*, *gadd45 β*) which consequently inhibit JNK signaling/phosphorylation (Fig. 1.1) allowing for survival (De Smaele *et al.*, 2001; Tang *et al.*, 2001). These reports using genetically modified cell lines have become widely accepted in the cell stress signaling field. However, earlier work in this field reported that NF- κ B's activation of *xiap* and *gadd45 β* activate JNK through the up-regulation of upstream MAPkinases (Takekawa and Saito, 1998). These discrepancies may be a result of the cell lines used as well as the culturing technique (single recombinant TNF- α cytokine treatment, monolayer vs. spheroid) performed to obtain the signaling results.

The extracellular environment surrounding a cell dictates its physiological state, resulting in proliferation, quiescence or cell death. Internal transduction cascades convey messages from the external environment to the cell through multiple overlapping signaling pathways. Using spheroid cell culture as a model provides an *in vitro* system which allows for a more realistic cellular response by allowing for cell to cell communication and contact due to the nature of the 3-D structure. External stresses imposed on such systems can be monitored and assessed at endogenous protein and cytokine levels, allowing for the determination of the combined effects of multiple cytokines at physiological levels/ratios. This may invoke responses on converging pathways culminating in an overall response that is different from that observed in

monolayers where single exogenous effectors (cytokines) are added. Interestingly, TNF- α , IL-1b and IL-8 are cytokines that impart overlapping effects in apoptosis and survival (Chen and Goeddel, 2002; Ichijo, 1999; Manna and Ramesh, 2004). Their downstream signaling involves the activation of both NF- κ B and JNK (Manna and Ramesh, 2004; Zhang and Chen, 2004). Therefore, observing endogenous combinational cytokine signaling within multicellular aggregates under external stress may invoke signaling pathways that lead to cellular outcomes (apoptosis/survival) not previously observed. As such conditions allow for direct signaling to neighboring cells providing a “tissue- like” response (Schmeichel and Bissel, 2003), the overall cellular response of networked pathways may be directly related to cytokine profiles. If this is the case, multicellular aggregates will provide a more holistic understanding of the inputs and outputs of such pathways.

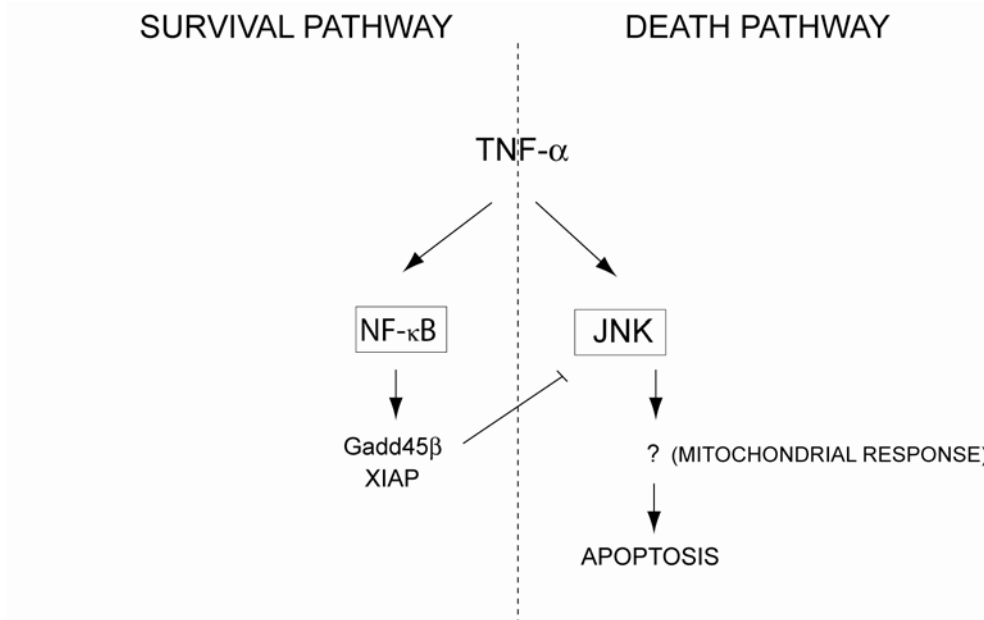


Fig. 1.1 Schematic representation of TNF- α -induced pathways modulating apoptosis and survival. Previous studies have shown that NF- κ B activation prevents JNK signaling by upregulation of Gadd45 β and XIAP. This was performed by blocking the NF- κ B-dependent pathway by either NF- κ B knockout mutations or antisense *gadd45 β* plasmids which led to sustained JNK activation and apoptosis. However these results were obtained using single addition of cytokine (TNF- α) at concentrations which may not be physiologically relevant.

Overview of Thesis

The initial study using HEK293 cells as the model cell line is presented in **Chapter 2**. A novel signaling relationship between NF- κ B (a transcription factor) and JNK (a MAPKinase) (Fig. 1.2A) was identified. Endogenous stress signaling within HEK293 multicellular aggregates identified the relationship between NF- κ B and JNK as co-operative and further suggested Gadd45 β as the mediator of this cross-talk. This result was controversial and in some cases contradictory to numerous previous reports. These opposing results suggest that a more complex cascade or mechanism was required for operation of the spheroid signaling pathway. Under the experimental conditions used in this work (3-D cell culture of HEK293 cells) NF- κ B signaling together with JNK activation was required for cell survival. Chemical inhibition studies provided further evidence that inactivation of either NF- κ B or JNK signaling induces cell death within HEK293 multicellular aggregates during external stress conditions, with NF- κ B directly influencing the activation/phosphorylation of downstream JNK signaling.

Using cytokine profiling, the endogenous combinational signaling (TNF- α , IL-1b and IL-8) of cytokines within the HEK293 multicellular aggregates during the external stress was identified. The resultant co-activation of the NF- κ B and JNK pathways amplified further production of downstream cytokines (TNF- α , IL-1b and IL-8) by an AP-1 transcription factor response (c-jun, ATF3) (Fig. 1.2A). This cyclical activation propagated the signal throughout the spheroid and appeared to be critical for HEK293 cells to recover from the external stress and proliferate normally when returned to monolayers (return to normal cell cycle). The synergistic effects of these extracellular

signaling molecules may explain the discrepancy of the signaling events observed during the course of this work (Compare Fig. 1.1 to Fig. 1.2A). These conflicting results may be resolved with the use of 3-dimensional cell culture techniques where endogenous signaling routes are invoked.

The next investigation, (**Chapter 3**) utilized HEK293 cells grown as monolayers. This experiment attempted to mimic the intercellular signaling response observed within the spheroids, using recombinant cytokines singularly and in combination. The results supported the role of extracellular signaling molecules acting in combination (TNF- α , IL-1b and IL-8) for cell survival. Only when TNF- α , IL-1 β and IL-8 were supplied in combination could the entire initial endogenous signaling route observed in the previous aggregate system (**Chapter 2**) be obtained. These results provide direct evidence that HEK293 cells utilize cytokine profiles to affect signal transduction events that lead to specific cell fate decisions during stress.

The final research question to be addressed in this thesis was if the patterns observed in HEK293 spheroids were present in aggregates of primary and carcinogenic cells (**Chapter 4**). As mentioned previously, transformation state and/or cell line may determine the availability of operational signaling pathways that can be utilized by a cell to survive stress conditions. HEK293 cells are adenovirally infected giving them an immortal phenotype (Graham *et al.*, 1977). Therefore, it was of interest to test both primary and carcinogenic cell lines for both their ability to survive long-term storage as a multicellular aggregate and to determine which pathways were operational in each. HFF-2, a human foreskin fibroblast, was chosen as the primary cell line to be tested and T98G (a glioblastoma cell line) was used as the carcinoma. The reasons behind these choices

were as follows: primary human epithelial cell lines (HFF-2) unlike many endothelial derived cells (mammary and glandular tissues) (Bates *et al.*, 2000) to our knowledge have not been tested for their ability to form aggregates, and T98G is a true p53 mutant carcinoma which is contrasted against the p53/pRb signaling impaired HEK293 cells (impaired by adenoviral transformation).

Interestingly, the T98G and HFF-2 cells activated an alternate pathway from that observed with the HEK293 aggregates. IFN- γ production activated Gadd45 α and the p38 MAPKinase pathway. Both cell lines displayed increased levels of AP-1 transcription factors c-jun and ATF3 similar to what was observed within the HEK293 cells. While the HEK293 cell line utilized a cyclical TNF- α , IL-1 β , and IL-8 pathway, the HFF-2 and T98G cells employed IFN- γ (Fig. 1.2B). Although both extracellular cytokine and upstream intercellular signaling differed between the HFF-2/T98G and HEK293 stress responses, the activation of a cyclical pathway appeared similar. All three cell lines activated a signal transduction cascade using cytokines which activated a MAPkinase pathway (p38 or JNK). The MAPkinase signal then induced an identical AP-1 transcription factor response further increasing cytokine production.

Differences in cell survivability from this external stress were also determined by performing the NF- κ B inhibition studies as previously described for the HEK293 cells. T98G cells like the HEK293 cells could not return to proliferating monolayers without activation of NF- κ B. HFF-2 cells however appeared unaffected by this treatment. A switch in signaling was observed from p38 to JNK MAPKinase activation in both T98G and HFF-2 cells lines during NF- κ B inhibition. This discrepancy in lethality suggests that cellular transformation state may determine the degree in which JNK activation

becomes either apoptotic or antiapoptotic. Although different gene expression patterns may exist due to tissue specific requirements of these cell lines, the availability of the classical quiescent/apoptotic pathways (p53/Rb) may be the ultimate determinant in ability to withstand these avascular type stresses. These results also suggest NF- κ B as a target for a specific/selective treatment for cancer and transformed cell lines without affecting primary untransformed tissue. Furthermore these studies demonstrate that the 3-dimensional model can be applied to cell lines in multiple cellular transformation states, and these findings have important implications for the study and control of avascular cancer progression and wounding response mechanisms which are discussed in Chapter 4.

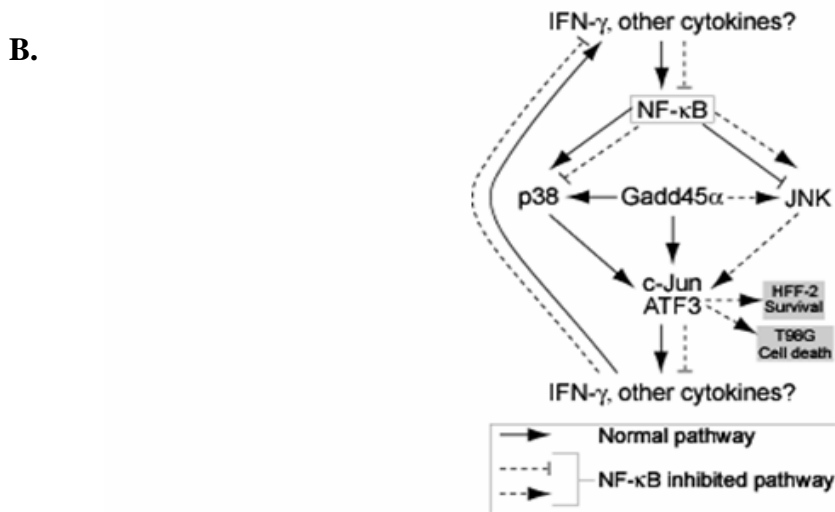
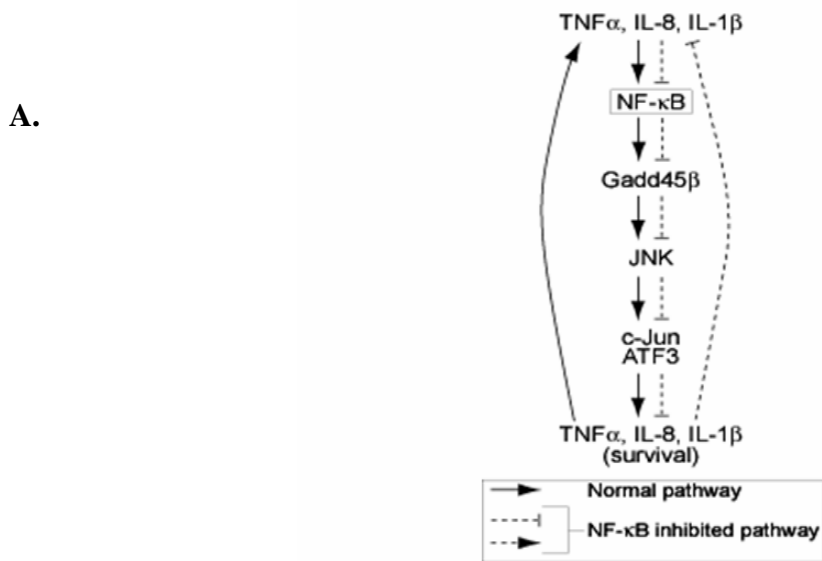


Fig. 1.2 Schematic representation of identified signaling pathways. **(A)** Signaling relationship between NF- κ B and JNK identified with work reported herein using HEK293 cells in aggregate cell culture. NF- κ B activates JNK signaling leading to survival. **(B)** Signal transduction cascades operational within HFF-2 and T98G cells as aggregate cell culture during external stress. Compare with (A) for signaling differences from the HEK293 cell line.

References

- Bates CB, Edwards NS, Yates JD. 2000. Spheroids and cell survival. *Crit Rev Oncol Hematol* 36: 61-74.
- Bloom FR, Price P, Lao GF, Xia JL, Crowe JH, Battista JR, Helm RF, Slaughter S, Potts M. 2001. Engineering mammalian cells for solid-state sensor applications. *Biosensors Bioelectronics* 16:603-608.
- Chen G, Goeddel DV. 2002. TNF-R1 signaling: a beautiful pathway. *Science* 31:1634-5.
- Coller HA, Sang L, Roberts JM. 2006. A new description of cellular quiescence. *PLoS Biol.* Mar;4(3):e83. Epub
- Crowe JH, Crowe LM. 2000. Anhydrobiosis: a unique biological state. *American Zoologist* 40:986-986.
- Davis RJ. 2000. Signal transduction by the JNK group of MAP kinases. *Cell* 103: 239-252.
- de Castro AG, Tunnacliffe A. 2000. Intracellular trehalose improves osmotolerance but not desiccation tolerance in mammalian cells. *FEBS Letters* 487:199-202.
- De Smaele E, Zazzeroni F, Papa S, Nguyen DU, Jin R, Jones J, Cong R, Franzoso G. 2001. Induction of gadd45beta by NF-kappaB downregulates pro-apoptotic JNK signalling. *Nature* 414: 308-313.
- Franzoso G, Zazzeroni F, Papa. 2003. JNK : a killer on a transcriptional leash. *Cell Death Differ* 10; 13-15.
- Graham FL, Smiley J, Russell WC, Nair R. 1977. Characteristics of a human cell line transformed by DNA from human adenovirus type 5. *J Gen Virol* 36: 59-74.
- Gray JV, Petsko GA, Johnson GC, Ringe D, Singer RA, Werner-Washburne M. 2004. "Sleeping beauty": quiescence in *Saccharomyces cerevisiae*. *Microbiol Mol Biol Rev* 68:187-206.
- Guo N, Puhlev I, Brown DR, Mansbridge J, Levine F. 2000. Trehalose expression confers desiccation tolerance on human cells. *Nat Biotechnol* 18:168-171.
- Huang Z, Tunnacliffe A. 2004. Response of human cells to desiccation: comparison with hyperosmotic stress response. *J Physiology* 558:181-19.
- Ichijo H. 1999. From receptors to stress-activated MAP kinases. *Oncogene* 18:6087-6093.

Jack GD, Mead EA, Garst JF, Cabrera MC, Desantis AM, Slaughter SM, Jervis J, Brooks AI, Potts M, Helm RF. 2006. Long term metabolic arrest and recovery of HEK293 spheroids involves NF-kappaB signaling and sustained JNK activation. *J Cell Physiol* 206: 526-36.

Jacks T, Weinberg RA. 2002. Taking the study of cancer cell survival to a new dimension. *Cell* 111: 923-925.

Lamb JA, Ventura JJ, Hess P, Flavell RA, Davis RJ. 2003. JunD mediates survival signaling by the JNK signal transduction pathway. *Mol Cell* 11:1479-1489.

Manna SK, Ramesh GT. 2005. Interleukin-8 induces Nuclear Transcription Factor-kB through TRAF6-dependent pathway. *J Biol Chem* 280:7010-7021.

Matsuo T. 2001. Trehalose protects corneal epithelial cells from death by drying. *J Ophthalmol* 85:610-612.

Puhlev I, Guo N, Brown DR, Levine F. 2001. Desiccation tolerance in human cells. *Cryobiology* 42(3):207-217.

Rider TH, Petrovick MS, Nargi FE, Harper JD, Mathews RH, Bertolin LT, Blanchard DJ, Young AM, Chen J, Hollis MA. 2003. A B Cell-Based Sensor for Rapid Identification of Pathogens. *Science* 301:213-215.

Schmeichel KL, Bissell MJ. 2003. Modeling tissue-specific signaling in three dimensions. *J Cell Sci* 116: 2377-2388.

Sutherland RM. 1988 Cell and microenvironment interactions in tumor microregions - the multicell spheroid model. *Science* 240: 177-184.

Takekawa M, Saito H. 1998. A family of stress-inducible GADD45-like proteins mediate activation of the stress-responsive MTK1/MEKK4 MAPKKK. *Cell* 95:521-30.

Tang G, Minemoto Y, Dibling B, Prucell NH, Li Z, Karin M, Lin A. 2001. Inhibition of JNK activation through NF-kB target genes. *Nature* 414: 313-317.

Walenta S, Doetsch J, Mueller-Klieser W, Kunz-Schughart LA. 2000. Metabolic imaging in multicellular spheroids of oncogene-transfected fibroblasts. *J Histochem Cytochem* 48: 509-522.

Zhang Y, Chen F. 2004. Reactive oxygen species (ROS), Troublemakers between Nuclear Factor-kB (NF-kB) and c-Jun NH₂-terminal kinase (JNK). *Cancer Res* 64:1902-1905.

Chapter 2

NF- κ B signaling and sustained JNK activation are essential for long-term arrest and recovery of HEK293 multicellular aggregates

Abstract

A wide variety of adherent mammalian cells can be induced into a reversible state of metabolic arrest (quiescence) by a conversion to non-adherent multicellular aggregates. The use of multicellular aggregates offers a simple way to identify activated stress response signal transduction pathways by monitoring both cytokines and proteins at endogenous levels, without reliance upon genetic engineering or exogenous addition of cytokines and/or chemokines. This study describes the signaling events required for these “spheroids” to be maintained at room temperature under oxygen and nutrient-deprived conditions for extended periods of time (weeks) as well as converted back to adherent monolayers. The activated pathways for HEK293 spheroids required to maintain viability during the long-term arrest and recovery were found to be dependent on both NF- κ B signaling and sustained JNK activation. A cyclical cascade, presumably originating from an intercellular stress signal, leads to endogenous cytokine production (TNF- α , IL-1 β and IL-8) and propagation of the cellular stress signal through the co-activation of both NF- κ B and JNK. Increased levels of known downstream pathway signaling members, specifically Gadd45 β , c-jun and ATF3 were clearly observed as was the activation of c-jun (phosphorylation). The activation of these pathways aid in the ability of these cells to survive long-term storage and recovery as chemical inhibition of both NF- κ B nuclear translocation and JNK phosphorylation leads to significant cell death.

Introduction

The dynamic environment surrounding a cell inherently dictates its physiological state, resulting in proliferation, quiescence or cell death. Signal transduction pathways link the extracellular matrix to the internal workings of the cell through complex pathways. The use of multicellular aggregates provides an *in vitro* model system which allows for a more realistic and physiological cellular response by allowing for cell to cell communication and contact. Due to the nature of the 3-dimensional structures, external stresses imposed on such systems can be monitored and assessed at endogenous protein and cytokine levels rather than the addition of exogenous effectors. Endogenous cytokine production and signaling within spheroids allow for combined efforts of multiple cytokines at physiological levels which may invoke responses on similar converging pathways and illicit overlapping responses. Unlike monolayers in which exogenous effectors (cytokines) are usually added singularly to media at unrealistic concentrations, aggregates under stress conditions allow for endogenous cytokine production and direct signaling to neighboring cells mimicking *in vivo* tissue-like response.

TNF- α , IL-1 β and IL-8 are cytokines that elicit various overlapping effects involved in immune response, apoptosis and survival (Chen and Goeddel, 2002; Ichijo, 1999; Manna and Ramesh, 2005). Their downstream signaling involves the activation of both NF- κ B and JNK (Manna and Ramesh, 2005; Zhang and Chen, 2004), however, a full appreciation of the relationship between the NF- κ B and JNK pathways has thus far remained elusive. Studies using cells in which NF- κ B signaling is impaired have suggested that NF- κ B activation acts antagonistically by increasing transcription of multiple genes (*xiap*, *gadd45* β) which consequently inhibits JNK signaling (DeSmaele *et*

al., 2001; Takekawa and Saito, 1998). Conversely to these antagonistic functions, reports have suggested collaborative signaling events for the NF- κ B and JNK pathways. For example, NF- κ B's activation of *xiap* and *gadd45* β has alternatively been shown to activate JNK through the up-regulation of upstream kinases (Suzuki *et al.*, 2001; Takekawa and Saito, 1998). In addition, NF- κ B signaling has been suggested to increase downstream gene expression by acting synergistically with JNK and contributing to downstream JunD activation (Lamb *et al.*, 2003). These opposing results suggest that a more complex cascade or mechanism is required for the operation of this signaling pathway. To further complicate this area of research, JNK activation has been suggested to be critical in both apoptosis and cell survival (Davis, 2000), with correlative studies indicating that JNK activation participates in both apoptotic and/or antiapoptotic responses mediated from cytokine signaling (Lamb *et al.*, 2003).

During the course of our work on determining the inherent strategies available to human cells for long term (months) storage at room temperature, we took advantage of the phenomenon that many cell lines can be induced into a quiescent state by forming non-adherent multicellular aggregates (spheroids) when grown on agarose surfaces (Jack *et al.*, 2006). The purpose of the work reported here was to identify the signaling pathway(s) activated during storage and recovery of HEK293 multicellular aggregates when stored for 2 weeks in vacuum-sealed containers under media-free conditions at room temperature. A novel signaling route was presumed to be active since HEK293 cells like many tumor cells do not possess arrest pathways (p53, pRB) that would normally be activated under these stress conditions due to the incorporation of the human adenovirus type 5 (Graham *et al.*, 1977). This work reported herein delineates a novel

signaling pathway where endogenous cytokine (TNF- α , IL-1 β , and IL-8) production leads to sustained JNK activation (days) and as well as activation of NF- κ B. The cooperative activation of these two pathways aids in the ability of these cells to survive this long term stress. Furthermore, up-regulation of NF- κ B's known pathway signaling member Gadd45 β , does not eliminate or negatively affect JNK (phosphorylation status) or its downstream activation of c-jun as has been previously suggested (De Smaele *et al.*, 2001). Instead, the results presented here suggest a correlative role for Gadd45 β in increasing JNK activation leading to cell survival. Multicellular aggregates are an excellent *in vitro* model system for analysis of signal transduction pathways as they can be assayed for cytokines and proteins simultaneously at endogenous protein levels.

Materials and Methods

Cell Culture

HEK293 cells at passage 9 were cultured in DMEM supplemented with 10% fetal bovine serum, 5% non-essential amino acids and 5% CO₂/humidified air at 37 °C. Monolayers were grown in T-185 flasks to 60% confluency then split into T-185 flasks coated with a 1% agarose mix in a 2:1 media/water ratio. Cells were suspended in 30 ml of supplemented media and grown for 4 days in order to form multicellular spheroids. The suspension was removed from the flasks and centrifuged (1500 x g, 2 min) and the media removed. The pellet was returned to the flasks and then placed in antistatic bags (Dri-shield 2000 moisture barrier bag from Surmount Inc., USA; Cat. # 70068), which were sealed immediately under vacuum (Deni® Magic Vac™, Champion model; Keystone Manufacturing, USA). Vacuum-sealed flasks were stored for 2 weeks (in the

dark) at room temperature. Recovery was initiated by removing the flask from the bag and resuspending the spheroids in supplemented media and placing the flasks in a 5% CO₂/humidified air incubator maintained at 37 °C. Timepoints for transcriptional and protein analyses were: 0 h storage (prior to sealing in bags), 2 week storage (0 hr recovery), 6 h, 24 h, and 72 h recovery. For the NF-κB and JNK inactivation studies, the same conditions were repeated except that the media and agarose were supplemented with 100 nM of the NF-κB activation inhibitor 6-amino-4-(phenoxyphenylethylamino)quinazoline (Calbiochem) or 1 μM of the JNK activation inhibitor SP600125 (Calbiochem), respectively.

Fluorescence Activated Cell Sorting Analysis

Cells were harvested and washed twice with 10 ml of PBS, with an intermediate centrifugation step (1500 x g; 2 min). The CycleTEST™ PLUS DNA Reagent Kit (Becton-Dickinson) was used according to the directions from the manufacturer for cell suspensions. Cells were analyzed using a Beckman Coulter flow cytometer (EPICS-XL). Software used for data analysis was EPICS version 1.5.

Transcriptional Profiling and Analysis

All experiments were biological triplicates. Cells were harvested and total RNA was extracted using the RNeasy™ kit and protocols (Qiagen). Microarray protocols, equipment and data were fully MIAME compliant and have been deposited at the Gene Expression Omnibus website (Series: GSE1455; Samples: GSM24493-GSM24510). RNA quality was assessed by electrophoresis using the Agilent Bioanalyzer 2100 and

spectrophotometric analysis prior to cDNA synthesis. Between 1 and 10 μ g of total RNA from each sample was used to generate a high fidelity cDNA, which was modified at the 3' end to contain an initiation site for T7 RNA polymerase. Samples were subjected to gene expression analysis via the Affymetrix Human 133A high-density oligonucleotide array which queries 22,000 human probe sets. Hybridization, staining and washing of all arrays were performed in the Affymetrix fluidics module as per the manufacturer's protocol. Streptavidin phycoerythrin stain (SAPE, Molecular Probes) is the fluorescent conjugate used to detect hybridized target sequences. The detection and quantitation of target hybridization is performed with a GeneArray Scanner 3000 set to scan each array twice at a factory set PMT level and resolution. All arrays referred to in this study were assessed for "array performance" prior to data analysis by statistical analysis of control transcripts that were spiked into the samples and the hybridization cocktail to assess array performance. In addition, several genes were identified on each array to help assess the overall quality of signal intensity from all arrays, this analysis helped validate the reproducibility of each array at baseline to define the lower limit of sensitivity.

A data set of statistically significant genes was generated using a multi-class F-Test with variance stabilization encompassing 6 sample classes (Iobion Informatics). The false discovery rate (FDR) was corrected for multiple testing using the Benjamini-Hochberg approach to multiple testing. The Q-Value cutoff for the experiment was 0.05 with probe sets with Q-values greater than 0.05 considered insignificant expressors across the experiment. This resulted in a list of 3302 probe sets that was then reduced further using a (+/-) 6-fold change filter. The reduced data set was a list of 52 statistically

significant probe sets representing 38 genes that were either up or down regulated more than six fold from the experimental multi-class mean.

Quantitative real-time polymerase chain reactions (Q-PCR)

Q-PCR employed Taqman chemistry with probes and primers designed using Primer Express v.1.0 (ABI, Foster City CA). The following rules added to the default selection criteria provided by the software. First, all probes selected will contain more C's than G's with no more than four consecutive bases of the same kind. Second, both forward and reverse primers will be selected to have at least three of the last five bases be A's or T's preventing clamping at the 3' primer end. The following dye combinations for probe generation were used for detection and data normalization: FAM (for the genes of interest), HEX (for normalizer genes, see below) and BHQ1 (non-fluorescent quencher) and ROX (reference). Prior to comparative analysis, a validation experiment was performed in order to determine the relative efficiency of the probes designed for the genes of interest and a series of probes designed to a gene that does not change as a function all perturbations, which was selected based on their behavior in the microarray data set and will be subsequently used as reference genes for comparative analysis. Following probe and primer optimization all cDNA's were diluted and used in a 10 μ l PCR reaction containing: 5 μ l of ABI 2x Universal Master Mix, 1.25 μ l of each forward and reverse primers (final concentrations ranging from 200-900nM depending on the primer set), 1 μ l of probe (final concentrations ranging from 50-200nM depending on the probe/primer set) and RNAase/DNAase free water. All reactions were performed in triplicate and the experiment replicated three times. All reactions were performed in an

ABI 7900 with the following cycle parameters: 1 cycle of 50°C (2 min) followed by 95°C (10min.), 40 cycles of 95°C (15 sec) followed by 60°C (1 min). Data were collected at every temperature phase during every cycle. Raw data were analyzed using the Sequence Detection Software (ABI, Foster City CA) while relative quantification using the comparative threshold cycle (C_T) method was performed in Microsoft Excel.

Assay designs for GADD45 α : Fwd: TGGAGGAAGTGCTCAGCAAA, Reverse: GGCACAACACCACGTTATCG, Probe: FAM-CCCTGAGTCAGCGCACGATCACTG-BHQ1; *GADD45 β* : Fwd: GCATTGTCTCTCCC-CACACA, Reverse: AGGGTTCTGTAGGAGGGAAAAGA, Probe: FAM-CCCG-GGAGAGGGAGGCTCCA-BHQ1; *GADD45 γ* : Fwd: CCTGCACTGCATCCTCATTTC, Reverse: TCTCCAAGGCGGGATCCT, Probe: FAM-AACCCCAACGAGGACGCCTGG-BHQ1; *Normalizer gene (β -actin)*: Fwd: GGCACCCAGCACAAATGAAG, Reverse: CCGATCCACACGGAGTACTTG, Probe: HEX-TCAAGATCATTGCTCCTCCTGAGC-BHQ1.

Western Blotting

Cells were harvested and washed twice with 10 ml of PBS, with an intermediate centrifugation step (1500 x g; 2 min). Cell pellets were lysed for 20 min at 4 °C on a rotator using a lysis buffer containing 20mM HEPES, 300 mM NaCl, 2 mM EDTA, 2 mM sodium orthovanadate, 0.1% Triton X, 20 mg/ml PMSF and 1:500 dilution of protease inhibitor cocktail for mammalian cell culture (Sigma). Lysates were cleared by centrifugation at 15,000 x g and protein concentration was measured using Coomassie protein assay reagent (Pierce). Cleared lysates were separated on SDS-PAGE Criterion™

gels (BioRad) at equal protein loading levels (30 µg of total protein per lane). Protein transfer to a polyvinylidene difluoride membrane (Hybond-P, Amersham Biosciences) was accomplished using a semidry transfer apparatus and probed with the following primary antibodies: p53 (sc-263), p21 (sc-817) and polyclonal p130 (sc-317), p107 (sc-318), Gadd45 α (sc-792), Gadd45 β (sc-8776), Gadd45 γ (sc-8777), MEK-7 (sc-13071), MEK-4 (sc-837), p38 (sc-7972) p-p38 (sc-7973), JNK2 (sc-7345), c-Jun (sc-1694), p-c-Jun(sc-16312-R), ATF3 (sc-188), actin (sc-8432) (Santa Cruz Biotechnology); p-JNK (4671S), p-MEK7 (4171), p-MEK4 (44-474) (Cell Signaling Technology). Following application of secondary horseradish peroxidase-conjugated secondary antibody and subsequent washes, signal was generated using ECLTM (Amersham Biosciences). Signals were detected by autoradiography.

Multiplex cytokine assays

Cytokines levels were measured using the Bioplex Protein Array system (BioRad), according to the instructions of the manufacturer. This multiplexed, particle-based, flow cytometric assay utilizes anti-cytokine monoclonal antibodies linked to microspheres incorporating distinct proportions of two fluorescent dyes. Cytokines measured included interleukin-1b (IL-1b), IL-2, IL-4, IL-5, IL-6, IL-7, CXCL8 (IL-8), IL-10, IL-12 (p40), IL-13, IL-17, interferon- γ (IFN- γ), tumor necrosis factor- α (TNF- α), granulocyte colony stimulating factor (G-CSF), granulocytemacrophage colony stimulating factor (GM-CSF), CCL2 [monocyte chemoattractant protein-1 (MCP-1)/MCAF], CCL4 [macrophage inflammatory protein-1b (MIP-1b)], Treated and untreated spheroid cell lysates (0.15 mg/ml) were thawed and run in triplicate (50 µl per

sample). Antibody coupled beads were incubated with the plasma sample (antigen) after which they were incubated with biotinylated detection antibody before finally being incubated with streptavidin–phycoerythrin. For each cytokine, eight standards ranged from 2 to 32,000 pg/ml and the minimum detectable dose was <10 pg/ml.

Confocal Microscopy

Confocal microscopy was performed on a Zeiss LSM-510 laser-scanning microscope (Zeiss 10x objective). Cell staining was with the LIVE/DEAD Viability/Cytotoxicity Kit (Molecular Probes). The final concentration of ethidium homodimer was 4 mM and the final concentration of calcein AM was 3 mM. The staining solution was added to the sample and incubated at room temperature (in the dark) for 30 minutes. Images of whole spheroids were prepared by transferring spheroids to 35 mm glass-bottom petri dishes containing 100 µl stain (incubation as described above).

Results

Placement of monolayer HEK293 cells onto agarose leads to their reorganization into multicellular aggregates (spheroids, Fig. 2.1A, B), with spheroid sizes ranging from 100 to 250 µm in diameter. With the removal of media, these cells undergo a forced metabolic arrest surviving for up to six-weeks in vacuum-sealed anti-static bags at room temperature (Jack *et al.*, 2006). Confocal and FACS analyses revealed that the majority of cells were viable after a two-week storage period (Fig. 2.1B), with transition back to proliferating adherent monolayers occurring over a period of 72 hrs after resuspension of the spheroids in media and placement on glass slides (Fig 2.1A, B). Spheroid viabilities

after conversion to monolayers with and without a two-week storage were comparable, although the samples that were not stored appeared to recover faster. The majority of death occurred within the core of the spheroid where cell density is the highest. Monolayer formation from spheroids may create an overpopulation effect and mechanical forces may cause death in the core area upon outgrowth. While this may be a disadvantage for long term storage and recovery of labile cells, spheroid formation preconditions cells to survive prolonged storage. The implications of this phenomenon from the perspective of long-term cell storage is discussed elsewhere (Chapter 1).

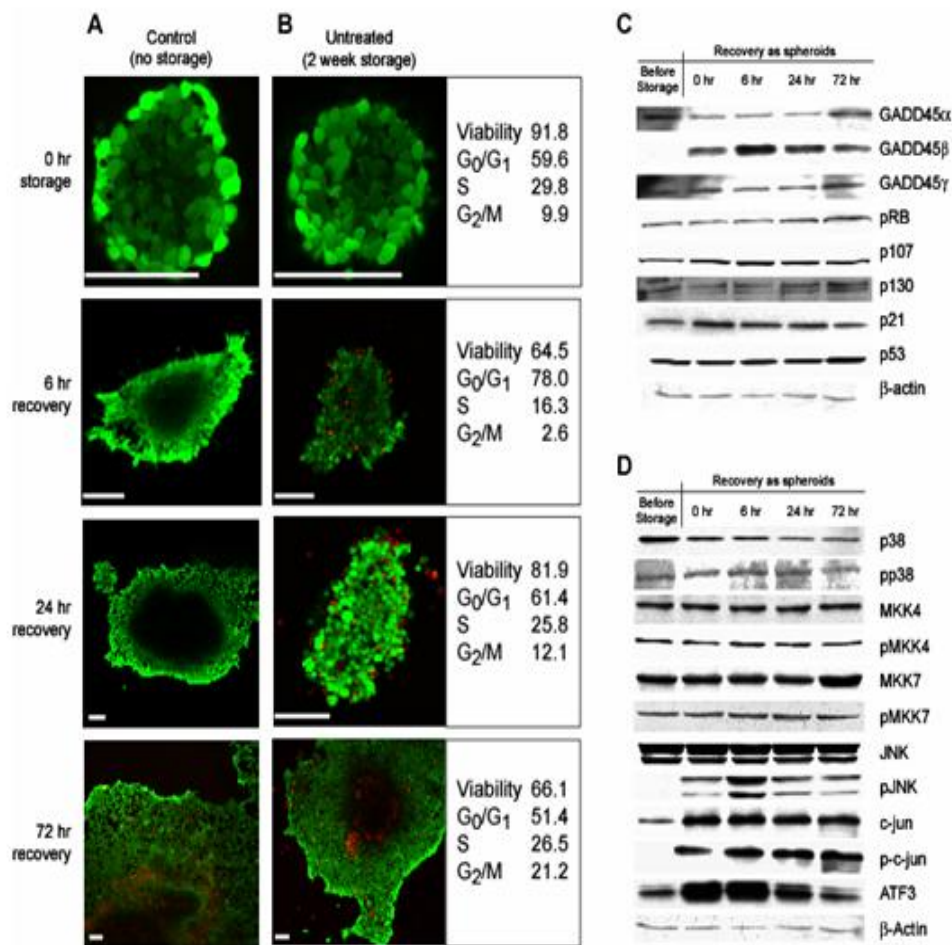


FIG. 2.1 HEK293 cells can be stored for extended periods of time as multicellular spheroids. **(A)** Confocal images of spheroids stained with the LIVE/DEAD stain (Molecular Probes) showing spheroid conversion back to monolayers. In this series of images there was no storage of the spheroid prior to conversion to monolayers. Outgrowth to adherent monolayer cells is evident at the 6h time point. **(B)** HEK293 cells before (first image) and after two week storage (6, 24 and 72h). Note that conversion back to monolayers takes slightly longer than for cells that were not stored. Scale bars for (A) and (B) = 100 μ m. Viabilities and cell cycle status are indicated for each time point for the stored cells. **(C)** Western blots showing that Gadd45 β is present directly after two-week storage and during recovery. The lack of a response from the standard quiescence markers (pRb, p107, p130, p21, p53) indicates that HEK293 spheroids are prevented from entering a state of quiescence via the retinoblastoma pathway. **(D)** Probing several signal transduction pathways revealed that protein levels for downstream effectors p-JNK, p-c-jun and ATF3 increased directly after storage.

Transcriptional profiling shows increased expression of *GADD45* β

As a first step at characterizing the system, DNA microarrays were used to monitor gene expression (relative to monolayer cells) after spheroid formation (0 hr storage), after storage as spheroids under media-free, hypoxic conditions in anti-static bags (0 hr recovery), and during recovery from arrest following 6, 24 and 72 hr of rehydration. The results were similar to those obtained for cells recovered as monolayers (Jack *et al.*, 2006), and a selective list of the most up- and down-regulated genes are presented in Fig. 2. An enhanced listing can be found in the Supplemental Materials, and a complete dataset can be accessed from the Gene Expression Omnibus (Series: GSE1455; Samples: GSM24493-GSM24510). All three *GADD45* genes showed marked induction, with *GADD45* β transcripts showing the greatest increase during the recovery phase (Table 2.1). The Growth-Arrest and DNA Damage inducible *GADD45* genes encode three small acidic proteins that share greater than 50% protein sequence identity (Zhan *et al.*, 1994). *GADD45* β encodes a protein with biological role(s) that range from the regulation of apoptosis to cellular quiescence—specific physiological states that are dependent on the cell type as well as the upstream signaling pathways that activate *GADD45* β transcription (Liebermann and Hoffman, 2002). Further analysis through quantitative PCR revealed preferential up-regulation of *GADD45* β that increased throughout the 72 hr recovery period (Table 2.1). *GADD45* α gene expression decreased slightly during the storage and recovery phase, while *GADD45* γ showed a response similar to that of *GADD45* β , although its fold-change was significantly less (10-fold vs. 116-fold; Table 2.1). Discrepancies between microarray and qPCR results are not without precedent. Cross-hybridization of probe targets is a common phenomenon in microarray protocols, and

may explain our findings. Nevertheless, the data provide strong evidence that elevated transcription of *GADD45β* is an important component of the survival process.

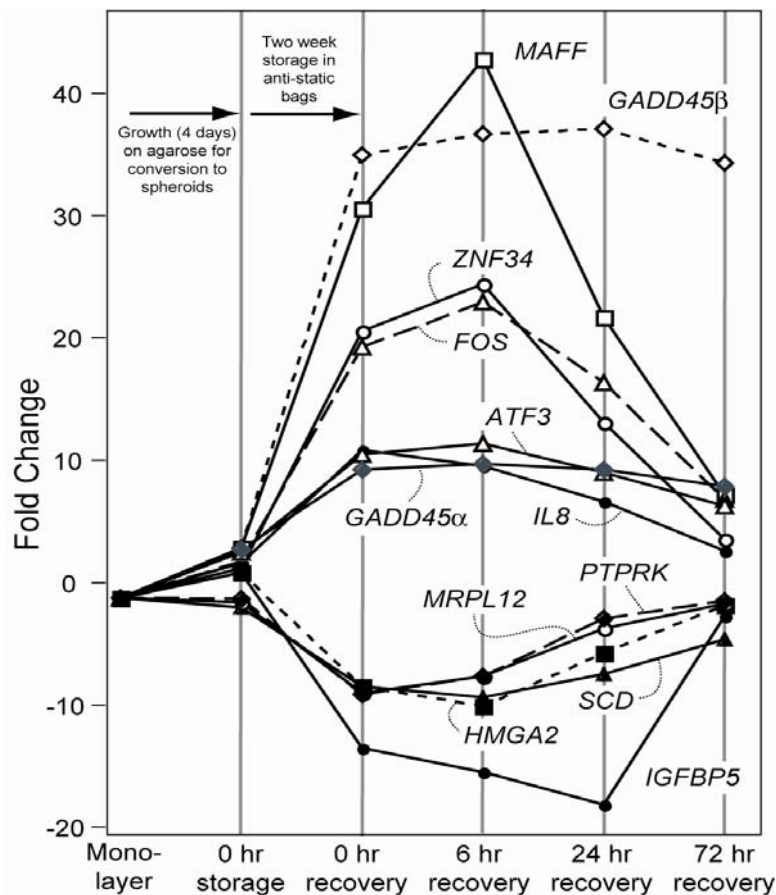


FIG. 2.2 A selective gene listing expression changes as determined by transcriptional profiling during storage and recovery of HEK293 multicellular aggregates. For a complete listing of the genes (36 in total) showing 6-fold up- and down-regulated, refer to the supplemental (pg 45). The complete dataset is available at the Gene Expression Omnibus (GEO Series: GSE1455)

Table 2.1 Comparison of Transcriptional Fold Changes for the *GADD45* Genes.

<i>GADD45</i> gene	Microarray Analysis Avg. Fold Induction ¹		Quantitative PCR Avg. Fold Induction ²	
<u><i>GADD45</i>α</u>				
0 hr Storage	2.95	(0.0138)	1	(0.64)
0 hr Recovery	9.48		-2.05	(0.15)
6 hr Recovery	9.97		-1.69	(0.19)
24 hr Recovery	9.45		0.96	(0.12)
72 hr Recovery	8.11		1.19	(0.14)
<u><i>GADD45</i>β</u>				
0 hr Storage	3.09	(0.0138)	1	(0.46)
0 hr Recovery	35.18		48.99	(0.27)
6 hr Recovery	36.92		39.02	(0.39)
24 hr Recovery	37.31		48.97	(0.23)
72 hr Recovery	34.56		115.98	(0.40)
<u><i>GADD45</i>γ</u>				
0 hr Storage	1.11	(0.0388)	1	(0.33)
0 hr Recovery	2.85		6.21	(0.23)
6 hr Recovery	3.43		5.74	(0.18)
24 hr Recovery	2.76		8.76	(0.21)
72 hr Recovery	2.15		10.76	(0.16)

¹Fold changes are relative to a monolayer control with P-values in parentheses.

²Fold changes are relative to the 0 hr storage sample, with standard deviations in parentheses.

Quiescence and recovery processes involve the NF- κ B and JNK pathways

To explore the role of Gadd45 proteins in cell quiescence, Gadd45 protein levels were determined by Western blotting, and compared to changes observed for the more common quiescence markers. Western analyses detected no changes in the levels of p53, its downstream transcriptional partner p21, or the phosphorylation levels of the pRb

family of proteins throughout the duration of the experiment (Fig. 2.1C). This confirms that the change in phenotype did not change the effect of E1A and E1B expressed adenovirus gene products (Parreno *et al.*, 2000; Querido *et al.*, 1997); spheroids respond similarly to monolayer cells in that signaling through classical quiescence pathways does not occur. Gadd45 β protein levels reached maximum during the initial phase of recovery, and the levels remained high throughout the 72 hr recovery period. The other family members, Gadd45 α and Gadd45 γ , showed no significant change in protein levels from the control time point through the 72hr recovery time point. This is in contrast to a recent report on cancer cell lines that linked decreased Gadd45 α and γ levels to increased survival (Zerbini *et al.*, 2004). The observed profile of GADD45 β , monitored at the transcriptional and protein levels, suggests that the gene is an integral component of the induced quiescence response strategy in HEK293 cells.

Gadd45 β has been linked with numerous downstream signaling cascades (Chi *et al.*, 2004; Papa *et al.*, 2004; Tang *et al.*, 2001). Interactions of Gadd45 β with p38, MEK4, and MEK7 blocks activation of these pathways, and is suggested to prevent signaling to downstream JNK1 and JNK2 (De Smaele *et al.*, 2001; Papa *et al.*, 2004). Since these are phosphorylation dependent pathways that can lead to apoptosis and/or quiescence, we chose to determine phosphorylation levels of p38, JNK1, JNK2, MEK4, and MEK7 throughout the time course of the experiment by Western blotting (Fig. 2.1D). While phosphorylation status of p38, MEK4, and MEK7 remained unchanged, both JNK1 and JNK2 were activated by phosphorylation after the two-week storage phase and remained active throughout the 72 hr recovery period. To further probe JNK activation, the total protein and phosphorylation status of c-jun, a direct downstream target of JNK, was

monitored. ATF3 levels were also probed as this protein is a target of c-jun activation, and its transcript was observed to increase significantly during recovery (Fig. 2.2). We observed an increase in the phosphorylation of c-jun, as well as the protein levels of both c-jun and ATF3 during recovery from 2 week storage. These results suggest a JNK-dependent pathway is active during the recovery phase.

Chemical inhibition of the NF- κ B and JNK pathways

Previous work has shown that *GADD45 β* expression is regulated by NF- κ B (De Smaele *et al.*, 2001; Tang *et al.*, 2001). When the storage and outgrowth experiment was performed in the presence of an inhibitor which prevents NF- κ B downstream transcriptional activation (Tobe *et al.*, 2003), cells were unable to form uniform spheroids (Fig. 2.3A). In addition, during recovery from storage, the cells were unable to attach and form monolayers, with the majority remaining suspended in the media. Most of the cells (85.4%) had died after 72hrs of recovery, providing strong evidence that cell survival is dependent upon NF- κ B activation (Fig. 2.3A). Interestingly, the majority of cells which remained alive after 72 hr were attached to neighboring cells (Fig. 2.3A); this association may have aided in their protection.

In order to further substantiate the dependency of *GADD45 β* induction and cell survival on NF- κ B activation, we compared the *Gadd45 β* protein levels of treated and untreated cells directly after two week storage (Fig. 2.3B). The *Gadd45 β* , c-jun and ATF3 protein levels were lower in the chemically-treated cells, and phosphorylation of both JNK and c-jun were also attenuated. These results support the hypothesis that the stress signaling events induced by storage are dependent upon activation of NF- κ B and

may be regulated through Gadd45 β . The results of the chemical block also suggest that JNK, c-jun activation, and ATF3 expression may be required for these cells to enter and exit from the quiescent state, and are dependent on NF- κ B signaling for their activation. These data contradict previous reports that NF- κ B activation of Gadd45 β downregulates pro-apoptotic JNK signaling (De Smaele *et al.*, 2001; Papa *et al.*, 2004).

The role of JNK activation in quiescence and protection during recovery was examined further with another chemical inhibitor, SP600125, which is specific for the JNK isoforms. The concentration of inhibitor used in these experiments was ten-fold less than was shown to completely inhibit JNK activation in Jurkat cells (Bennett *et al.*, 2001), nonetheless this lower concentration produced results similar to those obtained with the NF- κ B inhibitor (compare Figs 2.3A and 2.3C). Although the FACs analysis revealed similar viabilities between the treated and untreated cells (Fig. 2.1B, Fig. 2.3C)—the JNK inhibited cells failed to return to monolayer after the two week storage period, with the majority of cells remaining suspended in the media and arrested without returning to a normal proliferating state (Fig 2.3C).

Although JNK phosphorylation was not completely inhibited, the exposure to SP600125 resulted in a reduction in total p-JNK levels, and a difference in the duration of the response. This reduction was sufficient to reduce phosphorylated levels of the downstream c-jun as well. Somewhat surprisingly, the ATF3 levels remained high during the JNK inhibition study (Fig. 2.3D), but decreased over time under the normal recovery conditions (Fig. 2.1D). Although the reason for this behavior is currently unclear, these results support the claim of multiple MAPK pathways converging on ATF3 expression (Hartman *et al.*, 2004, Inoue *et al.*, 2004).

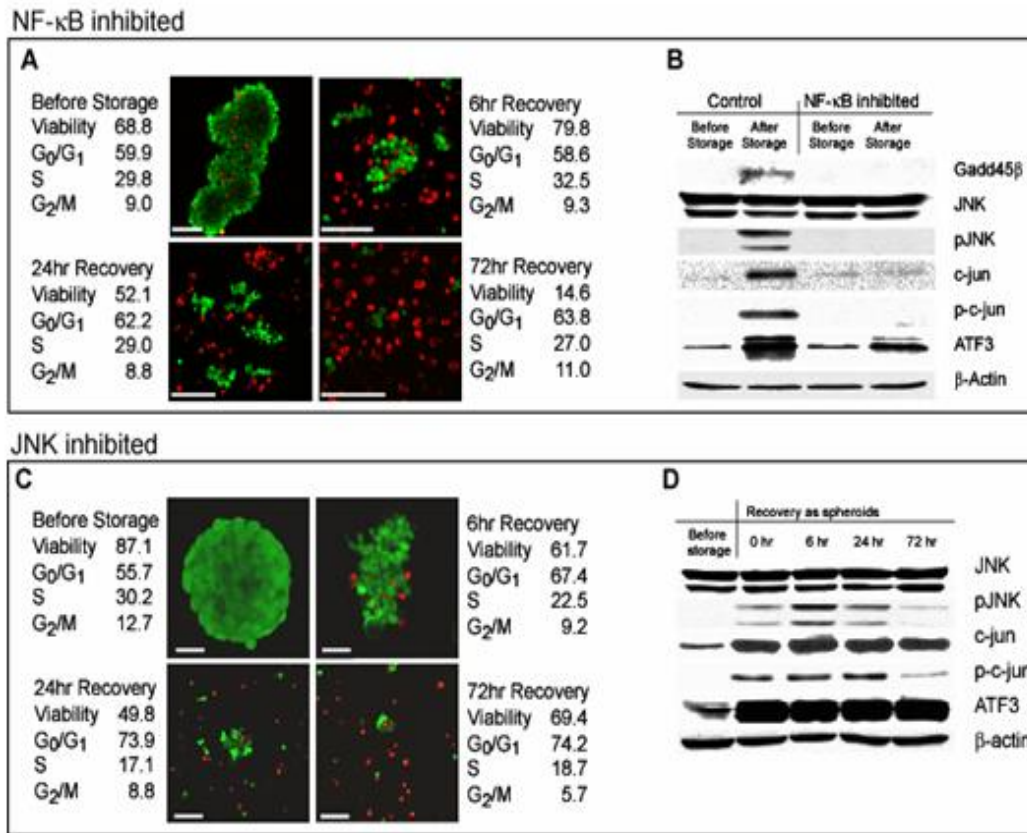


FIG. 2.3 The quiescence and recovery signal transduction pathway for HEK293 spheroids involves NF- κ B and JNK signaling pathways. (A) Same time points as shown in Fig. 2.1, but in this case the cells were exposed to an NF- κ B inhibitor during spheroid formation, storage and recovery. Scale bars = 100 μ m. (B) Inhibition of NF- κ B resulted in decreased Gadd45 β , p-JNK, p-c-jun and ATF3 protein levels. The low intensity of the Gadd45 β band in the stored control sample (relative to the same time point, 0hr recovery, Fig. 1C) is due to the low protein loading required to match the limited amount of protein available in the inhibited samples. Although faint, this band was present in all replicate experiments. (C) Same time points as in Figs. 2.1 and 2.2A, but in this case the cells were treated with SP600125 (JNK inhibitor) during spheroid formation, storage and recovery. Scale bars = 100 μ m. (D) Western analysis of the JNK inhibited spheroids. Decreased p-JNK and p-c-jun levels are evident while the ATF3 level remained high throughout the recovery period (compare levels and trends to Figs. 2.1D and 2.3B).

Role of cytokines

Another transcript that was observed to increase in the transcriptional analysis by microarrays was IL-8 (Fig. 2.2). This inflammatory chemokine activates and is regulated by the NF- κ B and JNK signaling pathways, typically triggered by a TNF- α or IL-1 β signal (Hoffmann *et al.*, 2002; Manna and Ramesh, 2005). A cyclical pathway was suspected to be in operation involving the activation of the NF- κ B and JNK stress pathways, consequently up-regulating the production of cytokines which would further propagate these signaling events throughout the cell as well as the aggregate. In order to investigate this hypothesis as well as explore the roles of cytokines in cellular quiescence, intra-spheroid cytokine levels were monitored via a multiplex cytokine assay during the storage and recovery process. Of the 17 cytokines assayed, TNF- α , IL-1 β , IL-8, and IL-4 showed the most markedly upregulated expression during the recovery period as well as large decreases in concentration when spheroids were grown in the presence of the NF- κ B inhibitor (Fig. 2.4). This strongly supports their dependence upon NF- κ B activation or its downstream signaling for production (Li-Weber and Krammer, 2003). Furthermore TNF- α , IL-1 β and IL-8, as well as being transcriptionally up-regulated by NF- κ B, also initiate both the NF- κ B and JNK signal transduction pathways (Manna and Ramesh, 2005; Zhang and Chen, 2004). The dramatic decrease in these cytokines by chemical treatment combined with the attenuated Gadd45 β , pJNK, p-c-jun and ATF3 protein levels (Fig 2.3B) strongly suggests endogenous cytokine production (TNF- α , IL-1 β , and IL-8) propagates the cyclical activation of NF- κ B and JNK pathways which are essential for both quiescence and recovery in multicellular aggregates.

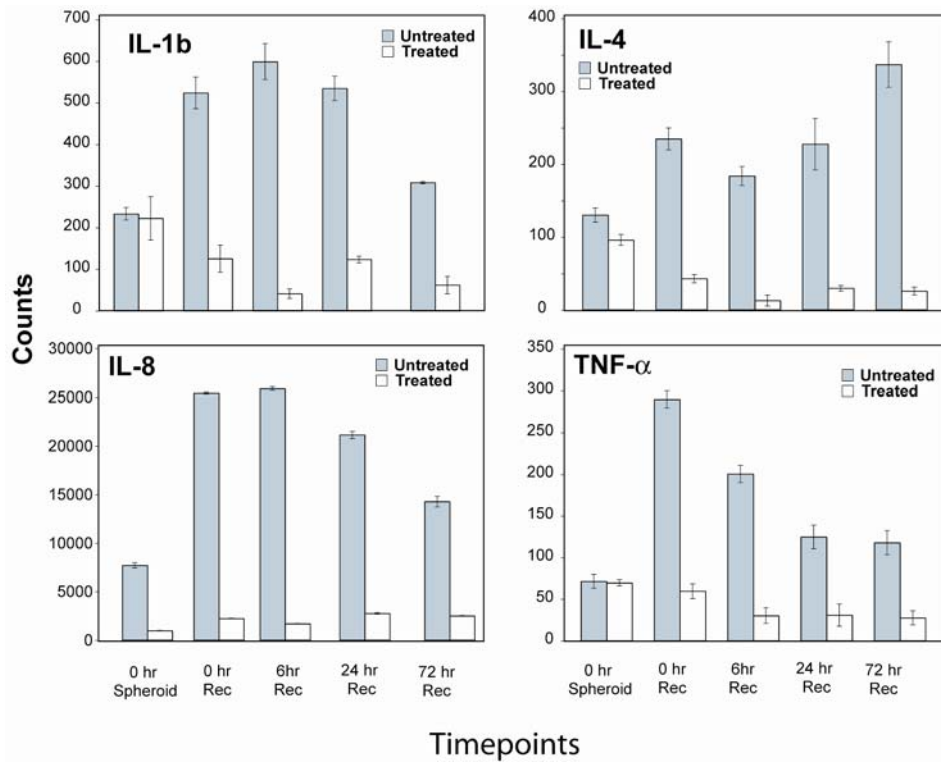


FIG. 2.4 Cytokine data for spheroids at the indicated timepoints as determined by fluorescence-based multiplex bead arrays. Shaded bars: untreated (control); clear bars: treated with the NF- κ B inhibitor. Data are presented in counts. See Supplemental for the complete dataset (17 cytokines).

Discussion

A strong relationship was observed between cytokine levels and signaling through the NF- κ B and JNK pathways. Cytokine signaling from TNF- α , IL-1 β , and IL-8 are known to activate both NF- κ B and JNK stress response pathways (Manna and Ramesh, 2005; Zhang and Chen, 2004). However previous investigations have produced a very diverse and contrasting array of results. Antagonistic and cooperative roles have been assigned to the activation of NF- κ B and its effect on JNK signaling (De Smaele *et al.*, 2001; Lamb *et al.*, 2003; Papa *et al.*, 2004; Suzuki *et al.*, 2001; Taketawa and Saito, 1998). The role of JNK upon activation of these pathways is also debated to be either pro-apoptotic or anti-apoptotic (Davis, 2004; De Smaele *et al.*, 2001; Lamb *et al.*, 2003). Although substantial evidence supports a functional role for the JNK signaling pathway in stress-stimulated apoptosis (De Smaele *et al.*, 2001), other studies have indicated that JNK activation may contribute to cell survival through cooperation with NF- κ B (Lamb *et al.*, 2003).

Adenovirally-infected HEK293 cells do not exhibit many of the classical arrest pathways (p53, pRb). As prolonged storage of HEK293 cells as multicellular aggregates is possible (Jack *et al.*, 2006), we hypothesized that an alternative signaling route was being invoked, and suspected the involvement of NF- κ B. Chemical inhibition of NF- κ B as well as JNK signaling showed markedly reduced cell viability and recovery when compared to controls. Together, these data demonstrate that the signaling events required for these cells to recover from the quiescent state are dependent upon activation of both NF- κ B and JNK with cytokine levels clearly influencing the overall response.

The results of these studies provide an outline of the cyclical signal transduction pathway required for these cells to enter and exit from a long term quiescent state. Cellular arrest in multicellular aggregates leads to production of endogenous cytokines (TNF- α , IL-1 β and IL-8) and their combined signaling to neighboring cells within the spheroids which consequently activates both NF- κ B and JNK pathways. The resultant activation of the NF- κ B and JNK pathways increases further production of downstream cytokines (TNF- α , IL-1 β and IL-8). This cyclical activation propagates the signal throughout the spheroid leading to the observed sustained activation of both the NF- κ B and JNK pathways. This process appears to be critical for HEK293 cells to recover and proliferate normally (return to normal cell cycle) as inhibition of either pathway results in compromised survival.

The transcription factor NF- κ B has been shown to upregulate multiple genes which are suggested to regulate the signaling of JNK (De Smaele *et al.*, 2001; Tang *et al.*, 2001). Gadd45 β 's upregulation by NF- κ B has been linked to the control of JNK signaling through upstream kinase regulation (De Smaele *et al.*, 2001; Takekawa and Saito, 1998). The role of Gadd45 β in the control of JNK signaling is still under debate with studies suggesting both inhibitory and stimulatory effects of Gadd45 β expression on JNK activation (De Smaele *et al.*, 2001; Takekawa and Saito, 1998). The significant increase in Gadd45 β levels observed in these studies during storage and recovery appear to have no inhibitory effect on downstream JNK activation, which is in conflict with several recently published reports (De Smaele *et al.*, 2001; Tang *et al.*, 2001). The signaling results obtained within this work may be due to the multicellular aggregate system and choice of cell line. Nonetheless, these results suggest a stimulatory effect of

Gadd45 β on JNK activation. Gadd45 β may be one of several links between the NF- κ B and JNK signaling pathways, allowing for the crosstalk and/or cooperativity reported here.

Chemical inhibition of NF- κ B signaling decreased Gadd45 β protein levels and attenuated the activation of downstream JNK as well as known members of their converging signaling cascades, specifically AP-1 family members c-jun and ATF3, with the net result being loss of adherence capabilities (death) and recovery as monolayers. This inhibition also resulted in reduced cytokine production (TNF- α , IL-1 β , IL-8) indicating that they are also dependent upon the activation of the NF- κ B signaling cascade to further propagate their production. The chemical inhibition of JNK signaling also produced similar results. Activation and upregulation of downstream c-jun was diminished causing a reduced ability of these cells to return to monolayers and proliferate normally. These combined results suggest that a cyclical signaling pathway is required for these cells to survive a long term storage and recovery. The pathway relies on the production of cytokines which activate downstream NF- κ B and JNK pathways leading to increased production of these cytokines and propagation of this stress response cascade.

Sustained JNK activation (days) in cells with impaired NF- κ B signaling has been shown to elicit an antiapoptotic response (Reuther-Madrid *et al.*, 2002). Cooperation between NF- κ B and transient (hours) JNK and JunD activation has also been shown to increase antiapoptotic gene expression and increase survivability (Lamb *et al.*, 2003). Our work, however, appears to be the first example of sustained JNK activation working in cooperation with NF- κ B's transcriptional upregulation of downstream genes to allow for cells to maintain a high degree of viability under a long term stress. The observed

responses may be related to the nature of the signaling in multicellular aggregates and may be specific to HEK293 cells. Nonetheless, these studies indicate that the investigation of stress response pathways utilizing the multicellular aggregate model may provide new insights into the signal transduction cascades required for cells to endure specific stresses.

Clearly the “cellular microecology” (Sutherland, 1988) present in monolayer cells will be vastly different to that of a spheroid. It is known that “exposure of cells to the spatial constraints imposed by a 3D milieu determines how cells perceive and interpret biochemical cues from the surrounding microenvironment [e.g. the extracellular matrix, growth factors and neighboring cells” (Schmeichel and Bissel, 2003). Multicellular aggregates may be a more realistic depiction of *in vivo* cells (tissue) and offer the ability to rapidly and strategically obtain both cytokines and proteins for further assay. Such systems have been demonstrated to provide an appreciably different picture of quiescence relative to monolayers and have been proposed to offer a new dimension to studies centered on tumor biology (Jacks and Weinberg, 2002) and inflammation-based cancer studies (Pikarsky *et al.*, 2004). We demonstrate here that the 3-dimensional model can be applied to cell lines other than tumors, and our findings have important implications for the study and control of quiescence, aging and longevity in mammalian cells. Our results suggest that JNK activation under some conditions and in some cellular states may lead to an increase in cell survivability. At least for cell types with signaling pathways similar to that of our model (*i.e.*, virally-infected cells and possibly some cancer states), JNK activation may not be of use as a therapeutic target since activation may lead to progression of the disease state, making this target a poor choice for therapy.

Efforts have been made to characterize changes in gene expression profiles of monolayer versus three-dimensional cell cultures (Ghosh *et al.*, 2005). Data presented suggest profound effects on gene expression due to this culturing technique. Research efforts described within these studies do not support such a drastic change in expression profiles from conversion of cell cultures from monolayer to spheroids. Rather the changes in expression occur due to the long term stress imposed on such systems. This discrepancy may be due to the size and length of growth as spheroids, allowing for the creation of larger necrotic spheroid cores. The size of the spheroid may induce stress on many more cells within the spheroid and allow for a more drastic change in the gene expression profile.

This research focuses on developing strategies for the long-term storage of viable mammalian cells without reliance upon cryogenics and/or genetic engineering. Phenotypic manipulation of HEK293 cells permits prolonged storage at room temperature without exogenous addition of stabilizers and/or manipulation of the genome. The ability to maintain viability under these conditions results from activation of a NF- κ B signal transduction cascade that utilizes Gadd45 β as a response mediator. Our findings have important implications for the study, and control, of quiescence (including hibernation and torpor), aging and longevity in mammalian cells. Subsequent chapters in this thesis will describe the inherent signal transduction pathway in operation during entry and exit from quiescence of virally-infected, carcinoma and primary cell lines.

References

Bennett BL, Sasaki DT, Murray BW, O'Leary EC, Sakata ST, Xu W, Leisten JC A, Motiwala A, Pierce S, Satoh Y, Bhagwat SS, Manning AM, Anderson DW. 2001. SP600125, an anthrapyrazolone inhibitor of Jun N-terminal kinase. *Proc Natl Acad Sci USA* 98:13681-13686.

Chen G, Goeddel DV. 2002. TNF-R1 signaling: a beautiful pathway. *Science* 31:1634-5.

Chi H, Lu B, Takekawa M, Davis RJ, Flavel RA. 2004. GADD45beta/GADD45gamma and MEKK4 comprise a genetic pathway mediating STAT4-independent IFNgamma production in T cells. *EMBO J* 23:1576-1586.

Davis RJ. 2000. Signal transduction by the JNK group of MAP kinases. *Cell* 103:239-52.

De Smaele E, Zazzeroni F, Papa S, Nguyen DU, Jin R, Jones J, Cong R, Franzoso G. 2001. Induction of gadd45beta by NF-kappaB downregulates pro-apoptotic JNK signalling. *Nature* 414:308-313.

Ghosh S, Spagnoli GC, Martin I, Pliegert S, Demougin, P, Heberer M, Reschner A. 2005. Three-dimensional culture of melanoma cells profoundly affects gene expression profile: A high density oligonucleotide array study. *J Cell Physiol* 204:522-31.

Graham FL, Smiley J, Russell WC, Nair R. 1977. Characteristics of a human cell line transformed by DNA from human adenovirus type 5. *J Gen Virol* 36:59-74.

Hartman MG, Lu D, Kim ML, Kociba GJ, Shukri T, Buteau J, Wang X, Frankel WL, Guttridge D, Prentki M, Grey ST, Ron D, Hai T. 2004. Role for activating transcription factor 3 in stress-induced B-cell apoptosis. *Mol Cell Biol* 24:5721-5732.

Hoffmann E, Dittrich-Breiholz O, Holtman H, Kracht M. 2002. Multiple control of interleukin-8 gene expression. *J Leukoc Biol* 5:847-855.

Ichijo, H. 1999. From receptors to stress-activated MAP kinases. *Oncogene* 18:6087-6093.

Jack GD, Mead EA, Garst JF, Cabrera MC, Desantis AM, Slaughter SM, Jervis J, Brooks AI, Potts M, Helm RF. 2006. Long term metabolic arrest and recovery of HEK293 spheroids involves NF-kappaB signaling and sustained JNK activation. *J Cell Physiol* 206: 526-36.

Inoue K, Zama T, Kamimoto T, Aoki R, Ikeda Y, Kimura H, Hagiwara M. 2004. TNF α -induced ATF3 expression is bidirectionally regulated by the JNK and ERK pathways in vascular endothelial cells. *Genes Cells* 1:59-70.

Jacks T, Weinberg RA. 2002. Taking the study of cancer cell survival to a new dimension. *Cell* 111:923-925.

Lamb JA, Ventura JJ, Hess P, Flavell RA, Davis RJ. 2003. JunD mediates survival signaling by the JNK signal transduction pathway. *Mol Cell* 11:1479-1489.

LaRue KEA, Khalil M, Freyer JP. 2004. Microenvironmental regulation of proliferation in multicellular spheroids is mediated through differential expression of cyclin-dependent kinase inhibitors, *Cancer Res* 64:1621-1631.

Li-Weber M, Krammer PH. 2003. Regulation of IL4 gene expression by T cells and therapeutic perspectives. *Nat Rev Immunol* 7:534-43.

Liebermann DA, Hoffman B. 2002. Myeloid differentiation (MyD)/growth arrest DNA damage (GADD) genes in tumor suppression, immunity and inflammation. *Leukemia* 16:527-541.

Manna SK, Ramesh GT. 2005. Interleukin-8 induces Nuclear Transcription Factor- κ B through TRAF6-dependent pathway. *J Biol Chem* 280:7010-7021.

Papa S, Zazzeroni F, Bubici C, Jayawardena S, Alvarez K, Matsuda S, Nguyen DU, C.G. Pham CG, Nelsbach AH, Melis T, De Smaele E, Tang WJ, D'Adamio L, Franzoso G. 2004. Gadd45beta mediates the NF-kappaB suppression of JNK signalling by targeting MKK7/JNKK2. *Nat Cell Biol* 2:146-153.

Parreno M, Garriga J, Limon A, Mayol X, Beck GR, Moran E, Grana X. 2000. E1A blocks hyperphosphorylation of p130 and p107 without affecting the phosphorylation status of the retinoblastoma protein. *J Virol* 74:3166-3176.

Pikarsky E, Porat RM, Stein I, Abramovitch R, Amit S, Kasem S, Gutkovich-Pyest E, Urieli-Shoval S, Galun E, Ben-Neriah Y. 2004. NF- κ B functions as a tumor promoter in inflammation-associated cancer. *Nature* 431:461-466.

Querido E, Teodoro JG, Branton PE. 1997. Accumulation of p53 induced by the adenovirus E1A protein requires regions involved in the stimulation of DNA synthesis. *J Virol* 71:3526-3533.

Reuther-Madrid JY, Kashatus D, Chen S, Li X, Westwick J, Davis RJ, Earp HS, Wang CY, Baldwin AS. 2002. The p65/RelA subunit of NF-kappaB suppresses the sustained, antiapoptotic activity of Jun kinase induced by tumor necrosis factor. *Mol Cell Biol* 22:8175-83.

Schmeichel KL, Bissell MJ. 2003. Modeling tissue-specific signaling and organ function in three dimensions. *J Cell Sci* 116:2377-2388.

Sutherland RM. 1988. Cell and environment interactions in tumor microregions : The multicell spheroid model. *Science* 240:177-184.

Suzuki Y, Nakabayashi Y, Takahashi R. 2001. Ubiquitin-protein ligase activity of X-linked inhibitor of apoptosis protein promotes proteasomal degradation of caspase-3 and enhances its anti-apoptotic effect in Fas-induced cell death. *Proc Natl Acad Sci* 98:8662-7.

Takekawa M, Saito H. 1998. A family of stress-inducible GADD45-like proteins mediate activation of the stress-responsive MTK1/MEKK4 MAPKKK. *Cell* 95:521-30.

Tang G, Minemoto Y, Dibling B, Prucell NH, Li Z, Karin M, Lin A. 2001. Inhibition of JNK activation through NF- κ B target genes. *Nature* 414:313-317.

Tobe M, Isobe Y, Tomizawa H, Nagasaki T, Takahashi H, Fukazawa T, Hayashi H. 2003. Discovery of quinazolines as a novel structural class of potent inhibitors of NF- κ B activation. *Bioorg Med Chem* 11:383-391.

Yoo J, Ghiassi M, Jirmanova L, Balliet AG, Hoffman B, Fornace AJ, Liebermann DA, Bottinger EP, Roberts AB. 2003. Transforming growth factor-beta-induced apoptosis is mediated by Smad-dependent expression of Gadd45 β through p38 activation. *J Biol Chem* 278:43001-43007.

Zerbini LF, Wang Y, Czibere A, Correa RG, Cho JY, Ijiri K, Wei W, Joseph M, Gu X, Grall F, Goldring MB, Zhou JR, Liebermann TA. 2004. NF- κ B-mediated repression of growth arrest- and DNA-damage-inducible proteins 45 α and γ is essential for cancer cell survival. *Proc Natl Acad Sci USA* 101: 13618-13623.

Zhan Q, Lord KA, Alamo I, Hollander MC, Carrier F, Ron D, Kohn KW, Hoffman B, Liebermann DA, Fornace AJ. 1994. The gadd and MyD genes define a novel set of mammalian genes encoding acidic proteins that synergistically suppress cell growth. *Mol Cell Biol* 14:2361-2371.

Zhang Y, Chen F. 2004. Reactive oxygen Species (ROS), Troublemakers between Nuclear Factor- κ B (NF- κ B) and c-Jun NH₂-terminal Kinase (JNK). *Cancer Res* 64:1902-1905.

Chapter 2 Supplemental Information

Contents

Table 2.S1 Microarray Master Key.

Table 2.S2 Transcriptional analysis fold change values for probe-sets that were up- or down- regulated at least 6-fold during the spheroid storage and recovery.

Table 2.S3 Raw fluorescence intensities for probe-sets that were up- or down-regulated at least 6-fold during the spheroid storage and recovery.

FIG. 2.S1 Graphical depiction of the most highly up- and down- regulated genes during spheroid storage and recovery. Note that several probe-sets in Table S1 are for the same gene. Only the most up- or down- regulated probe-set is shown on the graph.

FIG. 2.S2 Comparison of cytokine levels with and without NF- κ B inhibition.

Table 2.S1 Microarray Master Key (data available a GEO Website).

Experiment

GSE1455 Two week storage and recovery of HEK 293 cells at ambient temperature

Accession	Title	.cel/.dat/.exp/.chp
GSM24493	RHE2_T1_R1, Control Monolayer	Hu1_Helm_S2_U133A
GSM24494	RHE2_T1_R2, Control Monolayer	Hu2_Helm_S2_U133A
GSM24495	RHE2_T1_R3, Control Monolayer	Hu3_Helm_S2_U133A
GSM24496	RHE2_T2_R1, 0 hr desiccation	Hu35_b_Helm_S2_U133A
GSM24497	RHE2_T2_R2, 0 hr desiccation	Hu36_b_Helm_S2_U133A
GSM24498	RHE2_T2_R3, 0 hr desiccation	Hu37_b_Helm_S2_U133A
GSM24499	RHE2_T3_R1, 0 hr rehydration	Hu38_Helm_S2_U133A
GSM24500	RHE2_T3_R2, 0 hr rehydration	Hu39_Helm_S2_U133A
GSM24501	RHE2_T3_R3, 0 hr rehydration	Hu40_Helm_S2_U133A
GSM24502	RHE2_T4_R1, 6 hr rehydration	Hu41_Helm_S2_U133A
GSM24503	RHE2_T4_R2, 6 hr rehydration	Hu42_Helm_S2_U133A
GSM24504	RHE2_T4_R3, 6 hr rehydration	Hu43_Helm_S2_U133A
GSM24505	RHE2_T5_R1, 24 hr rehydration	Hu44_b_Helm_S2_U133A
GSM24506	RHE2_T5_R2, 24 hr rehydration	Hu45_Helm_S2_U133A
GSM24507	RHE2_T5_R3, 24 hr rehydration	Hu46_Helm_S2_U133A
GSM24508	RHE2_T6_R1, 72 hr rehydration	Hu47_Helm_S2_U133A
GSM24509	RHE2_T6_R2, 72 hr rehydration	Hu48_Helm_S2_U133A
GSM24510	RHE2_T6_R3, 72 hr rehydration	Hu49_Helm_S2_U133A

Table 2.S2 Probe gene sets that change at least 6-fold during storage and recovery.

Probe set	Gene Name	NCBI Gene ID	Description	Mono-layer	0 hr stor.	0 hr recov.	6 hr recov.	24 hr recov.	72 hr recov.
207574_s_at	GADD45B	NM_015675	GADD45beta	-1.00	3.09	35.18	36.92	37.31	34.56
209305_s_at	GADD45B	NM_015675	GADD45beta	-1.00	2.29	31.64	32.44	32.58	31.32
36711_at	MAFF	NM_012323	MAFF, transcription factor MAFF	-1.00	3.08	30.81	42.99	21.89	7.39
219801_at	ZNF34	NM_030580	Zinc finger protein 34 (KOX 32)	-1.01	1.39	20.77	24.63	13.30	3.75
209189_at	FOS	NM_005252	FOS, v-fos FBJ murine osteosarcoma viral oncogene homolog	-1.00	1.93	19.50	23.14	16.57	7.03
209304_x_at	GADD45B	NM_015675	GADD45beta	-1.00	1.88	15.92	16.46	16.50	15.24
208311_at	GPR50	NM_004224	GPR50, G protein-coupled receptor 50	-1.01	1.12	13.27	9.66	7.64	3.43
214696_at	MGC14376	NM_032895	MGC14376, small hypothetical protein	-1.01	-1.01	12.09	16.01	15.28	9.07
220046_s_at	Cyclin L	NM_020307	cyclin L ania-6a, cyclin L ania-6a	-1.00	-1.10	12.02	12.09	9.45	3.48
202859_x_at	IL8	NM_000584	IL8, interleukin 8	-1.01	1.80	11.09	9.78	6.86	2.84
203378_at	PCF11	NM_015885	PCF11, PCF11p homolog	-1.00	1.17	10.95	13.30	7.17	3.15
211506_s_at	IL8	NM_000584	IL8, interleukin 8	-1.00	1.68	10.88	9.45	6.26	2.17
202672_s_at	ATF3	NM_001674	ATF3, activating transcription factor 3	-1.01	2.72	10.69	11.57	9.23	6.52
204148_s_at	POMZP3	NM_012230	POMZP3 fusion protein isoform 1	-1.00	1.72	10.48	9.41	7.35	3.99
214230_at	CDC42	NM_001791	CDC42, cell division cycle 42 (GTP binding)	-1.01	1.04	10.43	11.69	3.84	1.34
222309_at	C6orf62	NM_030939	C6orf62, hypothetical protein	-1.01	1.11	10.24	11.95	5.10	2.08
214683_s_at	CLK1	NM_004071	CLK1, CDC-like kinase	-1.01	1.36	10.09	12.18	7.87	4.04
201289_at	CYR61	NM_001554	CYR61, cysteine-rich, angiogenic inducer 61, Insulin-like growth factor-binding protein 10	-1.00	1.30	9.95	6.60	4.87	2.68
214790_at	SUSP1	NM_015571	SUSP1, SUMO-1-specific protease	-1.00	1.95	9.56	11.73	3.71	1.40
221841_s_at	KLF4	NM_004235	KLF4, Kruppel-like factor 4	-1.00	2.19	9.50	11.62	11.12	7.26
203725_at	GADD45A	NM_001924	GADD45alpha	-1.00	2.95	9.48	9.97	9.45	8.11
203855_at	KIAA0893	NM_014969	KIAA0893, protein contains WD40 repeats	-1.02	1.50	9.24	10.20	10.40	6.89
218940_at	C14orf138	NM_024558	C14orf138, hypothetical protein	-1.00	1.46	9.17	10.88	5.55	2.78
210910_s_at	POMZP3	NM_012230	POMZP3 fusion protein isoform 1	-1.00	1.24	9.07	7.85	5.78	3.31
218929_at	CARF	NM_017632	CARF, interacts with ARF	-1.00	-1.08	8.96	8.39	5.72	2.88
216985_s_at	STX3A	NM_004177	STX3A, syntaxin 3A	-1.01	1.15	8.83	9.58	6.75	3.48
222074_at	UROD	NM_000374	UROD, uroporphyrinogen decarboxylase	-1.01	-1.15	8.29	8.23	4.31	1.89
37028_at	PPP1R15A	NM_014330	PPP1R15A, protein phosphatase 1, regulatory subunit 15A	-1.00	1.38	8.10	8.05	6.37	2.93
201694_s_at	EGR1	NM_001964	EGR1, early growth response 1	-1.04	1.80	8.02	7.50	6.53	3.36

212019_at	CSIG	AY154473	CSIG, cellular senescence inhibited protein; PBK1	-1.00	1.13	7.96	13.31	7.19	2.84
208740_at	SAP18	NM_005870	SAP18, sin3 associated polypeptide p18	-1.01	1.17	7.95	10.48	8.40	4.69
219603_s_at	ZNF226	NM_015919	ZNF226, zinc finger protein 226	-1.00	2.02	7.94	8.51	5.14	2.59
206552_s_at	TAC1	NM_003182	TAC1, tachykinin 1 precursor isoform beta	-1.00	1.54	7.88	8.41	9.42	6.76
209457_at	DUSP5	NM_004419	DUSP5, dual specificity phosphatase 5	-1.00	1.68	7.68	8.04	8.31	5.28
214169_at	UNC84A	NM_025154	UNC84A, unc-84 homolog A (C. elegans)	-1.00	1.25	7.54	8.31	4.27	1.94
205807_s_at	TUFT1	NM_020127	TUFT1, tuftelin 1	-1.00	1.63	7.38	8.09	7.28	4.33
213951_s_at	TCFL4	NM_013383	TCFL4, transcription factor-like 4	-1.00	1.57	7.17	8.87	6.64	4.09
211998_at	H3F3B	NM_005324	H3 histone, family 3B	-1.00	1.19	7.09	8.22	6.55	3.34
201939_at	SNK	NM_006622	SNK, serum-inducible kinase	-1.00	-1.00	7.05	9.83	8.99	6.24
214016_s_at	SFPQ	NM_005066	SFPQ, splicing factor proline/glutamine rich	-1.00	1.38	6.82	8.50	10.08	6.41
209803_s_at	TSSC3	NM_003311	TSSC3, tumor suppressing subtransferable candidate 3	-1.00	2.05	6.62	8.82	9.93	9.49
201739_at	SGK	NM_005627	serum/glucocorticoid regulated kinase	-1.00	-1.07	6.54	9.03	9.57	6.35
202815_s_at	HIS1	NM_006460	HIS1, HMBA-inducible	-1.00	-1.15	6.19	8.90	8.29	4.70
209211_at	KLF5	NM_001730	KLF5, Kruppel-like factor 5	-1.00	1.40	6.01	8.07	7.51	5.65
213750_at	CSIG	AY154473	CSIG, cellular senescence inhibited protein; PBK1	-1.00	-1.05	5.70	8.22	7.39	3.20
202814_s_at	HIS1	NM_006460	HIS1, HMBA-inducible	-1.00	1.03	4.63	8.44	9.85	5.65
221577_x_at	PLAB	NM_004864	PLAB, prostate differentiation factor	-1.00	1.40	1.42	1.75	5.38	10.07
201218_at	CTBP2	NM_001329	C-terminal binding protein 2 isoform 1	-1.00	1.14	-8.12	-2.86	1.13	1.58
208025_s_at	HMGA2	NM_003483.2	HMGA2, high mobility group AT-hook 2	-1.00	1.03	-8.24	-9.88	-5.50	-1.59
211708_s_at	SCD	NM_005063	SCD, stearoyl-CoA desaturase	-1.01	-1.82	-8.24	-9.15	-7.22	-4.40
203931_s_at	MRPL12	NM_002949	Mitochondrial ribosomal protein L12	-1.00	-1.39	-8.79	-7.40	-3.53	-1.52
203038_at	PTPRK	NM_002844	PTPRK, protein tyrosine phosphatase, receptor type, K precursor	-1.00	-1.07	-8.91	-7.41	-2.68	-1.27
203386_at	TBC1D4	NM_014832	TBC1D4, TBC1 domain family, member 4	-1.00	-1.11	-9.09	-8.05	-4.25	-1.82
211959_at	IGFBP5	NM_000599	IGFBP5, Human insulin-like growth factor binding protein 5	-1.01	1.05	-	-	-	-2.50

Table 2.S3 Fluorescence intensities for the most highly up- and down-regulated genes.

Probe set	Gene Name	Description	Mono-layer	0 hr stor.	0 hr recov.	6 hr recov.	24 hr recov.	72 hr recov.
207574_s_at	GADD45B	GADD45B	1182	3822	41579	43640	44106	40856
209305_s_at	GADD45B	GADD45B	1359	3237	43029	44093	44283	42571
36711_at	MAFF	MAFF, transcription factor MAFF	221	700	6871	9510	4842	1667
219801_at	ZNF34	Zinc finger protein 34 (KOX 32)	769	1072	16065	18944	10245	2900
209189_at	FOS	v-fos FBJ murine osteosarcoma viral oncogene homolog	871	1684	17426	20159	14433	6137
209304_x_at	GADD45B	GADD45B	2683	5190	42741	44167	44281	40900
208311_at	GPR50	GPR50, G protein-coupled receptor 50	913	1035	12505	8829	7000	3217
214696_at	MGC14376	MGC14376, small hypothetical protein	490	488	6049	7846	7490	4473
220046_s_at	Cyclin L	cyclin L ania-6a, cyclin L ania-6a	2706	2475	32607	32724	25564	9488
202859_x_at	IL8	IL8, interleukin 8	849	1551	9946	8301	5825	2475
203378_at	PCF11	PCF11, PCF11p homolog	677	796	7427	9006	4854	2164
211506_s_at	IL8	IL8, interleukin 8	575	970	6727	5451	3607	1285
202672_s_at	ATF3	ATF3, activating transcription factor 3	3526	9767	37823	40816	32559	23157
204148_s_at	POMZP3	POMZP3 fusion protein isoform 1	635	1101	6719	5986	4677	2558
214230_at	CDC42	CDC42, cell division cycle 42 (GTP binding protein)	852	884	9085	9998	3295	1142
222309_at	C6orf62	C6orf62, hypothetical protein	273	309	2853	3264	1417	584
214683_s_at	CLK1	CLK1, CDC-like kinase	869	1192	8801	10583	6844	3543
201289_at	CYR61	CYR61, cysteine-rich, angiogenic inducer 61, Insulin-like growth factor-binding protein 10	904	1185	9149	5964	4402	2436
214790_at	SUSP1	SUSP1, SUMO-1-specific protease	228	453	2208	2683	850	322
221841_s_at	KLF4	KLF4, Kruppel-like factor 4	764	1676	7656	8887	8519	5625
203725_at	GADD45A	GADD45alpha	3398	10103	32283	33881	32106	27658
203855_at	KIAA0893	KIAA0893, protein contains WD40 repeats	1261	1896	11923	12918	13118	8762
218940_at	C14orf138	C14orf138, hypothetical protein	486	714	4597	5291	2707	1373
210910_s_at	POMZP3	POMZP3 fusion protein isoform 1	579	719	5327	4552	3347	1941
218929_at	CARF	CARF, interacts with ARF	953	888	8602	7990	5455	2761
216985_s_at	STX3A	STX3A, syntaxin 3A	816	945	7288	7823	5520	2853
222074_at	UROD	UROD, uroporphyrinogen decarboxylase protein phosphatase 1, regulatory subunit 15A	629	549	5297	5206	2709	1188
37028_at	PPP1R15A	PPP1R15A	2400	3325	19482	19340	15302	7068
201694_s_at	EGR1	EGR1, early growth response 1	1289	2336	10498	9687	8454	4353
212019_at	CSIG	CSIG, cellular senescence inhibited protein; PBK1	437	494	3516	5821	3152	1254
208740_at	SAP18	SAP18, sin3 associated polypeptide p18	1171	1369	9403	12301	9847	5530
219603_s_at	ZNF226	ZNF226, zinc finger protein 226	621	1279	5154	5317	3218	1617
206552_s_at	TAC1	TAC1, tachykinin 1 precursor isoform beta	280	432	2306	2354	2652	1971
209457_at	DUSP5	DUSP5, dual specificity phosphatase 5	940	1607	7539	7601	7812	5050
214169_at	UNC84A	UNC84A, unc-84 homolog A (C. elegans)	638	799	4922	5337	2730	1242
205807_s_at	TUFT1	TUFT1, tuftelin 1	1517	2472	11324	12274	11046	6633
213951_s_at	TCFL4	TCFL4, transcription factor-like 4	997	1580	7336	8851	6625	4127
211998_at	H3F3B	H3 histone, family 3B	5076	6051	36022	41742	33245	16996
201939_at	SNK	SNK, serum-inducible kinase	583	582	4332	5732	5245	3771
214016_s_at	SFPQ	SFPQ, splicing factor proline/glutamine rich	2371	3301	16239	20198	23936	15216
209803_s_at	TSSC3	TSSC3, tumor suppressing subtransferable candidate 3	386	792	2734	3414	3842	3721

201739_at	SGK	SGK, serum/glucocorticoid regulated kinase	1039	977	7176	9389	9945	6858
202815_s_at	HIS1	HIS1, HMBA-inducible	1514	1326	9414	13472	12550	7129
209211_at	KLF5	KLF5, Kruppel-like factor 5	271	381	1697	2215	2047	1570
213750_at	CSIG	CSIG, cellular senescence inhibited protein; PBK1	1167	1114	6709	9614	8655	3745
202814_s_at	HIS1	HIS1, HMBA-inducible	2756	2871	12896	23287	27166	15603
221577_x_at	PLAB	PLAB, prostate differentiation factor	605	856	862	1059	3256	6102
201218_at	CTBP2	CTBP2, C-terminal binding protein 2 isoform 1	6149	7060	759	2183	7042	9751
208025_s_at	HMGA2	HMGA2, high mobility group AT-hook 2	7999	8270	974	814	1456	5056
211708_s_at	SCD	SCD, stearyl-CoA desaturase (delta-9-desaturase)	13936	8219	1695	1530	1931	3174
203931_s_at	MRPL12	MRPL12, mitochondrial ribosomal protein L12	10950	7886	1255	1649	3101	7277
203038_at	PTPRK	pY phosphatase, receptor type, K precursor	5154	4845	579	697	1927	4075
203386_at	TBC1D4	TBC1D4, TBC1 domain family, member 4	4522	4081	500	565	1069	2481
211959_at	IGFBP5	Human insulin-like growth factor binding protein 5	13066	14145	989	861	731	5334

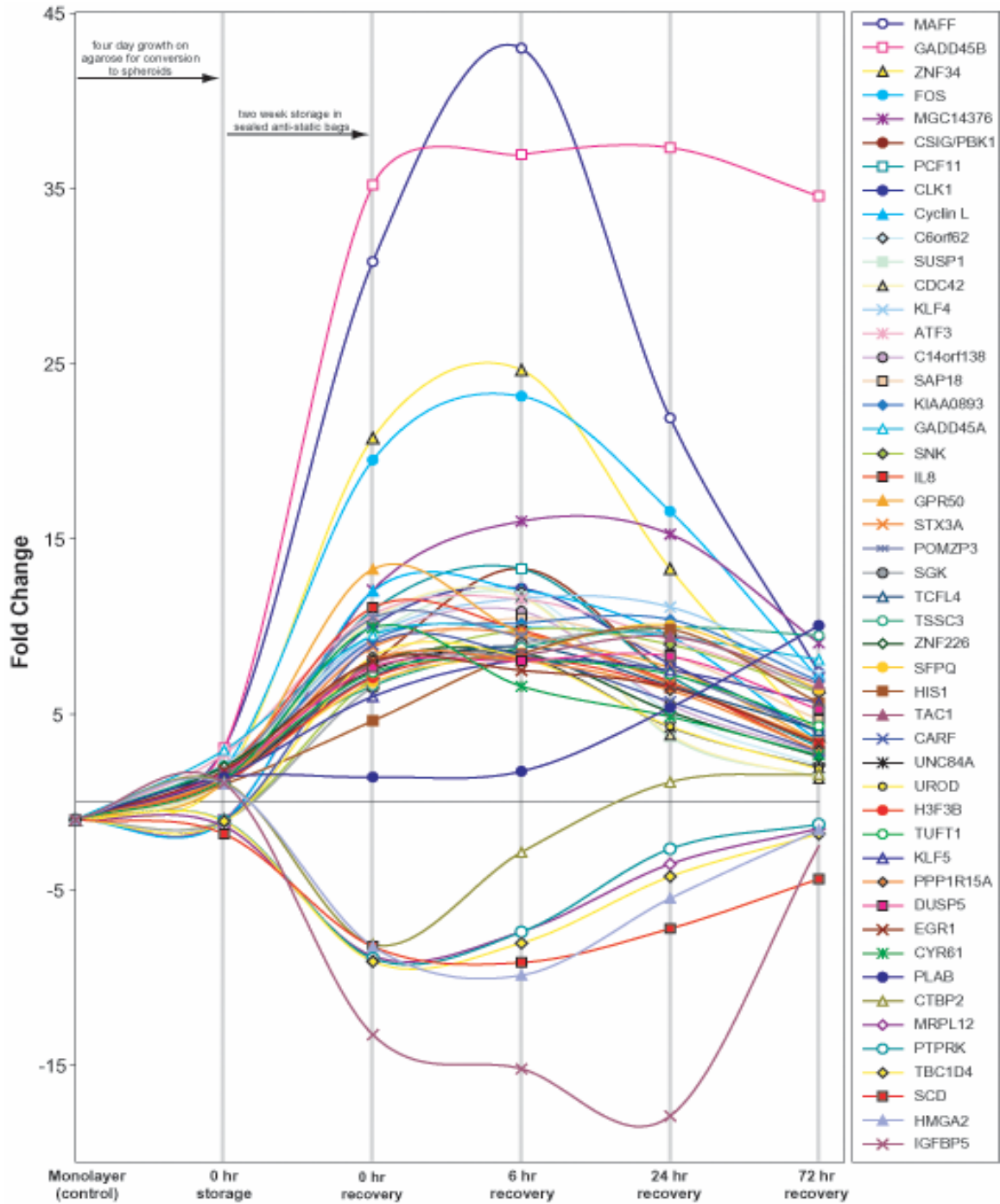


FIG. 2.S1 Graphical depiction of the most highly up- and down-regulated genes during spheroid storage and recovery. Note that several probe-sets listed in Tables S1 and S2 are for the same gene; only the most up- or down-regulated probe-set is shown in the graph.

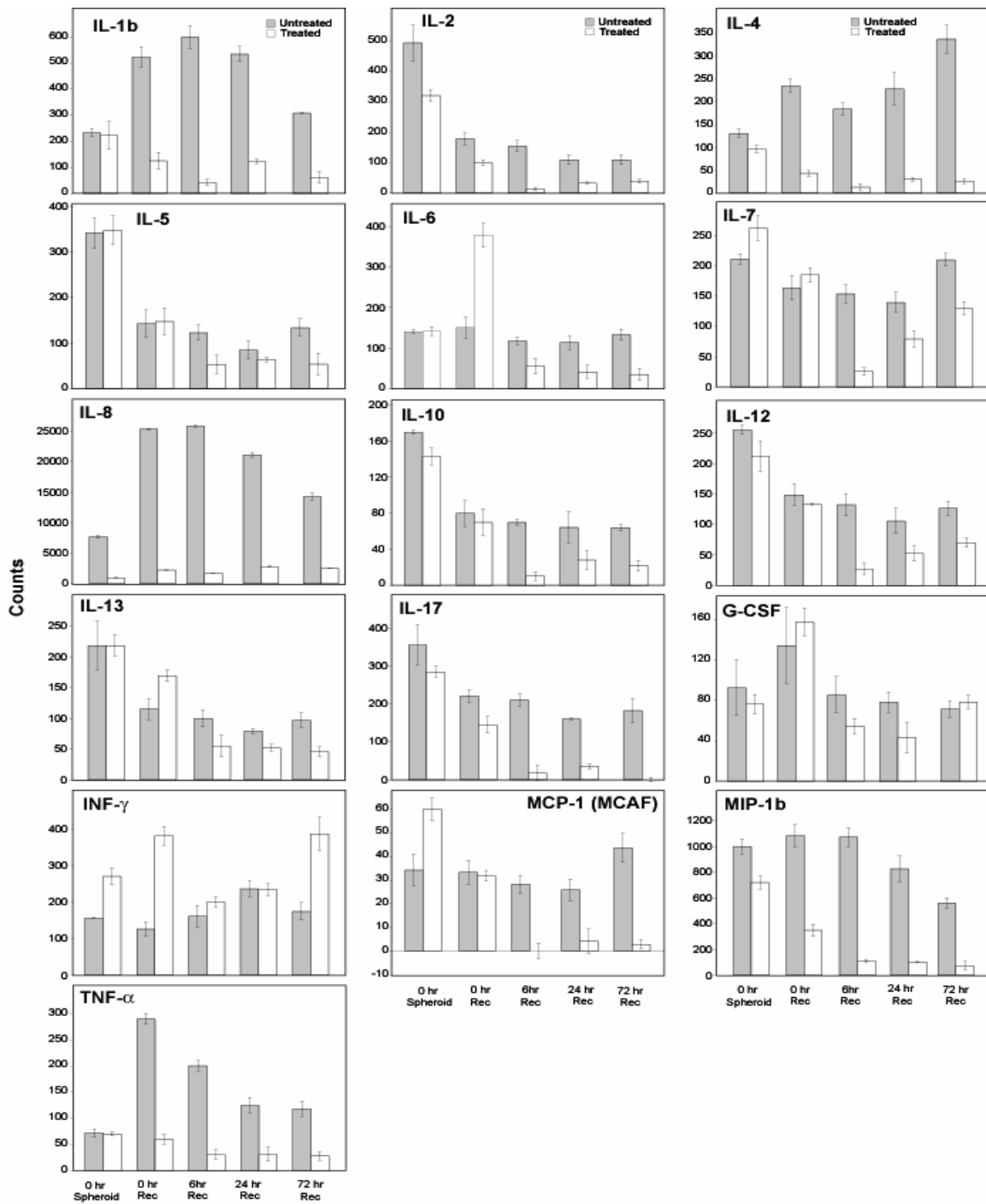


FIG. 2.S2 Cytokine data for spheroids at the indicated timepoints as determined by the fluorescence-based bead multiplex array. Shaded bars = untreated; clear bars = treated with the NF-kB inhibitor. Data are presented in counts.

Chapter 3

Cytokines influence HEK293 signal transduction cascades in a synergistic fashion

Abstract

Cytokines exist *in vivo* as mixtures, yet tissue culture studies delineating how cells respond to these molecules are often performed using individual effectors added exogenously. HEK293 multicellular aggregates (spheroids) survive long term arrest by endogenous combinatorial cytokine (TNF- α and IL-1 β) and chemokine (IL-8) signaling to sustain co-activation of NF- κ B and JNK. This chapter provides experimental evidence that when HEK293 cells are grown as adherent monolayers and exposed to the recombinant cytokines and chemokines (TNF- α , IL-1 β and IL-8) which were observed in the aggregates, a “spheroid signal transduction response” results. This response however is only observed when these recombinant signaling molecules are used in combination indicating that endogenous signal transduction cascade mechanisms are clearly cytokine-profile dependent.

Introduction

Cytokines within tissues exist as dynamic mixtures or profiles. Thus, tissue culture-based cytokine/chemokine studies that employ combinatorial additions are physiologically relevant (Gouwy *et al.*, 2005). The connections between the proinflammatory cytokines TNF- α , IL-1 β and the chemokine IL-8 are well established. TNF- α and IL-1 β have been shown to activate themselves (Ghivizzani *et al.*, 1997; Ulfgren *et al.*, 2000), each other (Brennan *et al.*, 1989; Williams *et al.*, 2000), and the production of chemokine IL-8 (Rathanaswami *et al.*, 1993; Hosaka *et al.*, 2005; Kuldo *et al.*, 2005). Furthermore, TNF- α , IL-1 β , and IL-8 are known to interact with the NF- κ B and JNK stress response pathways (Manna and Ramesh, 2005; Zhang and Chen, 2004) initiating overlapping effects involving the immune response, apoptosis, and cell survival (Chen and Goedell, 2002; Ichijo, 1999). While relationships between the cytokines and chemokines involved in immune and apoptosis/cell death responses have been well documented (Gouwy *et al.*, 2005; Kuldo *et al.*, 2005; Lee, 2002), the combinational signaling involved in cell survival has not.

When exposed to a long term arrest, HEK293 multicellular aggregates produce TNF- α , IL-1 β and IL-8 (Chapter 2). Their combined signaling to neighboring cells within the aggregates leads to co-activation of the NF- κ B and JNK pathways, further amplifying TNF- α , IL-1 β , and IL-8 production by an AP-1 transcription factor response. This cyclical activation appeared to be critical for HEK293 cells to recover from arrest and proliferate normally when returned to adherent monolayer growth conditions. In order to demonstrate the importance of cytokine profiles on cell signaling, we questioned if it was

possible to mimic the spheroid signaling response by supplementing adherent monolayer HEK293 cells with recombinant TNF- α , IL-1 β , and IL-8.

Materials and methods

Cell culture

HEK293 cells at passage 9 were cultured in DMEM supplemented with 10% fetal bovine serum, 1% non-essential amino acids and 5% CO₂/humidified air at 37 °C. Cells were grown in T-185 flasks to 40% confluency, at which time the media was supplemented with either TNF- α , IL-8 or IL-1 β cytokines (recombinant, Biosource International), a combination of all three, or PBS (used for cytokine solution buffer). Treatment levels were 5 and 15ng/ml for the individual cytokine treatments, and 5ng/ml of each cytokine in the mixed sample. Separate flasks were used for each treatment and timepoint (6, 24 and 72 h).

Cell Lysis and Western blotting

Harvesting of cells and preparation of protein lysates were performed as described [14]. Proteins were separated on SDS-PAGE CriterionTM gels (BioRad) at equal protein loading levels (60 μ g of total protein/lane). Protein transfer to polyvinylidene difluoride membranes (Hybond-P, Amersham Biosciences) was accomplished using a semi-dry transfer apparatus. The membranes were probed with the following primary antibodies: Gadd45 β (sc-8776), JNK2 (sc-7345), c-Jun (sc-1694), p-c-Jun (sc-16312-R), ATF3 (sc-188), actin (sc-8432) (Santa Cruz Biotechnology); p-JNK (4671S) (Cell Signaling Technology). Following application of secondary horseradish peroxidase-conjugated

secondary antibody and subsequent washes, signal was generated using ECLTM (Amersham Biosciences). Signals were detected by autoradiography.

FACS analysis

Cells were harvested by trypsinization and washed twice with 10 ml of PBS, with an intermediate centrifugation step (1500 x g; 2 min). The CycleTESTTM PLUS DNA Reagent Kit (Becton-Dickinson) was used according to the directions of the manufacturer for cell suspensions. Cells were analyzed using a Beckman Coulter flow cytometer (EPICS-XL). Software used for data analysis was EPICS version 1.5.

Transmitted light microscopy

Images of cells were captured at each timepoint and condition utilizing a Nikon Diaphot TMD Inverted Microscope using a Plan 10x 0.25 numerical aperture (160/-) objective, a clear interference filter, and 10x (CFW) eyepieces. Images were recorded on Ektachrome 160T Kodak emulsion (EPT 135-36) with a Nikon N6006 AF camera. Details on image processing are found in the Supplemental Information for Chapter 3.

Enzyme-linked immunosorbent assays

IL-8, TNF- α and IL-1 β levels from media samples were analyzed by ELISA by using kits from BioSource International. The ELISAs were performed according to the instructions supplied by the manufacturers. All analyses were performed in duplicate.

Protein identifications by LC-tandem ion trap mass spectrometry

Cell lysates were obtained as described previously in Chapter 2. Cleared lysates were separated on 12.5% SDS-PAGE CriterionTM gels (BioRad) at equal protein loading levels (100 µg of total protein per lane). Coomassie-stained gels were imaged (GS800, Bio-Rad) and compared selecting bands with intensity variations across the five samples. Five different bands were chosen and sampled across all five samples. Standard analysis protocols for reduction, cysteine carbamidomethylation, trypsinization and LC-tandem mass spectrometry were applied to each sample with identification via the MASCOT computer algorithm. See Supplemental Information in Chapter 3 for details.

Results and Discussion

Effects of cytokine treatments on cell morphology and viability

HEK293 cells grown as monolayers were exposed to TNF- α , IL-1 β and IL-8 individually (5 and 15ng/ml) and in combination (5 ng/ml each of TNF- α , IL-1 β and IL-8). Distinct changes in cellular morphology were observed for all cytokine treatments relative to a control at the 6 h timepoint. Rounded morphologies and the lack of cellular projections (lammellipodia) were found in all treated cells at this time, but by 24 h they had returned to morphologies typical of HEK293 cells (Fig. 3.1; Supplemental Data Fig. 3.S1). FACS analyses indicated that all cytokine treatments had little effect on viability, except when IL-1 β was added individually. This treatment, at both 5 and 15 ng/ml, resulted in a dramatic loss in viable cells at the 6 h time point with greater than 50% cell death (Fig. 3.2). This was not observed when IL-1 β was present in combination with

TNF- α and IL-8, and by the 24hr timepoint the IL-1 β treated cells had recovered sufficiently as to make them indiscernable from the control. These results indicate a difference in the degree to which these cytokines and chemokines elicit cellular stress responses. The IL-1 β treatment produced a level of stress such that at the 6 h timepoint, FACS cell preparation (which includes a trypsinization step) destroyed a large percentage of cells. This stress level was not observed when IL-1 β was present in combination with TNF- α and IL-8, indicating a protective effect for the combined treatment.

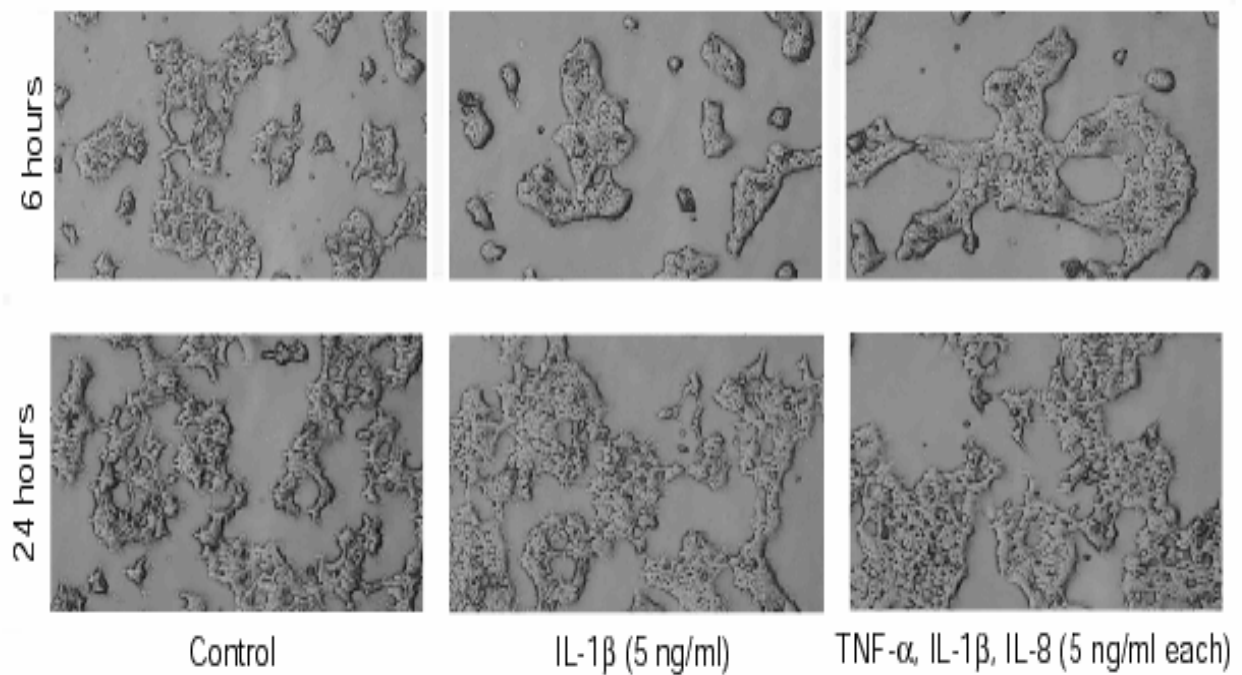


FIG. 3.1 Changes in cellular morphology due to TNF- α , IL-1 β and IL-8 treatments. Representative images of HEK293 cells at 6 and 24 h cytokine treatments are shown (see Supplemental Fig. 3.S1 for all images). Cells treated with individual cytokines or the cytokine mixture were rounded and lost the lamellipodia observed in the control. Cells exposed to all treatments appear to recover by 24 h and displayed similar morphologies similar to the control.

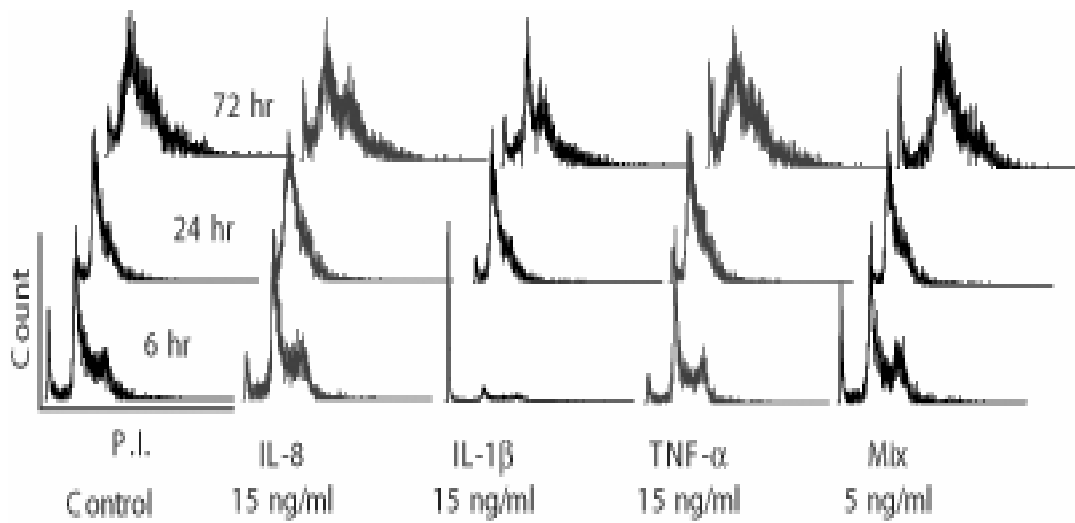


FIG. 3.2 The effects of cytokine treatments on cell viability. The IL-1 β treatment resulted in significant death at 6h (similar results were seen at both 5 and 15 ng/ml treatments). After 24 h all treatments had similar FACS profiles and viabilities.

Extracellular cytokine levels

As the morphological and viability assays suggested that the effect of cytokines diminished after 6 h, we decided to determine cytokine levels within the media during the course of the experiment using a commercial ELISA assay (Fig. 3.3). By 6 hours all cytokine levels were approximately 50% of their initial starting concentrations and remained relatively constant up to the 72 h timepoint. Whether this rapid initial decrease is attributed to either degradation or modification cannot be ascertained, but clearly a desensitization event occurred with the cells no longer responding to the cytokine for the remainder of the experiment.

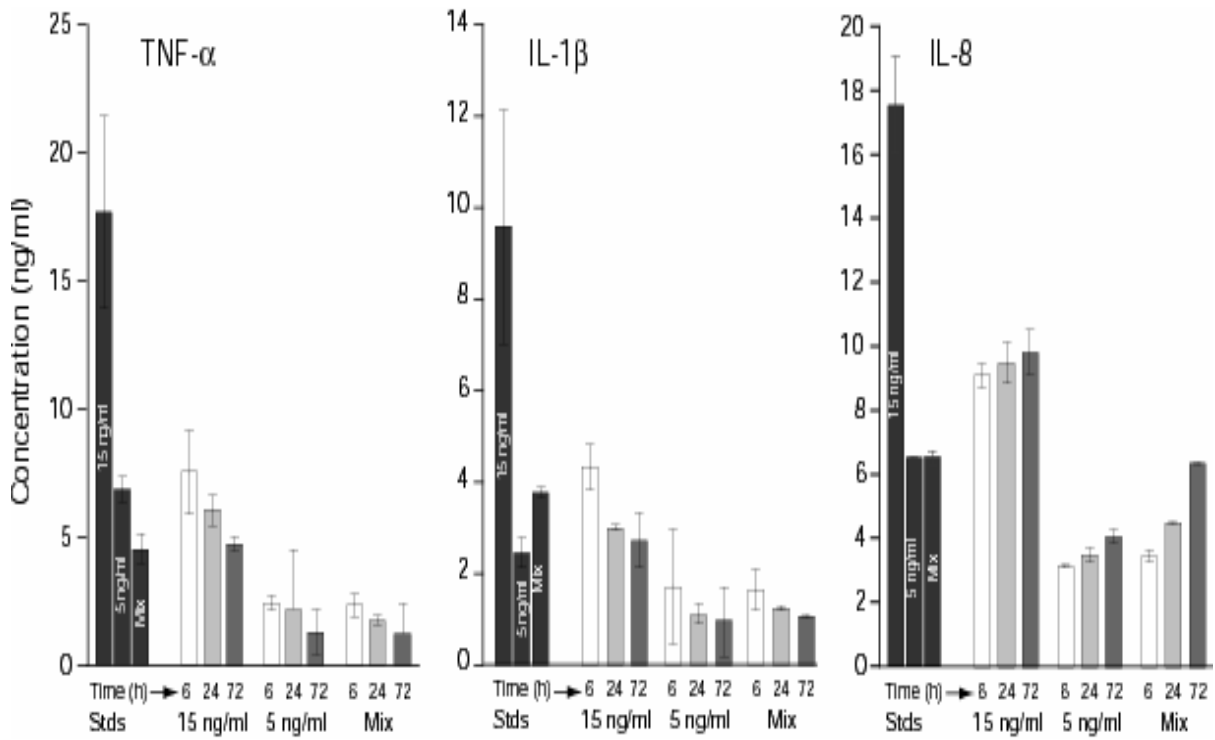


FIG. 3.3 Cytokine/chemokine concentrations in the media during the 72 h treatment. Cytokine levels dropped by approximately 50% after 6 h. TNF- α and IL-1 β levels remained relatively constant (slight decrease) up to the 72hr timepoint. Note that the concentration of IL-8 appeared to increase from 6-72 h, especially when used in combination with TNF- α and IL-1 β (Mix). Both are known activators of IL-8 production. Stds: prepared by direct addition of cytokines (in PBS) to media.

Effects of cytokines on activated signal transduction cascades

The HEK293 multicellular aggregate system under long term arrest and recovery activated a novel internal signaling pathway which enabled these cells to survive (Chapter 2). Evidence was provided that this intracellular cascade was activated due to the combination of endogenous cytokines and chemokines signaling within the aggregate (TNF- α , IL-1 β and IL-8). The survival pathway involved the sustained co-activation of NF- κ B and JNK in the presence of upregulated Gadd45 β levels, leading to activation of AP-1 transcription factors (c-Jun and ATF3). Chemical inhibition of either NF- κ B or JNK signaling diminished AP-1 activation and cytokine production within these aggregates resulting in cell death. In order to test the dependency of these pathways on TNF- α , IL-1 β and IL-8, Western blots were performed to establish the operational signaling pathways of HEK monolayer cells in the presence or absence of cytokine treatment (Fig. 3.4).

Individual cytokine treatments did not activate or upregulate the complete operational stress response pathway observed within multicellular aggregates (Fig. 3.4A and C). For example, the recovery of HEK293 aggregates to monolayers involved JNK and c-jun activation (phosphorylation) as well as an increase in ATF3. IL-1 β treatment, which resulted in the highest degree of cellular stress (Fig. 3.2) did not activate/upregulate JNK or downstream c-jun. Each individual cytokine treatment provided different response patterns, while only the combination gave the overall “spheroid” response at the 6 h timepoint. These results demonstrate that individual cytokines provide signaling responses that differ from combined treatments and suggest

strongly that understanding cell survival in culture will require an understanding of autocrine cytokine profiles.

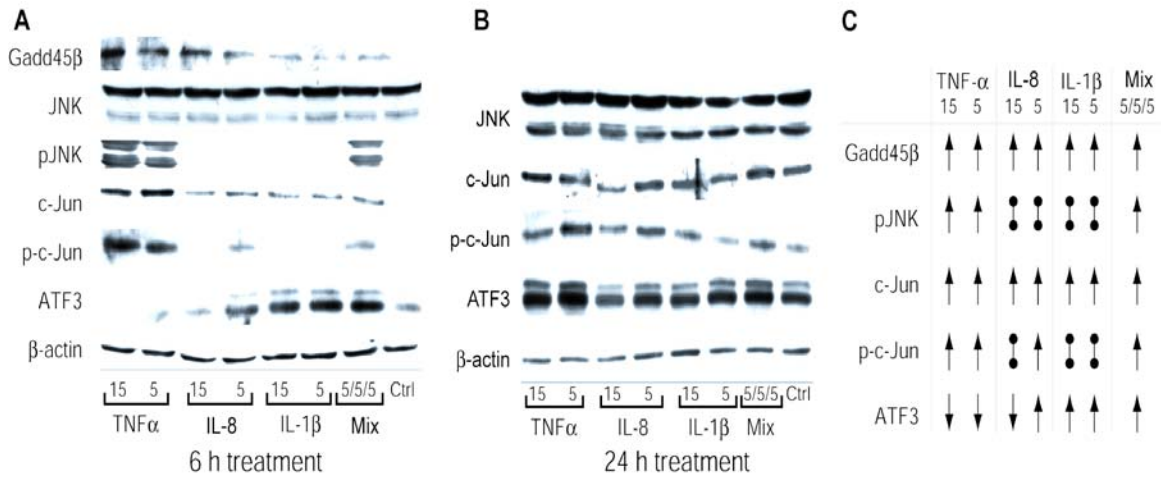


FIG. 3.4 Differential activation of intracellular signaling pathways due to TNF- α , IL-8 and IL-1 β . Previously identified members of a novel activated signal transduction cascade within multicellular aggregates [14] were probed for activation and upregulation due to cytokine treatments. (A) Western blots of HEK293 monolayer cell lysates a 6 h treatment with TNF- α , IL-8 and IL-1 β (15 or 5ng/ml) or in combination (5ng/ml each). (B) Western blots at 24 h timepoint. Gadd45 β and pJNK could not be detected at this timepoint (data not shown). For the 72 h western blots see Supplemental Fig. 3.S3. (C) Schematic for the activated pathways at 6hrs due to individual and combinational cytokine/chemokine treatments. Arrows indicate response direction, closed circles indicate no response. Only the combined treatment provided the spheroid signal response.

Stress-activated proteins identified by mass spectrometry

Cell lysates from the 6 h time point were separated by SDS-PAGE (Coomassie stained) in an effort to identify specific proteins that may be linked to the signal response. Visual observation identified several bands that differed in intensity across the sample treatments (Table 3.1, See Supplemental Fig. 3.S3 for gel images) and samples were submitted to mass spectrometric analyses. The high molecular weight band (120 kDa) was most intense in the IL-1 β treated sample and was found to contain PARP1, a protein associated with DNA repair, apoptosis and chromatin remodeling (Kim *et al.*, 2005). The lowest molecular weight band contained transgelin-2 that has been linked to chronic inflammation-induced ulcerative colitis model systems and has been suggested as a diagnostic marker for hepatocellular carcinomas (Yeo *et al.*, 2006; Shi *et al.*, 2005). Other proteins identified include those involved with stress responses (HSP74, ENPL), nuclear export and nucleolar function (CRM1/exportin, NUCL), and cell reorganization (ACTN4). Quantification of protein levels was not obtained within each sample. However, this dataset provides a starting point for linking cytokines to proteins and their combined roles in cell survival.

Table 3.1 Proteins identified from 1D SDS-PAGE gels by LC-tandem mass spectrometry.

Band	kDa	TNF- α	IL-8	IL-1 β	Mix	Control	Proteins identified
I	120	++	++	+++	+	+	ACLY, NUCL, PARP1, UBE1
II	105	+	-	-	+++	+++	HSP74, NUCL, SND1, UBE1, XPO1
III	104	-	-	+++	+	-	ACTN4, HSP74
IV	95	++	++	+++	+	+	ENPL (GRP94), C1TC
V	55	+++	+	-	++	-	2AAA, HNRPK, HSP71, STIP1, TCPZ
VI	22	++	+++	+++	++	++	TAGL2, PRDX2, PSMB5, RS5, RS7, RS9

Molecular weights are approximate. Symbols (+/-) indicate relative band intensity from the 15 ng/ml treated samples (TNF- α , IL-8, IL-1 β), the combination sample (Mix, 5 ng/ml each) and the Control. Key: (-) band not visible; (+) faint; (++) darker; (+++) darkest band in all five lanes. All proteins listed as identified had MASCOT scores of at least 200 and selected peptides were confirmed manually for all proteins listed. See supplemental (Fig. 3.S3) for gel images, UniProt protein identifications, and tabulated MASCOT scores for proteins.

Concluding Remarks

Evidence for the synergistic actions *in vivo* of multiple cytokines (TNF- α and IL-1 β) in mediating cellular responses was described as early as 1987 (Movat *et al.*, 1987; Henderson and Pettipher, 1989). It is well documented that cytokines within tissues exist and signal in combinatorial fashion (Gouwy *et al.*, 2005) that act together in synergistic and antagonistic combinations (Janes *et al.*, 2006). Previous work described in Chapter 2 determined that the survival strategies inherent in multicellular aggregates require an endogenous autocrine signaling system employing TNF- α , IL-1 β and IL-8. In this study, direct evidence is provided that activation of this pathway within HEK293 cells is dependent upon the synergistic effects of these cytokines. HEK293 adherent monolayer

cells provided the spheroid response only when TNF- α , IL-1 β and IL-8 were present in combination. Determining mechanisms of cell survival will require a better understanding of the combinatorial autocrine component.

References

Chen G, Goedell DV. 2002. TNF-R1 signaling: a beautiful pathway. *Science* 31:1634-1635.

Brennan FM, Chantry D, Jackson A, Maini R, Feldmann M. 1989. Inhibitory effect of TNF alpha antibodies on synovial cell interleukin-1 production in rheumatoid arthritis. *Lancet* 2:244-247.

Ghivizzani SC, Kang R, Georgescu HI, Lechman ER, Jaffurs D, Engle JM, Watkins SC, Tindal MH, Suchanek MK, McKenzie LR, Evans CH, Robbins PD. 1997. Constitutive intra-articular expression of human IL-1beta following gene transfer to rabbit synovium produces all major pathologies of human rheumatoid arthritis. *J Immunol* 159:3604-3612.

Gouwy M, Struyf S, Proost, P, Van Damme J. 2005. Synergy in cytokine and chemokine networks amplifies the inflammatory response. *Cytokine Growth Factor Rev* 16:561-580.

Henderson B, Pettipher ER. 1989. Arthritogenic actions of recombinant IL-1 and tumor necrosis factor α in the rabbit: evidence for synergistic interactions between cytokines in vivo. *Clin Exp Immunol* 75:306-310.

Hosaka K, Ryu J, Saitoh S, Ishii T, Kuroda K, Shimizu K. 2005. The combined effects of anti-TNF α antibody and IL-1 receptor antagonist in human rheumatoid arthritis synovial membrane. *Cytokine* 32:263-269.

Ichijo H. 1999. From receptors to stress-activated MAP kinases. *Oncogene* 18:6087-6093.

Jack GD, Mead EA, Garst JF, Cabrera MC, DeSantis AM, Slaughter SM, Jervis J, Brooks AI, Potts M, Helm RF. 2006. Long term metabolic arrest and recovery of HEK293 spheroids involves NF-kappaB signaling and sustained JNK activation. *J Cell Physiol* 206:526-536.

Janes KA, Gaudet S, Albeck JG, Nielsen UB, Lauffenburger DA, Sorger PK. 2006. The response of human epithelial cells to TNF involves an inducible autocrine cascade. *Cell* **124**: 1225-1239.

Kim MY, Zhang, T, Kraus WL. 2005. Poly(ADP-ribosyl)ation by PARP-1: 'PAR-laying' NAD⁺ into a nuclear signal. *Genes Dev* 19:1951-1967.

Kuldo JM, Westra J, Asgeirsdottir SA, Kok RJ, Oosterhuis K, Rots JG, Schouten JP, Limburg PC, Molema G. 2005. Differential effects of NF- κ B and p38 MAPK inhibitors and combinations thereof on TNF- α and IL-1 β -induced proinflammatory status of endothelial cells in vitro. *Am J Physiol Cell Physiol* 289:C1229-C1239.

Lee MS. 2002. Cytokine synergism in apoptosis: Its role in diabetes and cancer. *J Biochem Mol Biol* 35:54-60.

Manna SK, Ramesh GT. 2005. Interleukin-8 induces nuclear transcription factor- κ B through TRAF6-dependent pathway. *J Biol Chem* 280:7010-7021.

Movat HZ, Burrowes CE, Cybulsky MI, Dinarello CA. 1987. Acute inflammation and a Schwartzman-like reaction induced by interleukin-1 and tumor necrosis factor. Synergistic action of the cytokines in the induction of inflammation and microvascular injury. *Am J Pathol* 129:463-476.

Rathanaswami P, Hachicha M, Wong WL, Schall TJ, McColl SR. 1993. Synergistic effect of interleukin-1 beta and tumor necrosis factor alpha on interleukin-8 gene expression in synovial fibroblasts. Evidence that interleukin-8 is the major neutrophil-activating chemokine released in response to monokine activation. *Arthritis Rheum* 36:1295-1304.

Shi YY, Wang HC, Yin YH, Sun WS, Li Y, Zhang CQ, Wang Y, Wang S, Chen WF. 2005. Identification and analysis of tumour-associated antigens in hepatocellular carcinoma. *Br J Cancer* 92:929-934.

Ulfgren AK, Anderson U, Engstrom M, Klareskog L, Maini RN, Taylor PC. 2000. Systemic anti-tumor necrosis factor alpha therapy in rheumatoid arthritis down-regulates synovial tumor necrosis factor alpha synthesis. *Arthritis Rheum* 43:2391-2396.

Williams RO, Marinova-Mutafchieva L, Feldmann M. 2000. Evaluation of TNF-alpha and IL-1 blockade in collagen-induced arthritis and comparison with combined anti-TNF-alpha/anti-CD4 therapy. *J Immunol* 165:7240-7245.

Yeo M, Kim DK, Park HJ, Oh TY, Kim JH, Cho SW, Paik YK, Hahm KB. 2006. Loss of transgelin in repeated bouts of ulcerative colitis-induced colon carcinogenesis. *Proteomics* 6:1158-1165.

Zhang Y, Chen F. 2004. Reactive oxygen species (ROS), Troublemakers between Nuclear Factor- κ B (NF- κ B) and c-Jun NH₂-terminal kinase (JNK). *Cancer Res* 64:1902-1905.

Chapter 3

Supplemental Information

Contents

Enhanced description of methodologies. Includes processing of light micrographs and details on the mass spectrometry-related work.

FIG. 3.S1 Light micrographs of HEK293 cells exposed to TNF- α , IL-8, and IL-1 β separately (5, 15 ng/ml) and in combination (Mix, 5 ng/ml each of TNF- α , IL-8 and IL-1 β).

FIG. 3.S2 Differential activation of intracellular signaling pathways due to TNF- α , IL-8 and IL-1 β showing all three timepoints (Fig. 3.4 in main text contains the 6 and 24 h images).

FIG. 3.S3 Coomassie-stained SDS-PAGE gels used for protein identification and the proteins identified.

Enhanced Methodologies

Processing and digital manipulation of light micrographs

Images shown in Fig. 3.1 (main text) and Fig. 3.S1 (Supplemental Data) were initially obtained on slide film using a light microscope (100X magnification). The slides were scanned and converted to grayscale colors in Adobe Illustrator. The resulting images were reduced in size and the colors were inverted to more clearly visualize the lamellipodia.

Protein identification methodology

Four 1-mm³ spots were excised manually from each band. Samples were destained, reduced with dithiothreitol, and alkylated with iodoacetamide. An in-gel tryptic digest was performed overnight at 37°C, with the digests halted by the addition of acetic acid, followed by gentle vortexing for 15 minutes. Samples were analyzed utilizing an Ultimate capillary HPLC system (LC Packings) interfaced with a ThermoFinnigan LCQ DecaXP ion trap mass spectrometer operating in the NSI mode. A pressure bomb was used to load 1 μ L of sample onto a pulled tip 75 μ m (ID) capillary column packed with 4 cm of Synergi 4 μ Hydro-RP (Phenomenex). Peptides were eluted over a linear gradient of 5% to 95% mobile phase B over 30 minutes at a flow rate of 100 nl/min where mobile phase A was 0.5% acetic acid and mobile phase B was MeCN with 0.5% acetic acid. The

most abundant peptides were sampled twice before exclusion; collision-induced LC/MS/MS spectra were processed by Xcalibur version 1.2 software.

MASCOT software (Release 2.0; Matrix Science, Boston MA) was employed to analyze the tandem mass spectrometry peak lists. MASCOT search parameters included: tryptic digest with a maximum of 1 missed cleavage, peptide mass tolerance of 2, fragment mass tolerance of 0.8, and carbamidomethyl fixed modification for cysteine. Protein identifications were considered significant and correct with a probability Mowse score ≥ 200 where an individual ion score ≥ 37 had a $p < 0.05$ for random matches. Selected MS² spectra were also evaluated manually for each protein listed in Table 3.2 (main text) and Figure 3.S2 (Supplemental) to confirm their presence. Proteins are listed in the Supplemental by their MASCOT score for one run. Selected duplicate runs showed similar results. While a higher score can infer more of a particular protein present, this interpretation should be used with caution as the score will depend on many factors including the complexity of the sample. Nonetheless, in several cases, proteins from the same band were identified in one treatment but not in others.

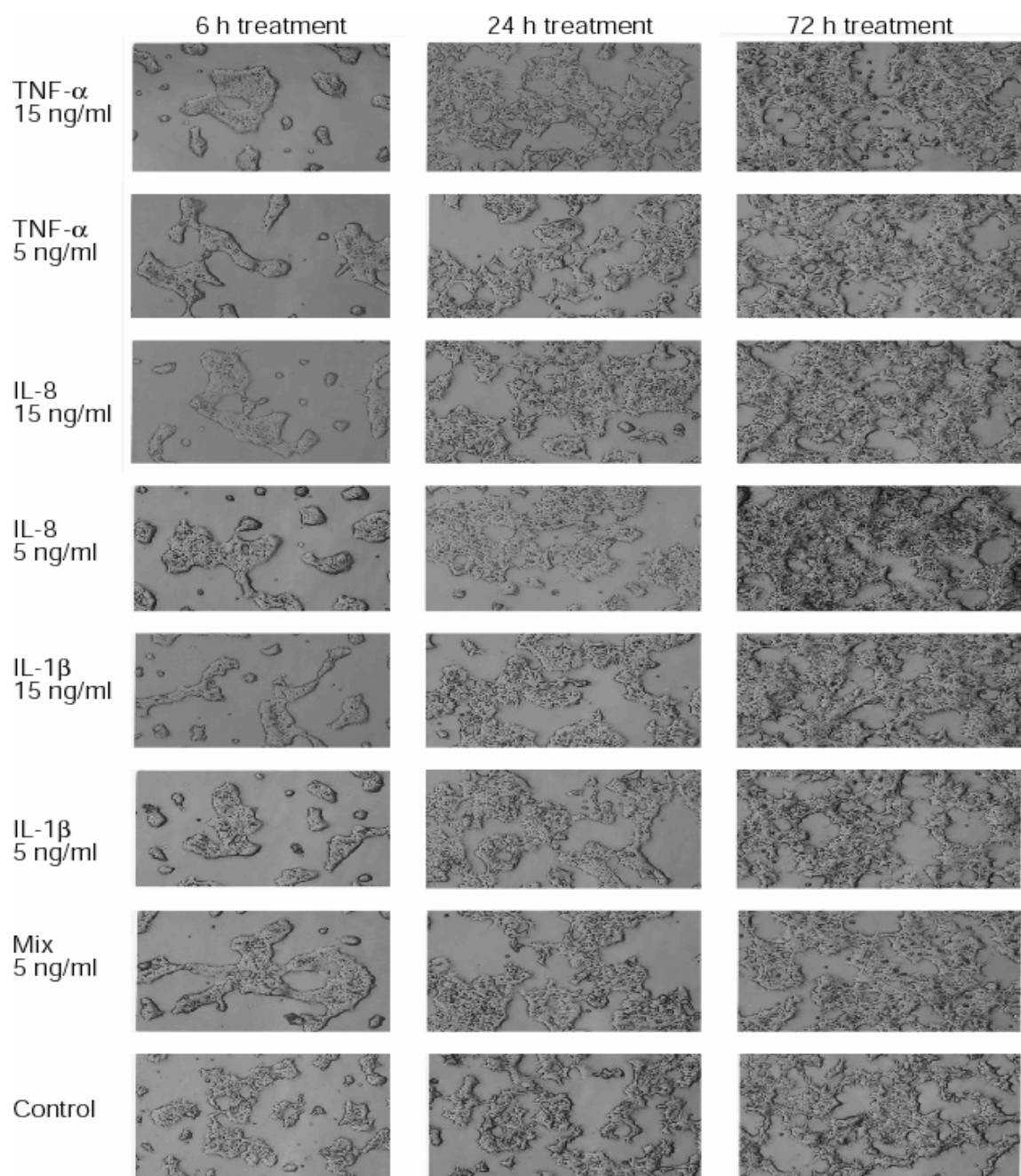


FIG. 3.S1 Light micrographs of HEK293 cells exposed to TNF-a, IL-8, and IL-1b separately (5, 15 ng/ml) and in combination (Mix, 5 ng/ml each of TNF-a, IL-8 and IL-1b).

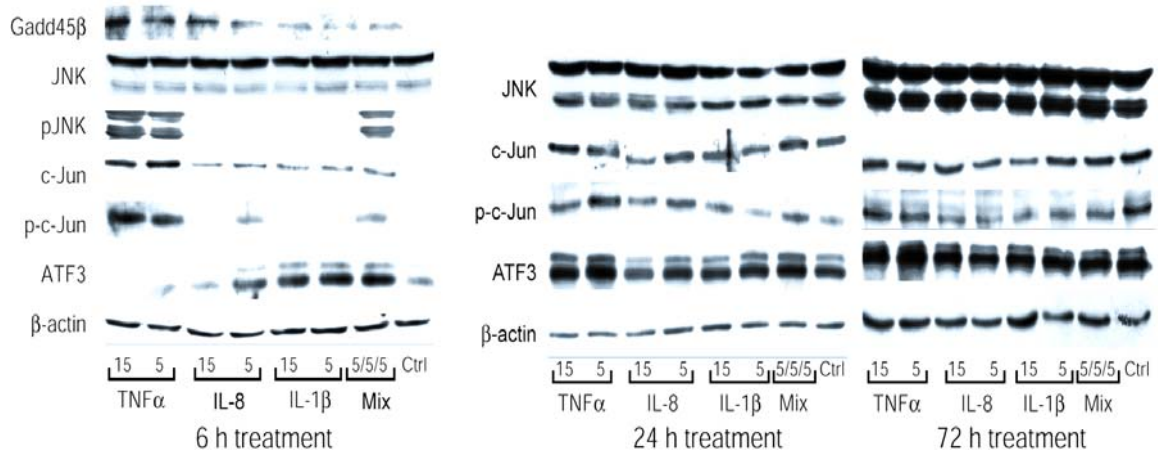
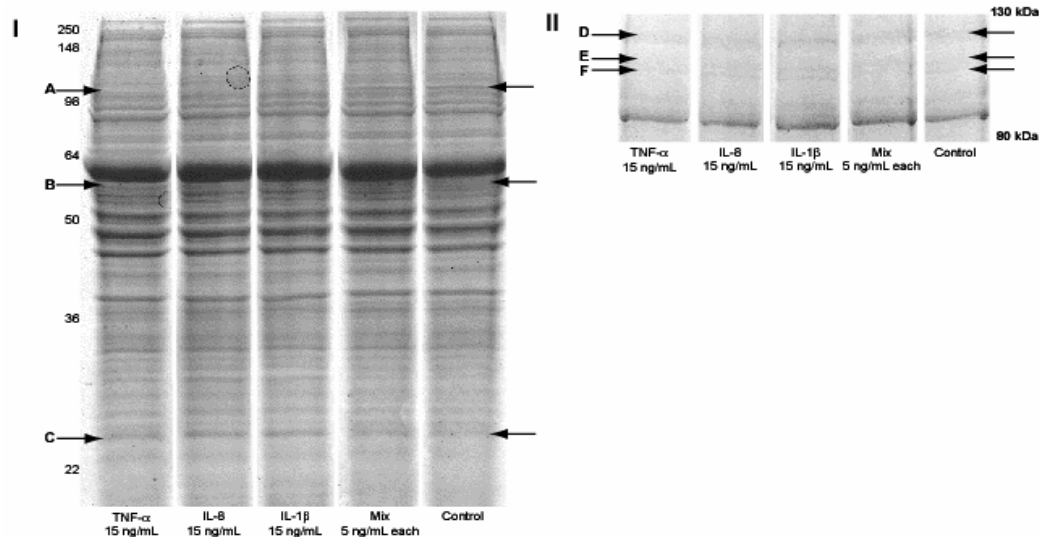


FIG. 3.S2 Differential activation of intracellular signaling pathways due to TNF- α , IL-8 and IL-1 β showing all three timepoints (Fig. 3.4 in main text contains the 6 and 24 h images).



Protein	Band*	MASCOT SCORES					UniProtKB/ Swiss-Prot	Protein Information
		TNF- α	IL-8	IL-1 β	Mix	Control		
ACLY	D (I)	441	536	292	464	150	P53396	ATP-citrate lyase
NUCL	D (I)	205	244	302	382	287	P19338	Nucleolin (Protein C23)
PARP1	D (I)	61	181	268	327	505	P09874	Poly [ADP-ribose] polymerase 1
UBE1	D (I)	287	170	116	137	nd	P22314	Ubiquitin-activating enzyme E1
HSP74	A (II)	458	723	241	680	793	P34932	Heat shock 70 kDa protein 4
NUCL	A (II)	783	488	582	776	724	P19338	Nucleolin (Protein C23)
SND1	A (II)	593	450	229	385	421	Q7KZF4	EBNA2 coactivator p100
UBE1	A (II)	906	770	1057	605	737	P22314	Ubiquitin-activating enzyme E1
XPO1	A (II)	407	316	173	373	291	O14980	Exportin-1
ACTN4	E (III)	188	311	157	160	175	O43707	Alpha-actinin-4
HSP74	E (III)	196	299	208	389	230	P34932	Heat shock 70 kDa protein 4
ENPL	F (IV)	533	186	187	316	657	P14625	Endoplasmic precursor (GRP94)
C1TC	F (IV)	331	226	155	373	338	P11586	C-1-tetrahydrofolate synthase
2AAA	B (V)	72	203	nd	168	nd	P30153	Ser/thr-protein phosphatase 2A 65 kDa regulatory subunit A
HNRPK	B (V)	298	311	207	180	94	P61978	Heterogeneous nuclear ribonucleoprotein K
HSP71	B (V)	317	129	48	249	210	P08107	Heat shock 70 kDa protein 1
STIP1	B (V)	232	114	49	221	126	P31948	Stress-induced phosphoprotein 1
TCPZ	B (V)	nd	nd	nd	365	156	P40227	T-complex protein 1 subunit zeta
TAGL2	C (VI)	282	454	408	525	355	P37802	Trangelin-2
PRDX2	C (VI)	247	365	239	195	235	P32119	Peroxiredoxin 2
PSB5	C (VI)	180	428	187	nd	115	P28074	Proteasome subunit beta type
RS5	C (VI)	300	291	183	203	317	P28074	40S ribosomal protein S5
RS7	C (VI)	227	373	278	360	457	P62081	40S ribosomal protein S7
RS9	C (VI)	207	318	159	343	376	P46781	40S ribosomal protein S9

*Roman numeral in parentheses correspond to Sample ID column in Table 2 (main text).

FIG. 3.S3 Coomassie-stained SDS-PAGE gels used for protein identification and the proteins identified. Two separate gels were run. I, A 12.5% gel run for full separation of the crude lysate. II, A 12.5% gel run for a longer period to help resolve bands in the 80-130 kDa region. Bands excised for analysis are labelled A-F. Protein identifications are listed in the Table below by band molecular weight so as to correspond directly to the sample listings found in Table 3.1.

Chapter 4

Activated stress response pathways within multicellular aggregates are transformation state dependent and utilize autocrine components

Abstract

Multicellular aggregates (spheroids) of primary human foreskin fibroblasts (HFF-2) and a glioblastoma cell line (T98G) entered and exited from long term (2 week) metabolic arrest utilizing an autocrine response. Cytokine production (specifically IFN- γ) activated a Gadd45 α /p38 pathway that led to increased AP-1 (c-jun and ATF3) transcription factor levels, augmenting cytokine production in a cyclical fashion. Whereas HFF-2 aggregates were capable of surviving long term arrest and recovery independent of JNK activation during NF- κ B inhibition, T98G aggregates were not. Such endogenous processes are not easily observed with adherent monolayer cell culturing systems, strongly suggesting that more emphasis needs to be placed on determining the operational signal transduction cascades within multicellular aggregates. Extracellular inputs such as spheroid formation, arrest, and regrowth as monolayers invoke intracellular signaling responses converging at the AP-1 transcription factor level. Variations in responses are both cell type and transformation state-dependent yet all cell lines studied maintained a cyclical cytokine component. The data are discussed in relation to contact inhibition, wounding response, and avascular tumor growth mechanisms.

Introduction

Increased understanding of how cells respond to stresses will derive from the application of systems-based models (Oda *et al.*, 2005; Janes and Lauffenburger 2006). Biomedical applications will result from these efforts when the model systems chosen reflect *in vivo* biology as closely as possible. Multicellular aggregates (also referred to as spheroids; Bates *et al.*, 2000) provide an *in vitro* model system which, by virtue of the direct cell-cell communication and contact, allow for more physiologically-relevant cellular responses (Schmeichel and Bissell, 2003). External stresses imposed on such systems can be monitored at endogenous protein and cytokine levels, often in multiplex fashion, providing responses based upon cytokine profiles, not individual cytokines. As the cells are in direct contact with one another, signaling to neighboring cells provides an autocrine-responsive environment with built-in feedback; a situation that cannot be easily obtained with adherent monolayer culturing techniques.

When adherent cells are grown on agarose surfaces, free-floating multicellular aggregates form that exhibit reduced metabolic activity (Bates *et al.*, 2000). This phenomenon was applied to the storage of human HEK293 cells under media-free, oxygen-limited conditions at room temperature for extended periods of time (Chapter 2). While the purpose of this work was to provide biomedical reagents (*ie.*, human cells) with robust storage characteristics, the protocols that were developed provide conditions similar to those of an avascular tumor. Spheroids, like avascular tumors, have restricted supplies of critical nutrients such as oxygen and glucose, and both spheroids and tumors respond to this stress through induced alterations in physiology and metabolism (Kunz-Schughart *et al.*, 1998). Nearly 20 years ago it was proposed that these aggregates may

serve as an *in vitro* model of tumor microregions at an early avascular stage of growth, and it was further suggested that the molecular basis of the biological processes found in these aggregates needs to be investigated more intensively (Mueller-Klieser, 1987). While mathematical models were employed to simulate avascular growth (Jiang *et al.*, 2005), signaling within and between cells grown in multicellular aggregates remains to be fully evaluated experimentally.

Multicellular aggregation and disassembly processes are similar to the wounding response. When spheroids are removed from agarose and plated using standard adherent monolayer culture conditions, adherence and subsequent migration away from the aggregate occurs, similar to tissue repair/remodeling processes. Wound healing is a complex process involving inflammation and cell-cell communication through cytokine networks that ultimately coordinate proliferation and migration (Takami *et al.*, 2005). Typical tissue culture model systems for investigating wounding response mechanisms utilize either cell spreading measurements (Dobrevá *et al.*, 2005) or plate scraping followed by characterization of the response (Harper *et al.*, 2005). The nature of 3-dimensional cell cultures promotes more direct cytokine signaling between neighboring cells (cell to cell contact) and may represent a valid model for *in vivo*-like wounding responses.

HEK293 cells are an immortalized cell line and cannot activate classical arrest pathways involving p53 and pRB due to the incorporation of the human adenovirus type 5 (Graham *et al.*, 1977). When submitted to long term arrest as spheroids, it was demonstrated that HEK293 cells invoked a novel survival signaling pathway where endogenous cytokine production (TNF- α , IL-1 β , and IL-8) led to the combined and

sustained JNK and NF- κ B activation (days) (Chapter 2). A similar response was observed when adherent HEK293 monolayers were treated with TNF- α , IL-8 and IL-1 β in combination (Chapter 3). These data were not congruent with those reported by others (De Smaele *et al.*, 2001; Papa *et al.*, 2004), where JNK activation in mouse embryonic fibroblasts (MEFs) led to cell death. It was questioned, therefore, if other human cell lines, such as primary non-transformed fibroblasts and cancer cells, invoked different survival pathways when exposed to the same arrest and recovery protocols utilized for the HEK293 study. Pathways that were activated in the primary and carcinoma cell lines were determined and compared to those of HEK293 cells at the levels of transcription, translation, and post-translation. These results are reported herein and highlight the complexities of signaling networks, the role of endogenous cytokines, effect of cell line and transformation state, and the efficacy of spheroids for understanding how external factors influence cell community behavior.

Materials and Methods

Cell Culture

HFF-2 cells were cultured in DMEM supplemented with 15% (v/v) fetal bovine serum and 5% CO₂ humidified air at 37 °C. T98G cells were cultured in EMEM with 10% FBS, 5% non-essential amino acids and 5% CO₂ humidified air at 37 °C. Monolayers were grown in T-185 flasks to 60% confluency then split into T-185 flasks coated with a 1% (w/v) agarose mix in a 2:1 media/water ratio. Cells were suspended in 30 ml of supplemented media and grown for 4 days in order to form multicellular spheroids (Jack et al, 2006). The suspension was removed from the flasks and centrifuged (1500 x g, 2 min) and the media removed. The pellet was returned to the agarose surface

and the flask was placed in vacuum bags (Dri-shield 2000 moisture barrier bag from Surmount Inc., USA; Cat. # 70068), which were sealed immediately under vacuum (Deni® Magic Vac™, Champion model; Keystone Manufacturing, USA). Vacuum-sealed flasks were stored for 2 weeks (in the dark) at room temperature.

Recovery was initiated by removing the flask from the bag and resuspending the spheroids in supplemented media and placing the flasks in a 5% CO₂/humidified air incubator maintained at 37 °C. Timepoints for transcriptional analysis were monolayer (control), 4 day growth spheroids, 2 week stored spheroids and 7 day growth back to monolayers. Time points for cytokine and protein analyses were: 0 h storage (spheroids prior to sealing in bags), 2 week storage (0 hr recovery), 6 h, 24 h, and 72 h recovery (as spheroids). For the NF-κB inactivation studies, the same conditions were repeated except that the media and agarose were supplemented with 100 nM of the NF-κB activation inhibitor 6-amino-4-(phenoxyphenylethylamino)quinazoline (Tobe *et al.*, 2003; Calbiochem).

FACS Analyses

Cells were harvested and washed twice with 10 ml of PBS, with an intermediate centrifugation step (1500 x g; 2 min). The CycleTEST™ PLUS DNA Reagent Kit (Becton-Dickinson) was used according to the directions from the manufacturer for cell suspensions. Cells were analyzed using a Beckman Coulter flow cytometer (EPICS-XL). Software used for data analysis was EPICS version 1.5.

Transcriptional Profiling and Quantitative Real Time PCR

All experiments were biological triplicates and were performed as described previously (Jack et al, 2006). Cells were harvested and total RNA was extracted using the RNeasy™ kit and protocols (Qiagen). Microarray protocols, equipment and data were fully MIAME compliant and have been deposited at the Gene Expression Omnibus website (Series: GSE4217-4218; Samples: GSM96262-96285), and an expanded version of the protocols can be found in the Supplementary Data. RNA quality was assessed by electrophoresis using the Agilent Bioanalyzer 2100 and spectrophotometric analysis prior to cDNA synthesis. Samples were subjected to gene expression analysis via Affymetrix Human 133_2.0Plus high-density oligonucleotide array which currently queries 46,000 human probe sets (each gene on the array is represented by 11 pairs of 25mer oligonucleotides that span the coding region for the 46,000 genes and EST's represented). Hybridization, staining and washing of all arrays were performed in the Affymetrix fluidics module as per the manufacturer's protocol. The detection and quantitation of target hybridization is performed with a GeneArray Scanner 3000 set to scan each array twice at a factory set PMT level and resolution. A data set of statistically significant genes was generated using a multi-class F-Test with variance stabilization encompassing 4 sample classes (Iobion Informatics). The false discovery rate (FDR) was corrected for multiple testing using the Benjamini-Hochberg approach to multiple testing. The Q-Value cutoff for the experiment was 0.05 with probe sets with Q-values greater than 0.05 considered insignificant expressors across the experiment. This resulted in a list of probe sets for each cell line that was then reduced further using a (+/-) 10-fold change filter.

Q-PCR employed Taqman chemistry with probes and primers designed using Primer Express v.1.0 (ABI, Foster City CA). Protocols, procedures and primer design were done as described previously (Chapter 2).

Western Blotting

Cells were harvested and washed twice with 10 ml of PBS, with an intermediate centrifugation step (1500 x g; 2 min). Cell pellets were lysed for 20 min at 4 °C on a rotator using a lysis buffer containing 20mM HEPES, 300 mM NaCl, 2 mM EDTA, 2 mM sodium orthovanadate, 0.1% Triton X, 20 mg/ml PMSF and 1:500 dilution of protease inhibitor cocktail for mammalian cell culture (Sigma). Lysates were cleared by centrifugation at 15,000 x g and protein concentration was measured using Coomassie protein assay reagent (Pierce). Cleared lysates were separated on SDS-PAGE Criterion™ gels (BioRad) at equal protein loading levels (30 µg of total protein per lane). Protein transfer to a polyvinylidene difluoride membrane (Hybond-P, Amersham Biosciences) was accomplished using a semidry transfer apparatus and probed with the following primary antibodies: Gadd45 α (sc-792), Gadd45 β (sc-8776), Gadd45 γ (sc-8777), p38 (sc-7972), JNK2 (sc-7345), c-Jun (sc-1694), p-c-Jun(sc-16312-R), ATF3 (sc-188), actin (sc-8432) (Santa Cruz Biotechnology); p-JNK (4671S), p-MEK4 (44-474) and p-p38 (9215L) (Cell Signaling Technology). Following application of secondary horseradish peroxidase-conjugated secondary antibody and subsequent washes, signal was generated using ECL™ (Amersham Biosciences). Signals were detected by autoradiography.

Multiplexed Cytokine Assays

Cytokines were measured using the Bioplex Protein Array system (BioRad), according to the instructions of the manufacturer. Cytokines measured included interleukin-1b (IL-1 β), IL-2, IL-4, IL-5, IL-6, IL-7, CXCL8 (IL-8), IL-10, IL-12 (p40), IL-13, IL-17, interferon- γ (IFN- γ), tumor necrosis factor- α (TNF- α), granulocyte colony stimulating factor (G-CSF), granulocytemacrophage colony stimulating factor (GM-CSF), CCL2 (monocyte chemoattractant protein-1, MCP-1, MCAF), CCL4 (macrophage inflammatory protein-1b, MIP-1b), spheroid cell lysates were prepared and ran as described previously (Chapter 2). For each cytokine, eight standards ranged from 2 to 32,000 pg/ml and the minimum detectable dose was <10 pg/ml.

Confocal Microscopy

Confocal microscopy was performed on a Zeiss LSM-510 laser-scanning microscope (Zeiss 10x objective). Cell staining was with the LIVE/DEAD Viability/Cytotoxicity Kit (Molecular Probes). The final concentration of ethidium homodimer was 4 mM and the final concentration of calcein AM was 3 mM. Staining was performed as described previously (Chapter 2).

Results

Primary fibroblast and glioblastoma multicellular aggregates undergo growth arrest and recovery from long term storage

Primary non-transformed cells and spontaneously transformed carcinoma cells were tested for their ability to undergo aggregation, long term arrest as aggregates, and

subsequent recovery as adherent monolayers. A human foreskin fibroblast was chosen as the primary cell line to be tested (HFF-2) and a glioblastoma cell line was used as the carcinoma (T98G). The T98G cell line is a true p53 mutant carcinoma, unlike the p53/pRb-signaling impaired HEK293 cells. Adherent monolayer cells were plated onto agarose and suspended in media for 4 days to allow aggregate formation. Both lines formed viable spheroids (Fig. 4.1A,C), similar to those of HEK293 cells (Chapter 2) and without the necrotic cores that form if the aggregates are submitted to longer growth periods (Ghosh *et al.*, 2005). The fully viable aggregates were collected by centrifugation and placed in either flasks to grow out as adherent monolayers (control, no storage), or returned to the surface of the agarose without liquid media and stored in moisture-sealed bags under partial vacuum for two weeks (Fig. 4.1A, C).

Recovery of the stored cells involved removal from the sealed container and plating under standard monolayer growth conditions. The HFF-2 and T98G cell lines returned to monolayers, and by 72h were proliferating with what appeared to be normal cell growth (Fig. 4.1). HEK293 cells also returned to normal adherent monolayers after the aforementioned storage and recovery process (Chapter 2). Of note is the variability in spheroid structure directly after the two-week storage regime (Fig, 4.1A, C). HFF-2 cells maintained a tight uniform spheroid whereas the T98G cell line tended to disaggregate upon incubation with fresh media, similar to the response of HEK293 cells. Thus cell lines representing three different transformation states, (virally-infected, carcinogenic, and primary) and tissue types (kidney, brain, and skin, respectively), can withstand this long term (2 week) stress as aggregates and return to normal adherent cells.

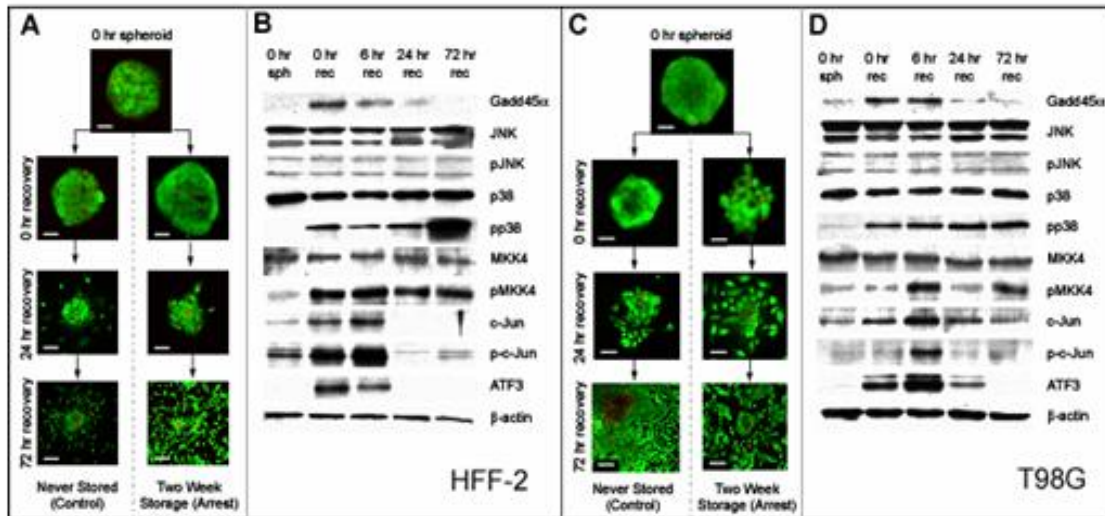


FIG. 4.1 HFF-2 and T98G multicellular aggregates can undergo long term arrest and recovery. **(A)** LIVE/DEAD (Molecular Probes) confocal images of HFF-2 aggregates. The top image is after four days growth to induce spheroid formation. Recovery as adherent monolayers (0, 24, and 72 h recovery) without a two week arrest period is shown on the left (control) and with a two week arrest on the right. Outgrowth as monolayers for both conditions is evident at the 24hr recovery timepoint. Scale bars, 100 μ m. **(B)** Western blots of HFF-2 cell lysates showing activated/upregulated Gadd45 α , MKK4, p38 and AP-1 intracellular signal transduction cascade during recovery timecourse. **(C)** Confocal images of T98G aggregates shown as described in (A). Note that spheroid formation and recovery processes appear very similar to what is observed with the HFF-2 cells. **(D)** Western blots of T98G pathway activation. Note the similarities to that obtained with the HFF-2 cells.

Signal transduction responses of cell lines differ upstream, but converge at the level of transcription factor

HEK293 cells relied upon activation of NF- κ B and Gadd45 β together with the JNK signaling pathway to recover from the long term arrest (Chapter 2). T98G and HFF-2 lines upregulated Gadd45 α that in turn activated MKK4/p38 during storage and recovery (Fig. 4.1B,D), a stress response similar to that described by others using monolayer systems (Bulavin *et al.*, 2003; Hildesheim *et al.*, 2004). Although the initial upstream transduction events for the HEK293 and T98G/HFF-2 lines were different, convergence occurred at the AP-1 transcription factor level. Upregulation of ATF3 and c-jun as well as the phosphorylation/activation of c-jun was observed for all three cell lines (Fig. 4.1B,D), supporting the concept that signaling convergence for the JNK (HEK293) and p38 (T98G and HFF-2) pathways at the transcription factor level (AP-1) leads to viable proliferating monolayers after long term arrest and recovery. This observation is in agreement with numerous reports that activation of several AP-1 transcription factors aid in antiapoptotic/survival responses during stress (Davis *et al.*, 2000; Lamb *et al.*, 2003), and further demonstrates that both c-jun and ATF3 can be activated by p38, independent of JNK kinase signaling (Frigo *et al.*, 2004; Kool *et al.*, 2003; Besirli *et al.*, 2003; Marinissen *et al.*, 1999). Thus, while the upstream signaling events differed between the HEK293 and T98G/HFF2 cell lines, convergence occurred at the transcription factor level, leading to cell survival during and after long term arrest.

Chemical inhibition of the NF- κ B pathway during spheroid arrest reveals that primary fibroblasts can survive independent of NF- κ B signaling

The NF- κ B signaling pathway was central to HEK293 survival during prolonged arrest and recovery as chemical inhibition of NF- κ B signaling led to cell death (Chapter 2). When the same NF- κ B chemical inhibition protocol was applied to the HFF-2 aggregates, the spheroids appeared less uniform in shape after arrest (compare Fig. 4.1A with Fig. 4.2A at 0 hr recovery), but returned to adherent proliferating monolayers. This result suggests strongly that primary fibroblasts are capable of aggregation, long term arrest, and recovery, independent of NF- κ B activation. T98G cells, while showing the same spheroid morphology directly after arrest and recovery (Fig. 4.2C), did not return to adherent monolayers and proliferate, but instead remained enlarged in an apparent non-adherent senescent state, a phenomenon identical to that observed with the NF- κ B inhibited HEK293 cells (Chapter 2). Thus, even though both the primary and glioblastoma cells activated Gadd45 α /p38-dependent pathways, the primary cell line (HFF-2) survived independent of NF- κ B activation, whereas the glioblastoma and immortalized cell lines (T98G and HEK293, respectively) required it. This chemical inhibition study demonstrates that even though initial pathway analyses indicate similar stress responses, probing deeper uncovers differences that are cell type and transformation state dependent.

Upon exposure to the NF- κ B inhibitor, MKK4 and p38 phosphorylation levels in HFF-2 and T98G cells remained relatively constant throughout spheroid formation and recovery (Fig. 4.2B,D), in contrast to what was observed without inhibition. While the JNK phosphorylation levels remained constant and barely detectable without NF- κ B

inhibition, reduction in NF- κ B signaling modulated pJNK levels during the recovery timecourse (Fig. 4.2B,D). Overall, these results with HFF-2 and T98G cells are in agreement with those reported with murine (MEF) cells where NF- κ B negatively regulates JNK signaling (Papa *et al.*, 2004). However, both the upstream Gadd45 α and downstream c-jun/ATF3 responses remained constant in the HFF-2 and T98G cell lines, with and without inhibition. Furthermore, no change in Gadd45 β protein levels (data not shown) or transcription levels (see Supplemental Table 4.S4) were detected with or without NF- κ B inhibition, suggestive of a Gadd45 β -independent JNK inactivation process. The other Gadd45 family members behaved in a similar fashion. While upregulation of *GADD45* α and γ transcripts were observed (Supplemental data, Table 4.S4), no change in Gadd45 γ protein levels could be detected. These results suggest that Gadd45 α can converge on multiple MAP kinase signaling pathways (JNK/p38), ultimately leading to similar downstream events (*ie.*, AP-1 activation).

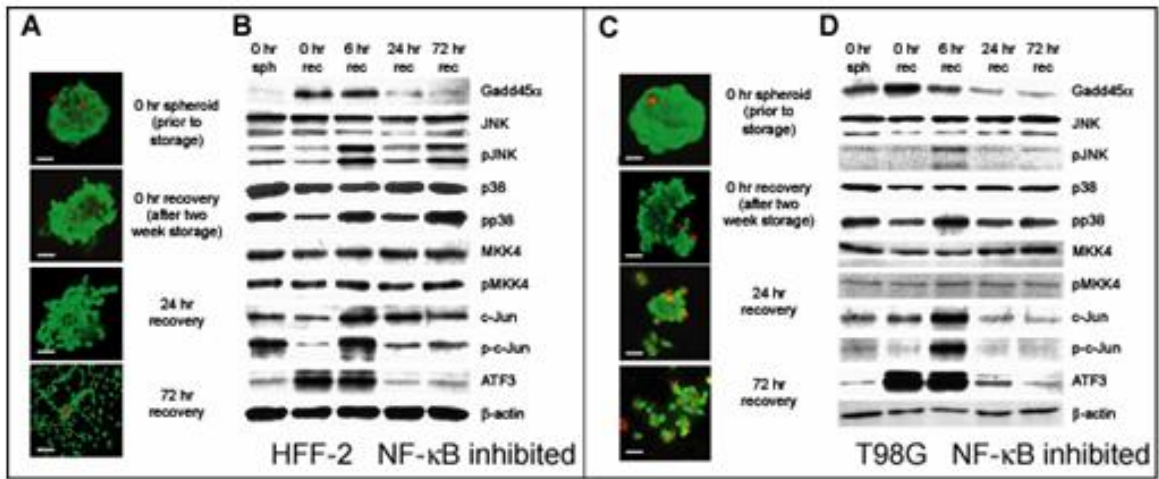


FIG. 4.2 HFF-2 and T98G multicellular aggregates respond differently to NF- κ B inhibition. (A) Confocal images of the HFF-2 arrest and recovery process in the presence of an NF- κ B inhibitor. Scale bars and timepoints are the same as in Figure 4.1. Note that the HFF-2 cells recover to adherent monolayers after storage. (B) Western blot analyses of HFF-2 cell lysates during NF- κ B inhibited timecourse. Note p38 and MKK4 show little change in activation (phosphorylation) status during the timepoints selected. However JNK phosphorylation occurs at the 6hr recovery timepoint. (C) Confocal images of T98G cells under NF- κ B inhibition timecourse. T98G cells displayed a higher degree of death when compared to HFF-2 cells and would not return to proliferating monolayer remaining suspended in media (D) Western blot analyses of T98G cells under NF- κ B inhibition. T98G cells show similar signaling patterns as observed with HFF-2 under these conditions.

Primary fibroblasts are better able to survive long term arrest as aggregates than glioblastoma cells and exhibit differing autocrine responses to arrest and recovery

Fluorescence activated cell sorting (FACS) assays further confirmed that HFF-2 cells maintained their viability throughout the arrest and recovery process, both with and without NF- κ B inhibition (Table 4.1). In addition, the return to adherent monolayers provided a shift from G₀/G₁ to G₂, indicative of an increase in proliferation. The T98G cells exhibited a higher degree of cell death directly after arrest as aggregates, and under NF- κ B-inhibited conditions could not return to proliferating monolayer cells (Fig. 4.2C). These results strongly suggest that even though the T98G glioblastoma cells naturally form avascular tumors, they are less capable of surviving “avascular-like” conditions when compared to the HFF-2 cells. Primary fibroblasts appear to be better able to enter and exit the quiescent aggregated state, and this process is independent of JNK activation during NF- κ B inhibition.

Table 4.1 Viability and cell cycle analysis data for HFF-2 and T98G spheroids during storage and recovery in the presence and absence of NF- κ B chemical inhibition.

Cell Line	Viability (%)	G ₀ /G ₁	S	G ₂ /M
HFF-2				
0hr Spheroid	90.62	79.30	5.60	13.80
0hr Recovery	93.58	75.70	1.70	22.10
6hr Recovery	80.60	65.40	5.60	25.90
24hr Recovery	70.30	68.00	6.90	22.80
72hr Recovery	85.70	62.30	6.60	26.70
HFF-2, NF-κB inhibited				
0hr Spheroid	73.00	86.40	2.20	10.70
0hr Recovery	94.80	89.20	0.50	9.90
6hr Recovery	92.78	88.90	0.50	9.90
24hr Recovery	88.10	84.20	2.40	12.30
72hr Recovery	80.80	69.30	3.70	22.50
T98G untreated				
0hr Spheroid	79.00	92.90	4.70	2.20
0hr Recovery	27.60	87.70	5.50	6.80
6hr Recovery	49.40	93.10	3.10	3.20
24hr Recovery	65.90	91.40	3.30	5.20
72hr Recovery	79.50	79.40	9.80	10.70
T98G, NF-κB inhibited				
0hr Spheroid	87.50	88.00	7.60	4.20
0hr Recovery	31.40	87.30	10.20	2.80
6hr Recovery	42.60	87.60	8.00	4.70
24hr Recovery	35.30	84.10	11.10	4.60
72hr Recovery	56.70	71.30	15.80	10.50

All values based upon FACS analyses (see Methods for details).

As significant cell death occurred during T98G arrest in the NF- κ B-inhibited state, we chose to determine changes in cytokine profiles within the aggregates during arrest and recovery. In order to maintain an environment of intercellular signaling, rather than recovering the spheroids as monolayer cells (Fig. 4.1 and 4.2), arrested cells were released by removing them from storage, adding fresh media, and allowing them to resume growth as spheroids under standard spheroid culture conditions. This same methodology was employed with the HEK293 experiments (Chapter 2). Of the 17 cytokines monitored, IL-8, IL-1 β , IL-6, MCP-1, and IFN- γ showed the greatest responses to spheroid formation, arrest and recovery (Fig. 4.3). HFF-2 cells showed very high levels of IL-8, even before arrest, indicating that spheroid formation (cell-cell contact) affects the production of this cytokine. Inhibition of NF- κ B signaling dramatically increased the production of IL-8, IL-1 β , IL-6 and MCP-1 throughout the course of the recovery in the HFF-2 cells, the complete opposite of what was observed in the HEK293 cells (Chapter 2). The upregulation of these cytokines may be due to the increase in JNK activation, which is a known activator (Xiao and Chodosh, 2005; Henley *et al.*, 2004; de Haij *et al.*, 2005). The glioblastoma (T98G) cells did not have high levels of IL-8 and IL-6 before arrest; increases in these cytokines occurred during storage. In contrast to the HFF-2 cells, T98G cells exhibited marginal changes in IL-6, IL-1 β and MCP-1 levels in response to NF- κ B inhibition.

IFN- γ production increased during storage in both the HFF-2 and T98G aggregates and exhibited the highest levels at the 0 hr recovery timepoint for both cell lines (Fig. 4.3). This cytokine is regulated by both NF- κ B and p38 through activation of AP-1 family members ATF3 and Jun (Corn *et al.*, 2003; Dong *et al.*, 2002). Its level decreased

dramatically as a result of NF- κ B inhibition, presumably through its dependency upon NF- κ B and a change in signal flux through the p38 pathway (Dong *et al.*, 2002; Corn *et al.*, 2003; Zhang and Kaplan, 2000). In contrast, the IFN- γ response in the HEK293 aggregates during storage and recovery, with or without NF- κ B inhibition, was marginal, potentially due to the lack of p38 signaling. Interestingly, IFN- γ is known to activate itself (Vila-del Sol and Fresno, 2005; Brysk *et al.*, 1995; Lee *et al.*, 2003) suggesting a cyclical pathway similar to that described previously for IL-8, TNF- α , and IL-1 β in the HEK293 cells (Chapter 2).

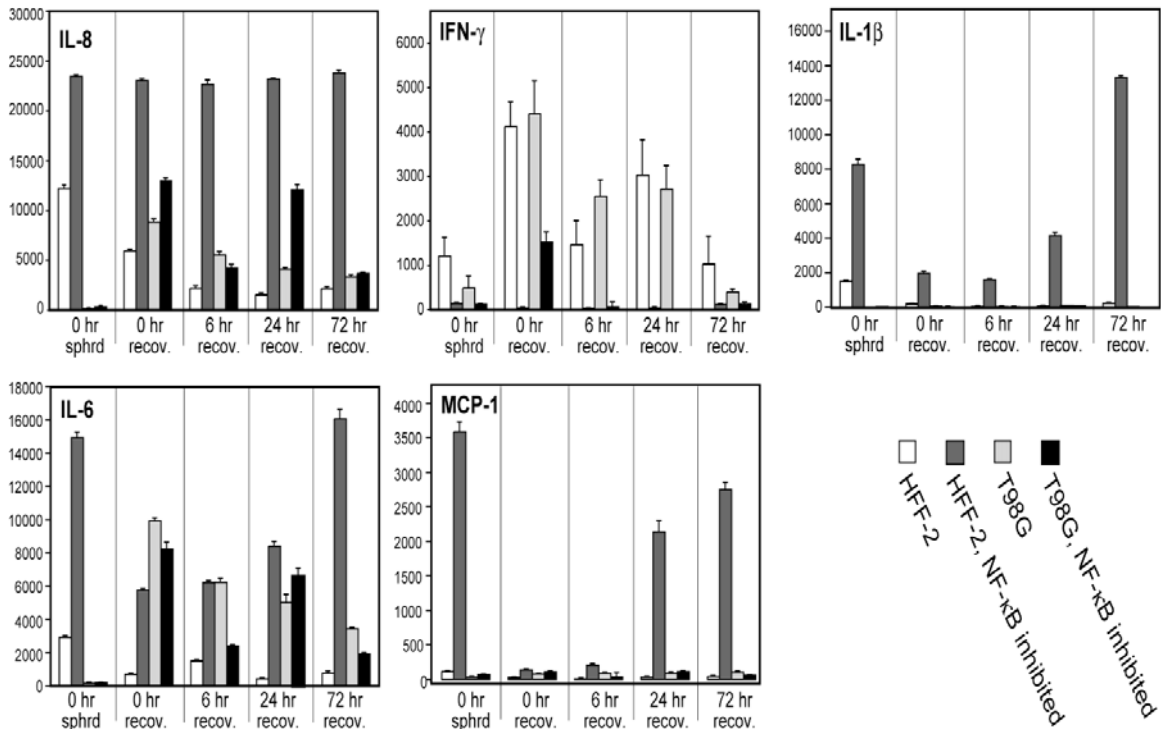


FIG. 4.3 Cytokine profiles for HFF-2 and T98G aggregates with and without NF- κ B inhibition are different. Analyses were performed prior to arrest (0 hr sphrd), after 2 week arrest (0 hr recov.), and during the recovery process (6, 24, 72 hr recov.). Note that in these experiments aggregates were recovered by removing them from storage and adding fresh media. Data are presented in counts.

Gene expression analyses provide evidence that primary fibroblast aggregates quickly return to a monolayer state whereas glioblastoma aggregates do not

T98G and HFF-2 arrest and recovery processes were evaluated for changes at the transcript level using their corresponding monolayer cells as controls. There were 67 and 50 genes, respectively, in the HFF-2 and T98G datasets that exhibited at least a 10-fold change in expression during the course of arrest and recovery (Supplemental Data Chapter 4, Tables 4.S1 and 4.S2). Of these genes, a subset of 11 were common to both cell lines, and the expression levels for these are shown in Fig. 4.4. While the mode of regulation (*ie.*, increase or decrease) were the same between the two cell lines, the timing of the responses were clearly different. The primary fibroblasts underwent significant gene expression changes during spheroid formation and returned to their initial monolayer state after the two week arrest. In contrast, the glioblastoma cells exhibited major changes in gene expression during the recovery process and never returned to the monolayer expression levels during the duration of the recovery phase (7 days growth under monolayer conditions). This trend was not limited to the 11 genes shown in Fig. 4.4; all genes above the 10-fold cutoff responded in a similar fashion (Supplemental Data Chapter 4, Figures 4.S1 and 4.S2).

Major differences were also found between the cell lines with regards to the putative cellular location of the proteins encoded by the highly regulated genes. Of the genes with significant fold changes (\pm 10-fold) for which location information was available, the primary fibroblasts dataset was significantly enriched in genes encoding extracellular (32%) and membrane-associated (26%) proteins. Several of the extracellular genes identified encode for cytokines and chemokines including *IL-8*, *IL-24*,

IL-1 β , *CCL8*, *CXCL1*, 2, 3, and 6. The glioblastoma dataset, in comparison, had only 17% extracellular and 13% membrane-associated genes identified. Taken together, the transcriptional profiling results support the concept that primary fibroblasts are better able to undergo the arrest and recovery process, possibly through manipulation of their extracellular environment.

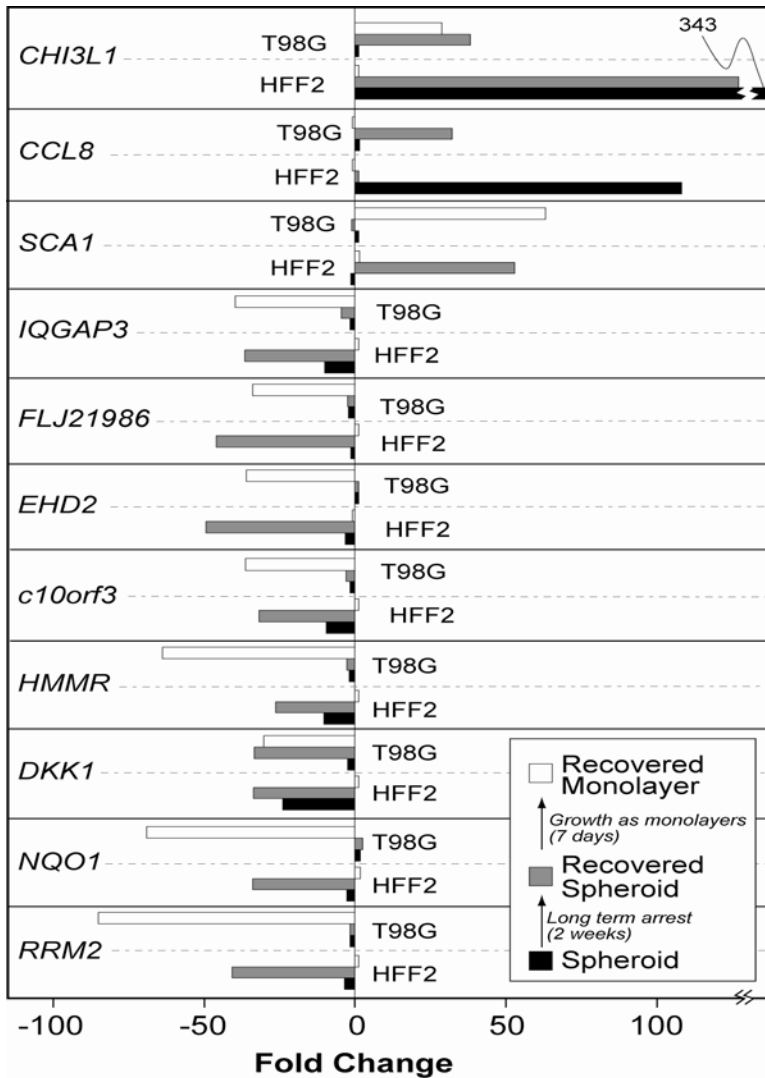


FIG. 4.4 Gene expression profiles for genes up- or down-regulated at least 10-fold (relative to a monolayer control) and found in both the HFF-2 and T98G cell lines. Genes are separated by cell line and time point (spheroid, recovered spheroid after two week arrest, and recovered monolayer), ordered from most down-regulated (ribonucleotide reductase, *RRM2*) to the most upregulated (chitinase 3-like 1; cartilage glycoprotein-39; *CHI3L1*). Values are relative to a monolayer control. Note that while the HFF-2 gene expression levels for the recovered monolayer had returned to monolayer control levels, the T98G line had not. For a more complete listing, see the Supplemental Data as well as the GEO website (GSE4217 and 4218).

Discussion

Chapter 2 demonstrated that HEK293 aggregates utilized a novel signaling pathway during arrest and recovery processes. As depicted in Fig. 4.5, a cyclical pathway was activated, involving cytokines (TNF- α , IL-1 β and IL-8) and intracellular signaling pathways (NF- κ B, Gadd45 β , JNK and AP-1). This signaling led to sustained co-activation of NF- κ B and JNK, permitting cells to survive long term arrest and recovery (Chapter 2). These observations were not compatible with previous work where JNK activation led to apoptosis and NF- κ B was reported to negatively regulate JNK signaling through Gadd45 β upregulation (DeSmaele *et al.*, 2001; Papa *et al.*, 2004). These disparate results could be due to the transformation state of the HEK293 cell line, where the immortalizing effects of the adenovirally expressed E1A and E1B gene products prevent antiproliferative signaling within the RB family of proteins (Parreno *et al.*, 2000; Berk, 2005) as well as the nuclear translocation of p53, blocking its transcriptional abilities. In addition, sequestration of p53 in the cytosol inhibits its ability to elicit a mitochondrial apoptotic response (Querido *et al.*, 1997; Berk, 2005; Moran, 1993). The inability of HEK293 cells to activate these classical quiescence/apoptosis cascades may explain the activated signaling pathway observed.

In order to reconcile these observed signaling differences, experiments were performed to monitor the response of two additional cell lines that differed in terms of their cell types and transformation states. Primary human foreskin fibroblasts (HFF-2) and a carcinogenic glioblastoma cell line (T98G) were examined for their ability to form multicellular aggregates, withstand a long term arrest, and subsequently recover from the arrest. As a primary cell line, HFF-2 cells are capable of activating the stress response

pathways which are impaired in the HEK293 cell line (p53 and Rb). T98G cells express p53 with a point mutation (phosphorylation site) which has been reported to inhibit its transactivational ability of several genes, including downstream p21. However; this mutation does not seem to inhibit p53's mitochondrial apoptotic response capabilities (Enns *et al.*, 2004; Ullrich *et al.*, 1993).

These studies show that the T98G and HFF-2 aggregates activated an alternative pathway from that observed with the HEK293 aggregates. IFN- γ production activated a Gadd45 α /p38 pathway leading to AP-1 (c-jun, and ATF3) activation (Fig. 4.5). Although both the cytokine and upstream intracellular signaling pathways were found to differ, cyclical activation was found in all three cell lines, resulting in a cascade from cytokines through a Gadd45 family member (α or β) to activate a MAPK pathway (p38 or JNK). The MAPK signal induces an AP-1 transcription factor response further increasing cytokine production. In summary, identical extracellular stresses (*i.e.*, inputs) imposed on two different cell lines led to divergent intracellular signaling pathways. These pathways subsequently converged at the AP-1 transcription factor level, leading to similar cellular responses (*i.e.*, outputs). We propose that the synergistic relationships between cytokines and chemokines (Kessler-Becker *et al.*, 2004; Gouwy *et al.*, 2005) play a central role in determining the overall cellular response.

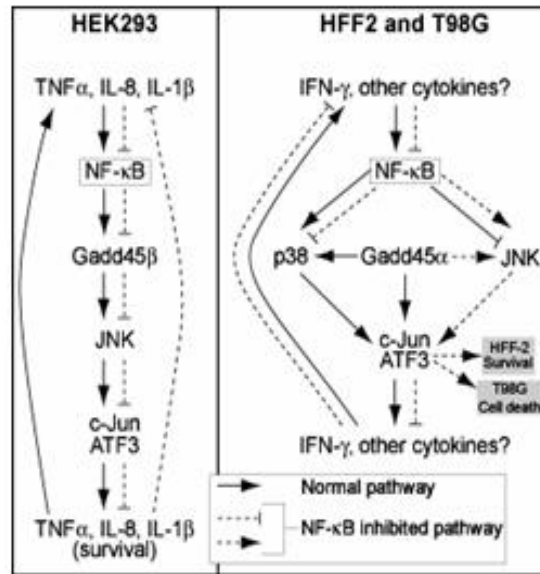


FIG. 4.5 Major activated signal transduction pathways within HEK293, HFF-2 and T98G aggregates during outgrowth as monolayers from a long term arrest as aggregates. While HEK293 cells depend on induction of both JNK and NF- κ B for survival, JNK activation has no effect on HFF-2 cell survival, but is lethal to T98G cells. The degree to which specific intracellular signaling pathways are activated depends on the cell line, cell transformation states and the external stimuli supplied (cellular inputs). These inputs lead to cellular responses or outputs (in this case migration and outgrowth as monolayers) that are modulated by cytokine profiles and autocrine loops.

The most significant differences in signaling among the three cell lines were observed when NF- κ B was inhibited. IFN- γ production was abolished and MKK4/p38 activation remained constant (no change throughout time course) within the HFF-2 and T98G aggregates. Surprisingly, Gadd45 α was still upregulated and JNK signaling was initiated, indicating that Gadd45 α is involved in several MAPK pathways, depending on the transcriptional activity of NF- κ B. These results are consistent with the work of others where NF- κ B was found to negatively regulate JNK signaling via Gadd45 β (De Smaele *et al.*, 2001; Papa *et al.*, 2004), but are not consistent with the results observed with our HEK293 studies (Chapter 2), suggesting that the signaling pathways for long term survival of HEK293 cells are transformation state or cell type specific. However, since Gadd45 β levels were not increased during long term arrest in both the primary fibroblast and glioblastoma cell lines, an additional factor such as XIAP may contribute to the inhibition of JNK by NF- κ B under these experimental conditions (Tang *et al.*, 2001). Chemical inhibition of NF- κ B did not affect AP-1 activation in either cell line, suggesting that both the p38 and JNK pathways converge on c-jun and ATF3.

The ability of the cell lines investigated to survive the long term arrest and subsequently recover as adherent monolayers suggests that pathway availability may be both transformation state and cell line dependent. T98G cells could not return to proliferating monolayers after their long term arrest as aggregates without activation of NF- κ B, similar to what we observed previously with HEK293 cells. HFF-2 cells appeared unaffected by this inhibition even though the HFF-2 and T98G lines activated a similar stress signal transduction route (Fig. 4.5). This discrepancy between lethality and signaling routes suggests cellular transformation state and cell type may determine the

degree to which JNK activation becomes either apoptotic or antiapoptotic. Although different gene expression patterns may exist due to tissue-specific requirements of these cell lines, the availability of the classical quiescent/apoptotic pathways (p53/Rb) may be the ultimate determinant in the ability to withstand these avascular-type stresses. NF- κ B has been shown to be constitutively active in most tumor cell lines and rarely found in active normal (untransformed) cells (Aggarwal, 2004). Furthermore suppression of NF- κ B in these tumor lines causes inhibited proliferation, cell cycle arrest and apoptosis (Aggarwal, 2004). The results from our research suggest that NF- κ B is a potential selective target in the treatment of cancer, as inhibition led to lack of proliferation and cell death under avascular growth conditions for both HEK293 and T98G cells without affecting the primary HFF-2 untransformed cell line.

The signal transduction pathways invoked by a human cell, tissue, or organ in response to an external stress are tremendously complex. In efforts to minimize complexity, investigations often focus on determining routes available to individual cell lines grown *in vitro*. Even with this “minimalist” approach, recent studies show that determining the framework of response cascades will require a systems-based model (Oda *et al.*, 2005; Janes *et al.*, 2005). As a strong justification for tissue culture-based investigations is to relate the observed molecular events to human health, efforts should be directed at developing model systems that best represent *in vivo* biology. Bearing this in mind, we expanded on our initial work with three-dimensional multicellular aggregates (Chapter 2), to define how both a primary fibroblast and a glioblastoma cell line undergo the process of aggregate formation, long term arrest, and recovery. Transcriptional profiling, multiplex cytokine assays and selected Western analyses provide strong

evidence that transformation state and cell type must be taken into consideration when modeling signal transduction cascades.

The multicellular aggregate system provides conditions similar to that of avascular tumor growth (depletion of oxygen and nutrients) and wounding response. Modification of the protocol or the conditions of the arrest and recovery (for example, long term arrest at 37 °C rather than room temperature) will provide cancer researchers a new tool for investigating the avascular stage of tumor development. Spheroids mimic avascular tumor stages or micrometastases in many aspects and were studied intensively as an experimental model reflecting an *in vivo*-like micromilieu (Walenta *et al.*, 2000). The “cellular microecology” (Sutherland, 1988) present in multicellular aggregates provide constraints due to cell-cell contact influencing how the aggregate reacts to stresses imposed by the surrounding environment (Schmeichel and Bissel, 2003). Such systems provide an appreciably different picture of quiescence relative to monolayers and offer a new dimension to studies centered on tumor biology (Zahir and Weaver, 2004; Jacks and Weinberg, 2002), inflammation-based cancer studies (Pikarsky *et al.*, 2004) and cell-matrix adhesions (Amatangelo *et al.*, 2005; Cukierman *et al.*, 2001)

These results suggest that aggregate systems will prove useful for understanding the wounding response. Model systems for such studies often utilize scraping of confluent tissue cultured cells (Harper *et al.*, 2005; Dobrevá *et al.*, 2006) followed by observation of new migration paths. The formation of aggregates and their release to adherent monolayers is also a cell migration/reorganizational response. The observation of IL-8 release during outgrowth within this study matches the observations that this is an important cytokine in the cell spreading response to wounding (Dobrevá *et al.*, 2006). In

addition, the p38 pathway was linked to TNF- α , IL-1 β , IL-6, IL-8, and MCP-1 mRNA stability (Ono and Han, 2000). These cytokines, except for TNF- α , were all found to be present at higher levels in the primary fibroblasts during arrest and recovery. Transcriptional profiling of the primary fibroblasts also revealed a dramatic increase in the gene encoding hepatocyte growth factor (HGF, Supplemental Table 4.S1). As endogenous addition of IL-1 β and INF- γ was recently shown to induce dermal fibroblast production of HGF (Takami *et al.*, 2005), a growth factor implicated in wound healing, it can be hypothesized that a slightly modified form of our protocol will be very useful for investigating the molecular aspects of the wounding response. Comparing and contrasting the quiescence pathways invoked by multicellular aggregates and confluent monolayers (contact inhibition; Faust *et al.*, 2005) may also prove to be extremely rewarding.

Cell culture-based studies aimed at determining the signaling processes involved in mammalian cell stress responses often show conflicting or seemingly incongruous results. While this is somewhat disconcerting, it is important to note that the use of different cell lines with varying degrees of genetic modification, exogenous addition of cytokines well above normal physiological levels, and our present inability to monitor all signaling pathways simultaneously are variables that can lead to results that initially appear incompatible. The interconnected nature of the signal transduction pathways (network) permits varying degrees of flux through separate pathways simultaneously, and these paths can diverge and converge in ways that are slowly coming to light (Hoffmann *et al.*, 2002; Bossio *et al.*, 2006; Janes *et al.*, 2006). In Chapter 2 it was demonstrated that long term arrest and recovery was dependent upon NF- κ B and Gadd45 β signaling

together with sustained JNK activation. Herein it is shown that while a carcinoma cell line is still dependent upon NF- κ B, its signaling partner is another member of the Gadd45 family, and signaling occurs through p38. Primary fibroblasts undergo arrest and recovery independent of NF- κ B yet still proceed through a p38 pathway. Three different cell types and transformation states provide three different routes to survival, all with cyclical cytokine production and signaling. These routes cannot be measured or modulated effectively in adherent monolayers. Multicellular aggregates provide higher ordered systems that can be used to describe signaling pathways within a cell, highlighting the role of autocrine responses and the synergistic relationships between cytokines and neighboring cells.

References

- Aggarwal BB. 2004. Nuclear factor- κ B: The enemy within. *Cancer Cell* 6: 203-208.
- Amatangelo MD, Bassi DE, Klein-Santo AJP, Cukierman E. 2005. Stroma derived three-dimensional matrices are necessary and sufficient to promote desmoplastic differentiation of normal fibroblasts. *Amer J Pathol* 167: 475-488.
- Bates CB, Edwards NS, Yates JD. 2000. Spheroids and cell survival. *Crit Rev Oncol Hematol* 36: 61-74.
- Berk AJ. 2005. Recent lessons in gene expression, cell cycle control, and cell biology from adenovirus. *Oncogene* 24: 7673-7685.
- Besirli CG, Johnson EM Jr. 2003. JNK-independent activation of c-jun during neuronal apoptosis induced by multiple DNA-damaging agents. *J Biol Chem* 278: 22357-22366.
- Bossio D, Marazzi I, Agresti A, Shimizu N, Bianchi ME, Natoli G. 2006. A hyper-dynamic equilibrium between promoter-bound and nucleoplasmic dimers controls NF- κ B-dependent gene activity. *EMBO J* 25: 798-810.
- Brysk MM, Selvanayagam P, Arany I, Brysk H, Tying SK, Rajaraman S. 1995. Induction of apoptotic nuclei by interferon-gamma and by predesquamin in cultured keratinocytes. *J Interferon Cytokine Res* 12: 1029-1035.
- Bulavin DV, Kovalsky O, Hollander MC, Fornace AJ Jr. 2003. Loss of Oncogenic H-ras-induced cell cycle arrest and p38 mitogen-activated protein kinase activation by disruption of Gadd45 α . *Mol Cell Biol* 23: 3859-3871.
- Corn RA, Aronica MA, Zhang F, Tong Y, Stanley SA, Kim SR, Stephenson L, Enerson B, McCarthy S, Mora A, Boothby M. 2003 T cell-intrinsic requirement for NF-kappaB induction in postdifferentiation IFN-gamma production and clonal expansion in a TH1 response. *J Immunol* 171: 1816-1824.
- Cukierman E, Pankov R, Stevens DR, Yamada KM. 2001. Taking cell-matrix adhesions to the third dimension. *Science* 294: 1708-1712.
- Davis RJ. 2000. Signal transduction by the JNK group of MAP kinases. *Cell* 103: 239-252.
- de Haij S, Bakker AC, van der Geest RN, Haegeman G, Vanden Berghe W, Aarbiou J, Daha MR, van Kooten C. 2005 NF-kappaB mediated Il-6 production by renal epithelial cells is regulated by c-jun NH2-terminal kinase. *J Am Soc Nephrol* 16: 1603-11.

- De Smaele E, Zazzeroni F, Papa S, Nguyen DU, Jin R, Jones J, Cong R, Franzoso G. 2001. Induction of gadd45beta by NF-kappaB downregulates pro-apoptotic JNK signalling. *Nature* 414: 308-313.
- Dobrev I, Waeber G, James RW, Widmann C. 2006. Interleukin-8 secretion by fibroblasts induced by low density lipoproteins is p38 MAPK-dependent and leads to cell spreading and wound closure. *J Biol Chem* 281: 199-205.
- Dong C, Davis RJ, Flavell RA. 2002 Map kinases in the immune response. *Annu Rev Immunol* 20: 55-72.
- Enns L, Bogen KT, Wiziak J, Murtha AD, Weinfeld M. 2004. Low-dose radiation hypersensitivity is associated with p53-dependent apoptosis. *Mol Cancer Res* 2: 557-566.
- Frigo DE, Tang Y, Beckman BS, Scandurro AB, Alam J, Borow ME, McLachlan JA. 2004. Mechanism of AP-1-mediated gene expression by select organochlorines through the p38 MAPK pathway. *Carcinogenesis* 25: 249-261.
- Faust D, Dolado I, Cuadrado A, Oesch F, Weiss C, Nebreda AR, Dietrich C. 2005. p38alpha MAPK is required for contact inhibition. *Oncogene* 24: 7941-7945.
- Ghosh S, Spagnoli GC, Martin I, Ploegert S, Demougin P, Heberer M, Reschner A. 2005. Three-dimensional culture of melanoma cells profoundly affects gene expression profile: A high density oligonucleotide array study. *J Cell Physiol* 204: 522-531.
- Gouwy M, Struyf S, Proost P, Van Damme J. 2005. Synergy in cytokine and chemokine networks amplifies the inflammatory response. *Cyto Growth Factor Rev* 16: 561-580.
- Graham FL, Smiley J, Russell WC, Nair R. 1977. Characteristics of a human cell line transformed by DNA from human adenovirus type 5. *J Gen Virol* 36: 59-74.
- Harper EG, Alvares SM, Carter WG. 2005. Wounding activates p38 map kinase and activation transcription factor 3 in leading keratinocytes. *J Cell Sci* 118: 3471-3485.
- Henley DV, Bellone CJ, Williams DA, Ruh MF. 2004. MAPK signaling pathways modulate IL-1beta expression in human keratinocytes. *Arch Biochem Biophys* 424: 112-118.
- Hildesheim J, Belova GI, Tyner SD, Zhou X, Vardanian L, Fornace AJ Jr. 2004. Gadd45 α regulates matrix metalloproteinases by suppression Δ Np63 α and β -catenin via p38 MAP kinase and APC complex activation. *Oncogene* 23: 1829-1837.
- Hoffmann E, Dittrich-Breiholz O, Holtmann H, Kracht M. 2002. Multiple control of interleukin-8 gene expression. *J Leukoc Biol* 72: 847-855.

Jack GD, Mead EA, Garst JF, Cabrera MC, Desantis AM, Slaughter SM, Jervis J, Brooks AI, Potts M, Helm RF. 2006. Long term metabolic arrest and recovery of HEK293 spheroids involves NF-kappaB signaling and sustained JNK activation. *J Cell Physiol* 206: 526-36.

Jacks T, Weinberg RA. 2002. Taking the study of cancer cell survival to a new dimension. *Cell* 111: 923-925.

Janes KA, Albeck JG, Gaudet S, Sorger PK, Lauffenburger DA, Yaffe MB. 2005. A systems model of signaling identifies a molecular basis set for cytokine-induced apoptosis. *Science* 310: 1646-1653.

Janes KA and Lauffenburger DA. 2006. A biological approach to computational models of proteomic networks. *Curr Opin Chem Biol* 10: 73-80.

Jiang Y, Pjesivac-Grbovic J, Cantrell C, Freyer JP. 2005. A multiscale model for avascular tumor growth. *Biophys J* 89: 3884-94.

Kessler-Becker D, Krieg T, Eckes B. 2004. Expression of pro-inflammatory markers by human dermal fibroblasts in a three-dimensional culture model is mediated by an autocrine interleukin-1 loop. *Biochem J* 379: 351-358.

Kool J, Hamdi M, Cornelissen-Steijer P, van der Eb AJ, Terleth C, van Dam H. 2003. Induction of ATF3 by ionizing radiation is mediated via a signaling pathway that includes ATM, Nibrin1, stress induced MAPkinases and ATF-2. *Oncogene* 22: 4235-4242.

Kunz-Schughart LA, Kreutz M, Knuechel R. 1998. Multicellular spheroids: a three-dimensional in vitro culture system to study tumour biology. *Int J Exp Pathol* 79: 1-23
Lamb JA, Ventura JJ, Hess P, Flavell RA, Davis RJ. 2003. JunD mediates survival signaling by the JNK signal transduction pathway. *Mol Cell* 11:1479-1489.

Lee J, Shin JS, Park JY, Kwon D, Choi SJ, Kim SJ, Choi IH. 2003. p38 Mitogen-activated protein kinase modulates expression of tumor necrosis factor-related apoptosis-inducing ligand induced by interferon- γ in fetal brain astrocytes. *J Neuroscience Res* 74: 884-890.

Marinissen MJ, Chiariello M, Pallante M, Gutkind JS. 1999. A network of mitogen-activated protein kinases links G protein-coupled receptors to the c-jun promoter: a role for c-jun NH2-terminal kinase, p38s, and extracellular signal-regulated kinase 5. *Mol Cell Biol* 19: 4289-4301.

Moran E. 1993 Interaction of adenoviral proteins with pRB and p53. *FASEB J* 7: 880-885.

- Mueller-Klieser W. 1987. Multicellular spheroids. A review on cellular aggregates in cancer research. *J Cancer Res Clin Oncol* 113: 101-122.
- Oda K, Matsuoka Y, Funahashi A, Kitano H. 2005. A comprehensive pathway map of epidermal growth receptor signaling. *Mol Sys Biol* msb4100014: E1-E17.
- Ono K, Han J. 2000. The p38 signal transduction pathway activation and function. *Cell Signal* 12: 1-13.
- Papa S, Zazzeroni F, Bubici C, Jayawardena S, Alvarez K, Matsuda S, Nguyen DU, C.G. Pham CG, Nelsbach AH, Melis T, De Smaele E, Tang WJ, D'Adamio L, Franzoso G. 2004. Gadd45 beta mediates the NF-kappa B suppression of JNK signalling by targeting MKK7/JNKK2. *Nat Cell Biol* 2: 146-153.
- Parreno M, Garriga J, Limon A, Mayol X, Beck GR Jr, Moran E, Grana X. 2000. E1A blocks hyperphosphorylation of p130 and p107 without affecting the phosphorylation status of the retinoblastoma protein. *J Virol* 74: 3166-3176.
- Pikarsky E, Porat RM, Stein I, Abramovitch R, Amit S, Kasem S, Gutkovich-Pyest E, Urieli-Shoval S, Galun E, Ben-Neriah Y. 2004. NF- κ B functions as a tumor promoter in inflammation-associated cancer. *Nature* 431: 461-466.
- Querido E, Teodoro JG, Branton PE. 1997. Accumulation of p53 induced by the adenovirus E1A protein requires regions involved in the stimulation of DNA synthesis. *J Virol* 71: 3526-3533.
- Schmeichel KL, Bissell MJ. 2003. Modeling tissue-specific signaling in three dimensions. *J Cell Sci* 116: 2377-2388.
- Sutherland RM. 1988 Cell and microenvironment interactions in tumor microregions - the multicell spheroid model. *Science* 240: 177-184.
- Takami Y, Motoki T, Yamamoto I, Gohda E. 2005. Synergistic induction of hepatocyte growth factor in human skin fibroblasts by the inflammatory cytokines interleukin-1 and interferon- γ . *Biochem Biophys Res Commun* 327: 212-217.
- Tang G, Minemoto Y, Dibling B, Prucell NH, Li Z, Karin M, Lin A. 2001. Inhibition of JNK activation through NF- κ B target genes. *Nature* 414: 313-317.
- Tobe M, Isobe Y, Tomizawa H, Nagasaki T, Takahashi H, Fukazawa T, Hayashi H. 2003. Discovery of quinazolines as a novel structural class of potent inhibitors of NF- κ B activation. *Bioorg Med Chem* 11: 383-391.
- Ullrich SJ, Sakaguchi K, Lees-Miller SP, Fiscella M, Mercer WE, Anderson CW, Appella E. 1993. Phosphorylation at Ser-15 and Ser-392 in mutant p53 molecules from human tumors is altered compared to wild-type p53. *Proc Natl Acad Sci* 90: 5954-5958.

Vila-del Sol V, and Fresno M. 2005. Involvement of TNF and NF-kappaB in the transcriptional control of cyclooxygenase-2 expression by INF-gamma in macrophages. *J Immunol* 174: 2825-2833.

Walenta S, Doetsch J, Mueller-Klieser W, Kunz-Schughart LA. 2000. Metabolic imaging in multicellular spheroids of oncogene-transfected fibroblasts. *J Histochem Cytochem* 48: 509-522.

Xiao J, and Chodosh J. 2005. Jnk regulates MCP-1 expression in adenovirus type 19-infected human corneal fibroblasts. *Invest Ophthalmol Vis Sci* 46: 3777-3782.

Zahir N, Weaver VM. 2004. Death in the third dimension: apoptosis regulation and tissue architecture. *Curr Opin Gen Dev* 14: 71-80.

Zhang S and Kaplan MH. 2000. The p38 mitogen-activated protein kinase is required for IL-12-induced IFN- γ expression. *J Immunol* 165: 1374-1380.

Chapter 4

Supplementary Information

Contents

Microarray methods

FIG. 4.S1 Graphical depiction of gene expression changes in HFF-2 cells during conversion to spheroids, arrest and subsequent recovery as adherent monolayers.

FIG. 4.S2 Graphical depiction of gene expression changes in T98G cells during conversion to spheroids, arrest, and subsequent recovery as adherent monolayers.

FIG. 4.S3 Cytokine profiles for the 12 other cytokines determined in the multiplex array for HFF-2 and T98G cells, with and without NF- κ B inhibition.

Table 4.S1 Genes in HFF-2 cells with at least a 10-fold change gene expression.

Table 4.S2 Genes in T98G cells with at least a 10-fold change gene expression.

Table 4.S3 Gene Expression Omnibus (GEO) Accession Information.

Table 4.S4 Comparison of quantitative PCR fold changes for *GADD45* genes in the presence and absence of NF- κ B chemical inhibition with HFF-2 and T98G cells.

Microarray Methods---Expanded

Total RNA was prepared from cells using the RNeasy total RNA extraction. RNA quality was assessed by electrophoresis using the Agilent Bioanalyzer 2100 and spectrophotometric analysis prior to cDNA synthesis. Ribo-SPIA™-based RNA amplifications and target preparations were carried out according to manufacturer instruction (Ovation™ Biotin System, <http://www.nugeninc.com/technology/index.shtml>, Nugen, San Carlos, CA). Briefly, 20ng of RNA was reverse transcribed into cDNA by reverse transcriptase using a DNA/RNA chimeric primer that is part DNA and part RNA. RNA was degraded by heat and fragments served as primers for second strand synthesis, yielding a double stranded cDNA with an RNA/DNA heteroduplex at one end. RNA portions of the heteroduplex portion of the ds-cDNA, were digested by RNase H, added to the reaction mixture together with a DNA polymerase and a second chimeric cDNA/cRNA primer (amplification primer). Amplification proceeds by primer extension, strand displacement and degradation of the RNA portion of the primer

extension product hybridized to the target, to reveal part of the priming site for subsequent primer hybridization and extension by strand displacement DNA synthesis. Accumulated cDNA amplification products were fragmented and labeled to generate biotinylated cDNA targets. Following fragmentation all components generated throughout the processing procedure (amplified cDNA, and fragmented cDNA) were analyzed by electrophoresis using the Agilent Bioanalyzer 2100 to assess the appropriate size distribution prior to microarray hybridization. Detailed protocols for sample preparation using the Affymetrix labeling protocols can be found at <http://www.affymetrix.com>.

All samples were subjected to gene expression analysis via the Affymetrix Human 133_2.0Plus high-density oligonucleotide array which currently queries 46,000 human probe sets. Currently each gene on the array is represented by 11 pairs of 25mer oligonucleotides that span the coding region for the 46,000 genes and EST's represented (clear overlapping of genes is evident). Each probe pair consists of a perfect match (PM) sequence that is complementary to the cDNA target and a mismatch (MM) sequence that has a single base pair mutation in a region critical for target hybridization; this sequence serves as a control for non-specific hybridization. Hybridization, staining and washing of all arrays was performed in the Affymetrix fluidics module as per the manufacturer's protocol. Streptavidin phycoerythrin stain (SAPE, Molecular Probes) is the fluorescent conjugate used to detect hybridized target sequences. The detection and quantitation of target hybridization is performed with a GeneArray Scanner 3000 set to scan each array twice at a factory set PMT level and resolution. All arrays referred to in this study were assessed for "array performance" prior to data analysis. This process involves the statistical analysis of control transcripts that are spiked into the samples themselves and the hybridization cocktail to assess array performance. In addition, several genes have been identified on each array to help assess the overall quality of signal intensity from all arrays. The results of this analysis helped validate the reproducibility of each array at baseline allowing us to define the lower level of sensitivity that will be employed to identify small changes in biologically relevant genes.

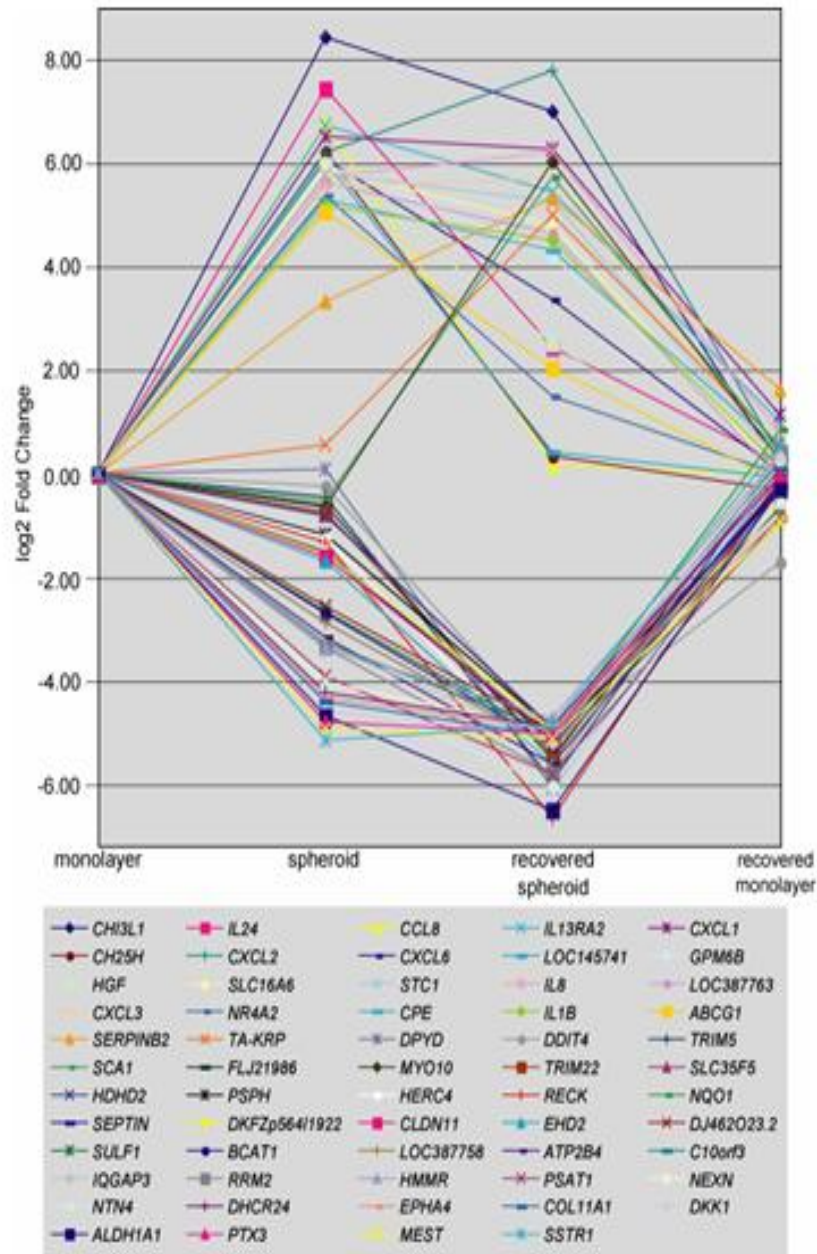


FIG. 4.S1 Log2 fold change trends for HFF-2 cells. Genes are arranged from left to right in rows, from most up-regulated (CHI3L1) to the most down-regulated (SSTR1) at the "spheroid" timepoint. Duplicate genes listings and unannotated genes are not listed.

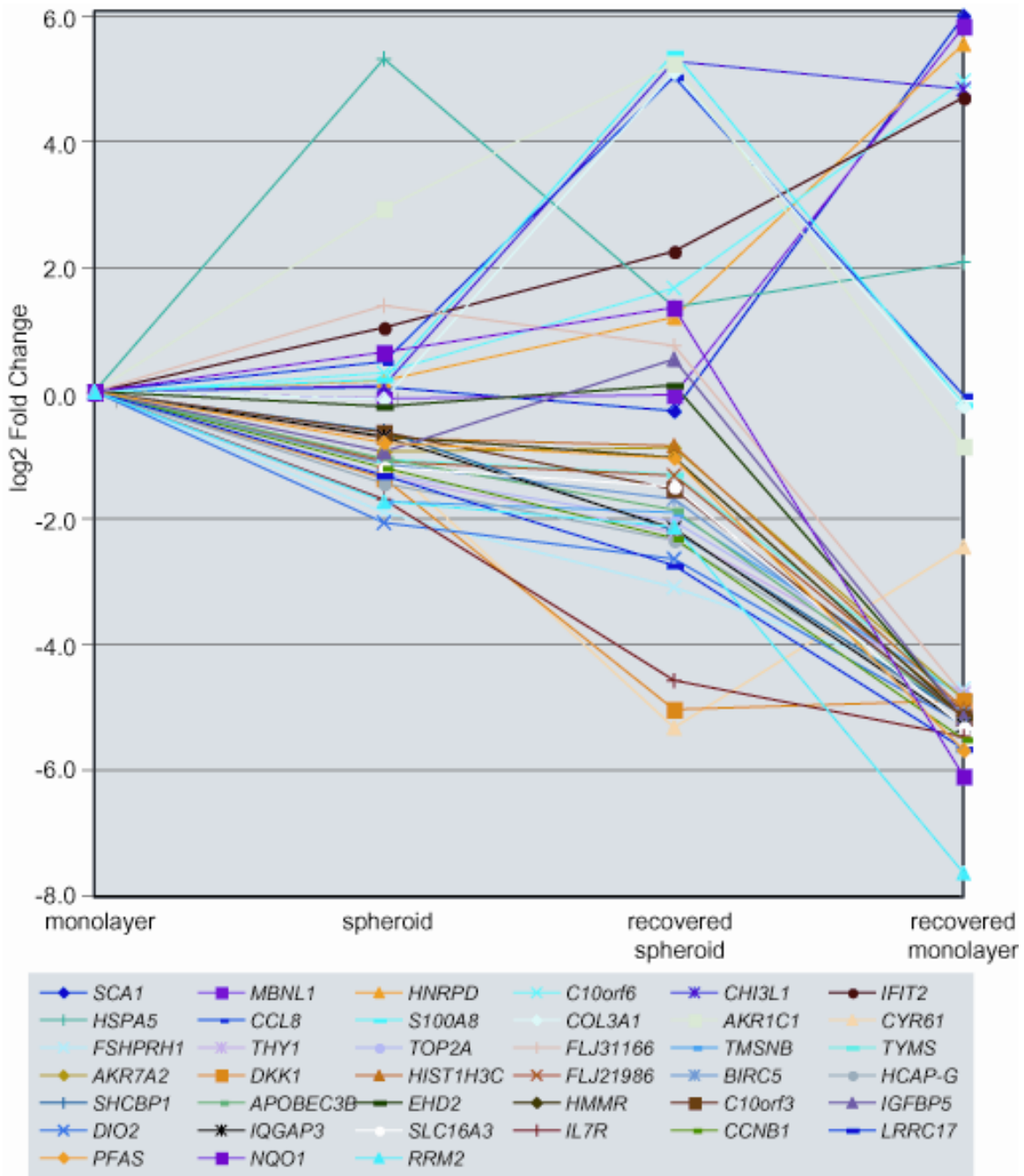


FIG. 4.S2 Log2 fold change trends for T98G cells. Genes are arranged from left to right in rows, from most up-regulated (SCA1) to the most down-regulated (RRM2) at the "recovered monolayer" timepoint. Duplicate genes listings and unannotated genes are not listed.

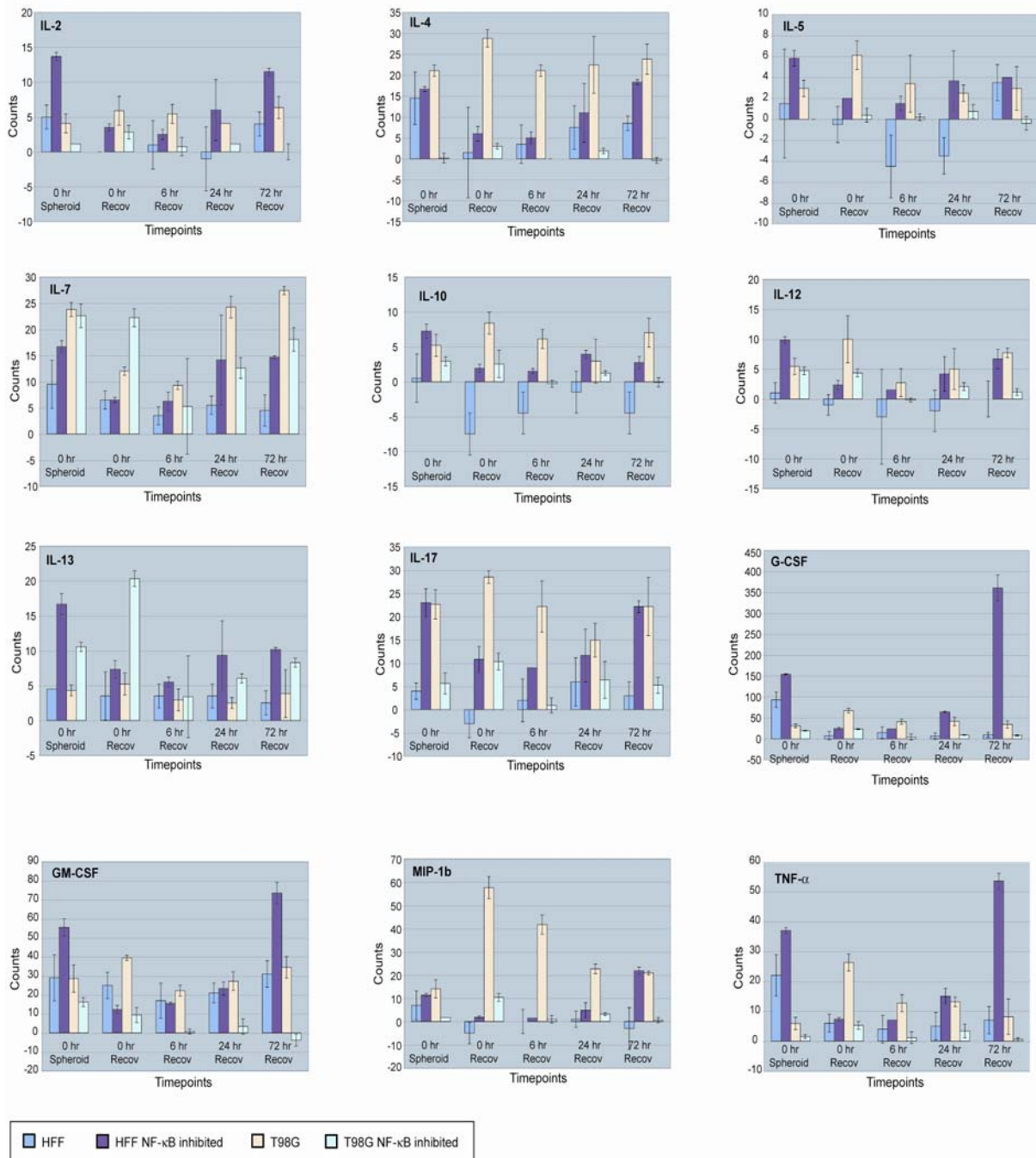


FIG. 4.S3 Changes in cytokine levels for the HFF-2 and T98G cells lines during spheroid formation, arrest and recovery, with and without NF- κ B inhibition. The cytokines shown here are the ones measured via the multiplex array (17 cytokines total) that did not show significant changes. Figure 3 in the main text displays the cytokines with the most dramatic changes in levels. Values are in counts with error bars (n=3).

Table 4.S1 Genes in HFF2 primary fibroblasts with greater or less than a 10-fold change in expression during the course of spheroid formation and recovery (NA, no information available).

Affymetrix Gene ID	UniGene Symbol	Mono-layer	Sphrd	Sphrd Recov	Mono-layer Recov	UniGene Cluster ID	UniGene Name
209395_at	CHI3L1	-1.01	343.45	126.73	1.08	Hs.382202	chitinase 3-like 1 (cartilage glycoprotein-39)
206569_at	IL24	-1.03	172.30	5.42	1.15	Hs.411311	interleukin 24
214038_at	CCL8	-1.00	107.74	1.12	-1.01	Hs.271387	chemokine (C-C motif) ligand 8
206172_at	IL13RA2	-1.01	105.90	43.42	2.00	Hs.336046	interleukin 13 receptor, alpha 2
204470_at	CXCL1	-1.00	90.56	76.90	2.19	Hs.789	chemokine (C-X-C motif) ligand 1 (melanoma growth stimulating activity, alpha)
209396_s_at	CHI3L1	-1.01	82.85	25.34	1.02	Hs.382202	chitinase 3-like 1 (cartilage glycoprotein-39)
227610_at	NA	-1.00	78.54	9.56	1.27	Hs.437875	Clone DNA100312 VSSW1971 (UNQ1971) mRNA, complete cds
225207_at	NA	-1.00	75.99	7.68	1.02	NA	NA
206932_at	CH25H	-1.01	74.41	1.27	-1.25	Hs.47357	cholesterol 25-hydroxylase
209774_x_at	CXCL2	-1.00	73.44	219.02	1.27	Hs.75765	chemokine (C-X-C motif) ligand 2
206336_at	CXCL6	-1.01	67.12	10.27	1.03	Hs.164021	chemokine (C-X-C motif) ligand 6 (granulocyte chemotactic protein 2)
241031_at	LOC145741	-1.01	65.80	1.33	-1.05	Hs.202656	hypothetical LOC145741
209167_at	GPM6B	-1.00	63.47	18.39	1.17	Hs.5422	glycoprotein M6B
209960_at	HGF	-1.01	62.89	5.70	-1.31	Hs.396530	hepatocyte growth factor (hepapoietin A; scatter factor)
230748_at	SLC16A6	-1.00	58.97	27.79	-1.02	Hs.42645	solute carrier family 16 (monocarboxylic acid transporters), member 6
204595_s_at	STC1	-1.02	55.33	38.18	1.15	Hs.25590	stanniocalcin 1
202859_x_at	IL8	-1.00	53.06	73.49	1.71	Hs.624	interleukin 8
227099_s_at	LOC387763	-1.04	48.65	24.83	-1.08	Hs.448680	hypothetical LOC387763
207850_at	CXCL3	-1.00	46.55	51.88	1.15	Hs.89690	chemokine (C-X-C motif) ligand 3
209169_at	GPM6B	-1.00	44.85	4.36	-1.07	Hs.5422	glycoprotein M6B
216248_s_at	NR4A2	-1.01	41.18	2.81	-1.01	Hs.82120	nuclear receptor subfamily 4, group A, member 2
201117_s_at	CPE	-1.01	39.27	19.75	1.38	Hs.75360	carboxypeptidase E
209170_s_at	GPM6B	-1.01	39.09	11.43	1.15	Hs.5422	glycoprotein M6B
205067_at	IL1B	-1.01	36.06	22.72	1.09	Hs.126256	interleukin 1, beta
204567_s_at	ABCG1	-1.00	32.96	4.11	-1.12	Hs.369055	ATP-binding cassette, sub-family G (WHITE), member 1
208075_s_at	NA	-1.00	27.48	-1.10	-1.18	NA	NA
211506_s_at	IL8	-1.01	10.82	79.80	-1.03	Hs.624	interleukin 8

204614_at	SERPINB2	-1.01	10.04	39.67	3.09	Hs.75716	serine (or cysteine) proteinase inhibitor, clade B (ovalbumin), member 2
239835_at	TA-KRP	-1.01	1.47	31.69	1.46	Hs.116665	T-cell activation kelch repeat protein
241773_at	NA	-1.00	1.14	46.74	1.39	NA	NA
204646_at	DPYD	-1.00	1.06	-67.24	-1.22	Hs.1602	dihydropyrimidine dehydrogenase
205234_at	SLC16A4	-1.00	-1.15	-31.42	-1.00	Hs.351306	solute carrier family 16 (monocarboxylic acid transporters), member 4
202887_s_at	DDIT4	-1.00	-1.19	-34.26	-3.29	Hs.111244	DNA-damage-inducible transcript 4
210705_s_at	TRIM5	-1.01	-1.36	-61.32	1.23	Hs.350517	tripartite motif-containing 5
1559249_at	SCA1	-1.00	-1.43	52.83	1.38	Hs.434961	spinocerebellar ataxia 1 (olivopontocerebellar ataxia 1, autosomal dominant, ataxin 1)
228728_at	FLJ21986	-1.00	-1.52	-45.89	1.29	Hs.440973	hypothetical protein FLJ21986
1554026_a_at	MYO10	-1.01	-1.56	65.05	1.20	Hs.61638	myosin X
213293_s_at	TRIM22	-1.00	-1.68	-43.35	-1.13	Hs.318501	tripartite motif-containing 22
225872_at	SLC35F5	-1.00	-1.73	-30.75	1.14	Hs.437608	solute carrier family 35, member F5
223155_at	HDHD2	-1.00	-1.75	-29.85	1.06	Hs.380822	haloacid dehalogenase-like hydrolase domain containing 2
205194_at	PSPH	-1.01	-2.26	-30.43	-1.28	Hs.512656	phosphoserine phosphatase
225989_at	HERC4	-1.00	-2.37	-51.83	1.30	Hs.96867	hect domain and RLD 4
205407_at	RECK	-1.00	-2.50	#####	-1.04	Hs.388918	reversion-inducing-cysteine-rich protein with kazal motifs
201467_s_at	NQO1	-1.00	-2.85	-33.80	1.81	Hs.406515	NAD(P)H dehydrogenase, quinone 1
230071_at	SEPTIN11	-1.00	-2.87	-35.70	-1.17	Hs.386784	septin 11
209596_at	DKFZp564I1922	-1.00	-2.92	-30.49	-1.59	Hs.72157	adlican
228335_at	CLDN11	-1.00	-3.03	-34.12	-1.26	Hs.31595	claudin 11 (oligodendrocyte transmembrane protein)
221870_at	EHD2	-1.00	-3.22	-49.34	-1.03	Hs.325650	EH-domain containing 2
45297_at	EHD2	-1.00	-3.26	-51.97	-1.05	Hs.325650	EH-domain containing 2
201890_at	RRM2	-1.00	-3.61	-40.81	1.30	Hs.226390	ribonucleotide reductase M2 polypeptide
225876_at	DJ462O23.2	-1.00	-5.93	-31.13	1.09	Hs.389516	hypothetical protein dJ462O23.2
212353_at	SULF1	-1.00	-6.31	-34.69	-1.59	Hs.409602	sulfatase 1
226517_at	BCAT1	-1.00	-6.46	-38.07	-1.20	Hs.438993	branched chain aminotransferase 1, cytosolic
225285_at	BCAT1	-1.00	-6.86	-32.44	-1.28	Hs.438993	branched chain aminotransferase 1, cytosolic
226769_at	LOC387758	-1.00	-7.34	-39.10	-1.93	Hs.32478	similar to RIKEN cDNA 1110018M03
212136_at	ATP2B4	-1.00	-8.94	-48.69	-1.20	Hs.343522	ATPase, Ca ⁺⁺ transporting, plasma membrane 4
218542_at	C10orf3	-1.00	-9.60	-31.71	1.21	Hs.14559	chromosome 10 open reading frame 3

229538_s_at	IQGAP3	-1.00	-9.96	-36.54	1.16	Hs.133294	IQ motif containing GTPase activating protein 3
209773_s_at	RRM2	-1.00	-10.20	-55.34	1.35	Hs.226390	ribonucleotide reductase M2 polypeptide
207165_at	HMMR	-1.00	-10.37	-26.40	1.27	Hs.72550	hyaluronan-mediated motility receptor (RHAMM)
229097_at	NA	-1.00	-11.64	-40.21	1.25	NA	NA
212135_s_at	ATP2B4	-1.00	-12.01	-37.23	-1.17	Hs.343522	ATPase, Ca ⁺⁺ transporting, plasma membrane 4
227061_at	NA	-1.00	-13.80	-37.59	-2.54	Hs.86538	CDNA FLJ44429 fis, clone UTERU2015653
223062_s_at	PSAT1	-1.00	-15.06	-56.00	-1.77	Hs.286049	phosphoserine aminotransferase 1
226103_at	NEXN	-1.00	-16.34	-31.11	1.10	Hs.22370	nexilin (F actin binding protein)
223315_at	NTN4	-1.00	-17.38	-65.29	-1.46	Hs.102541	netrin 4
200862_at	DHCR24	-1.00	-18.68	-29.62	-1.03	Hs.75616	24-dehydrocholesterol reductase
227449_at	EPHA4	-1.00	-20.01	-31.10	-1.81	Hs.244624	EphA4
37892_at	COL11A1	-1.00	-21.24	-33.32	1.07	Hs.439168	collagen, type XI, alpha 1
204602_at	DKK1	-1.00	-24.05	-33.58	1.26	Hs.40499	dickkopf homolog 1 (Xenopus laevis)
212224_at	ALDH1A1	-1.00	-25.43	-90.10	-1.23	Hs.76392	aldehyde dehydrogenase 1 family, member A1
229271_x_at	COL11A1	-1.00	-25.49	-26.59	-1.15	Hs.439168	collagen, type XI, alpha 1
206157_at	PTX3	-1.00	-27.80	-32.19	-1.02	Hs.2050	pentaxin-related gene, rapidly induced by IL-1 beta
202016_at	MEST	-1.00	-30.24	-34.91	-1.95	Hs.440459	mesoderm specific transcript homolog (mouse)
235591_at	SSTR1	-1.00	-35.55	-29.00	1.49	Hs.248160	somatostatin receptor 1
237435_at	NA	-1.00	-52.59	-73.06	1.32	NA	NA
204830_x_at	NA	-1.00	-63.78	-63.75	1.06	NA	NA

Table 4.S2 Genes in T98G glioblastoma cells with greater or less than a 10-fold change in expression during the course of spheroid formation and recovery (NA, no information available).

Gene ID	UniGene Symbol	Mono-layer	Sphrd	Sphrd Recov	Mono-layer Recov	UniGene Cluster ID	UniGene Name
1559249_at	SCA1	-1.00	1.06	-1.24	62.90	Hs.434961	spinocerebellar ataxia 1 (olivopontocerebellar ataxia 1, autosomal dominant, ataxin 1)
237440_at	EVE1	-1.00	1.16	1.03	58.94	NA	NA
1558111_at	MBNL1	-1.00	-1.08	-1.04	56.08	Hs.28578	muscleblind-like (Drosophila)
213359_at	HNRPD	-1.01	1.13	2.27	46.28	Hs.438726	heterogeneous nuclear ribonucleoprotein D (AU-rich element RNA binding protein 1, 37kDa)
228259_s_at	TIGA1	-1.00	-1.24	-1.06	40.81	NA	NA
235590_at	C10orf6	-1.02	1.23	3.13	30.87	Hs.447458	chromosome 10 open reading frame 6
238456_at	NA	-1.00	1.34	8.47	30.01	Hs.164151	CDNA FLJ36202 fis, clone TESTI2028296
209395_at	CHI3L1	-1.00	1.07	38.14	28.10	Hs.382202	chitinase 3-like 1 (cartilage glycoprotein-39)
226757_at	IFIT2	-1.01	2.02	4.70	25.68	Hs.169274	interferon-induced protein with tetratricopeptide repeats 2
230031_at	HSPA5	-1.00	39.31	2.55	4.16	Hs.310769	heat shock 70kDa protein 5 (glucose-regulated protein, 78kDa)
229947_at	NA	-1.01	2.56	59.35	1.44	Hs.98558	CDNA FLJ26876 fis, clone PRS09003
226189_at	NA	-1.00	1.19	34.98	1.22	Hs.367688	Clone IMAGE:4794726, mRNA
237250_at	NA	-1.00	1.78	29.52	1.20	Hs.48372	Full length insert cDNA clone YZ87G11
214038_at	CCL8	-1.00	1.39	32.23	-1.04	Hs.271387	chemokine (C-C motif) ligand 8
202917_s_at	S100A8	-1.00	1.15	41.89	-1.15	Hs.416073	S100 calcium binding protein A8 (calgranulin A)
211161_s_at	COL3A1	-1.00	-1.09	33.85	-1.17	Hs.443625	collagen, type III, alpha 1 (Ehlers-Danlos syndrome type IV, autosomal dominant)
1555854_at	AKR1C1	-1.00	7.52	37.40	-1.82	Hs.295131	aldo-keto reductase family 1, member C1 (dihydrodiol dehydrogenase 1; 20-alpha (3-alpha)-hydroxysteroid dehydrogenase)
201289_at	CYR61	-1.00	-2.12	-40.65	-5.54	Hs.8867	cysteine-rich, angiogenic inducer, 61
214804_at	FSHPRH1	-1.01	-3.78	-8.62	-26.50	Hs.348920	FSH primary response (LRPR1 homolog, rat) 1
208850_s_at	THY1	-1.00	-2.56	-4.71	-27.77	Hs.134643	Thy-1 cell surface antigen
201291_s_at	TOP2A	-1.00	-2.49	-4.19	-28.19	Hs.156346	topoisomerase (DNA) II alpha 170kDa
236646_at	FLJ31166	-1.00	2.59	1.66	-28.39	Hs.226422	hypothetical protein FLJ31166
205347_s_at	TMSNB	-1.00	-3.36	-3.79	-28.96	Hs.56145	thymosin, beta, identified in neuroblastoma cells
202589_at	TYMS	-1.00	-2.12	-2.49	-29.67	Hs.87491	thymidylate synthetase
214259_s_at	AKR7A2	-1.01	-1.94	-1.86	-29.70	Hs.512807	aldo-keto reductase family 7, member A2 (aflatoxin aldehyde reductase)
204602_at	DKK1	-1.00	-2.59	-33.29	-30.17	Hs.40499	dickkopf homolog 1 (Xenopus laevis)

231240_at	NA	-1.00	-4.64	-4.94	-31.61	NA	NA
208577_at	HIST1H3C	-1.00	-1.66	-1.82	-32.92	Hs.248176	histone 1, H3c
237435_at	NA	-1.01	-4.02	-22.84	-33.02	NA	NA
1568126_at	NA	-1.00	-1.93	-2.68	-33.22	NA	NA
228728_at	FLJ21986	-1.00	-2.15	-2.51	-33.88	Hs.440973	hypothetical protein FLJ21986
202094_at	BIRC5	-1.00	-2.22	-3.27	-35.05	Hs.1578	baculoviral IAP repeat-containing 5 (survivin)
218663_at	HCAP-G	-1.00	-2.75	-5.16	-35.60	Hs.528669	chromosome condensation protein G
219493_at	SHCBP1	-1.01	-1.55	-4.63	-35.62	Hs.123253	SHC SH2-domain binding protein 1
206632_s_at	APOBEC3B	-1.00	-2.10	-3.68	-35.74	Hs.226307	apolipoprotein B mRNA editing enzyme, catalytic polypeptide-like 3B
45297_at	EHD2	-1.00	-1.18	1.08	-35.88	Hs.325650	EH-domain containing 2
209709_s_at	HMMR	-1.00	-1.63	-2.06	-35.99	Hs.72550	hyaluronan-mediated motility receptor (RHAMM)
218542_at	C10orf3	-1.00	-1.57	-2.93	-36.29	Hs.14559	chromosome 10 open reading frame 3
211958_at	IGFBP5	-1.00	-1.93	1.43	-36.45	Hs.380833	insulin-like growth factor binding protein 5
203700_s_at	DIO2	-1.00	-4.25	-6.33	-39.53	Hs.436020	deiodinase, iodothyronine, type II
229538_s_at	IQGAP3	-1.00	-1.64	-4.51	-39.65	Hs.133294	IQ motif containing GTPase activating protein 3
202856_s_at	SLC16A3	-1.00	-2.30	-2.85	-40.30	Hs.386678	solute carrier family 16 (monocarboxylic acid transporters), member 3
210519_s_at	NQO1	-1.00	1.38	2.04	-41.82	Hs.406515	NAD(P)H dehydrogenase, quinone 1
221870_at	EHD2	-1.00	-1.15	1.06	-42.77	Hs.325650	EH-domain containing 2
226218_at	IL7R	-1.00	-3.27	-24.21	-44.77	Hs.362807	interleukin 7 receptor
214710_s_at	CCNB1	-1.00	-2.32	-5.04	-46.15	Hs.23960	cyclin B1
205381_at	LRRC17	-1.00	-2.52	-6.78	-51.19	Hs.288720	leucine rich repeat containing 17
213302_at	PFAS	-1.00	-1.76	-2.08	-52.27	Hs.88139	phosphoribosylformylglycinamide synthase (FGAR amidotransferase)
229490_s_at	NA	-1.00	-1.57	-4.76	-53.39	NA	NA
228729_at	CCNB1	-1.01	-2.11	-3.42	-54.70	Hs.23960	cyclin B1
229097_at	NA	-1.00	-1.18	-2.46	-60.23	NA	NA
207165_at	HMMR	-1.00	-1.99	-2.80	-63.66	Hs.72550	hyaluronan-mediated motility receptor (RHAMM)
201467_s_at	NQO1	-1.00	1.55	2.53	-69.08	Hs.406515	NAD(P)H dehydrogenase, quinone 1
201890_at	RRM2	-1.00	-1.65	-1.68	-85.08	Hs.226390	ribonucleotide reductase M2 polypeptide
209773_s_at	RRM2	-1.00	-3.36	-4.42	202.33	Hs.226390	ribonucleotide reductase M2 polypeptide

Table 4.S3 Microarray master key (data available at the GEO Website).

GSE4217 *Spheroid Formation and Recovery of Human Foreskin Fibroblasts at Ambient Temperature* (monolayer → spheroid → spheroid recovery → recovery as monolayers)

Accession	Title	.cel/.dat/.exp/.chp
GSM96262	HFF2_T1_R1, Monolayer	GSM96262
GSM96263	HFF2_T1_R2, Monolayer	GSM96263
GSM96264	HFF2_T1_R3, Monolayer	GSM96264
GSM96265	HFF2_T2_R1, Spheroid	GSM96265
GSM96266	HFF2_T2_R2, Spheroid	GSM96266
GSM96267	HFF2_T2_R3, Spheroid	GSM96267
GSM96268	HFF2_T3_R1, Spheroid Recovery	GSM96268
GSM96269	HFF2_T3_R2, Spheroid Recovery	GSM96269
GSM96270	HFF2_T3_R3, Spheroid Recovery	GSM96270
GSM96271	HFF2_T4_R1, Monolayer Recovery	GSM96271
GSM96272	HFF2_T4_R2, Monolayer Recovery	GSM96272
GSM96273	HFF2_T4_R3, Monolayer Recovery	GSM96273

GSE4218 *Spheroid Formation and Recovery of Human T98G Glioma Cells at Ambient Temperature* (monolayer → spheroid → spheroid recovery → recovery as monolayers)

Accession	Title	.cel/.dat/.exp/.chp
GSM96274	T98G_T1_R1, Monolayer	GSM96274
GSM96275	T98G_T1_R2, Monolayer	GSM96275
GSM96276	T98G_T1_R3, Monolayer	GSM96276
GSM96277	T98G_T2_R1, Spheroid	GSM96277
GSM96278	T98G_T2_R2, Spheroid	GSM96278
GSM96279	T98G_T2_R3, Spheroid	GSM96279
GSM96280	T98G_T3_R1, Spheroid Recovery	GSM96280
GSM96281	T98G_T3_R2, Spheroid Recovery	GSM96281
GSM96282	T98G_T3_R3, Spheroid Recovery	GSM96282
GSM96283	T98G_T4_R1, Monolayer Recovery	GSM96283
GSM96284	T98G_T4_R2, Monolayer Recovery	GSM96284
GSM96285	T98G_T4_R3, Monolayer Recovery	GSM96285

Table 4.S4 Comparison of quantitative PCR fold changes for *GADD45* genes in the presence and absence of NF- κ B chemical inhibition with HFF-2 and T98G cells.

Cell Line	<i>GADD45α</i> Fold Change		<i>GADD45γ</i> Fold Change		<i>GADD45β</i> Fold Change
HFF-2					
0hr Spheroid	1	+/- 0.3	1	+/- 0.54	N/D
0hr Recovery	11.42	+/- 0.57	2.52	+/- 0.83	N/D
6hr Recovery	7.45	+/- 1.95	-2.14	+/- 1.82	N/D
24hr Recovery	1.38	+/- 1.82	-4.28	+/- 1.56	N/D
72hr Recovery	1.17	+/- 1.3	1.22	+/- 1.31	N/D
HFF-2, NF-κB inhibited					
0hr Spheroid	1	+/- 1.31	1	+/- 1.05	N/D
0hr Recovery	4.6	+/- 0.39	1.44	+/- 0.54	N/D
6hr Recovery	1.9	+/- 0.25	-1.25	+/- 0.75	N/D
24hr Recovery	1.76	+/- 0.67	-1.47	+/- 1.32	N/D
72hr Recovery	-4.3	+/- 1.01	1.4	+/- 1.49	N/D
T98G					
0hr Spheroid	1	+/- 0.38	1	+/- 1.33	N/D
0hr Recovery	3.36	+/- 0.32	2.51	+/- 0.66	N/D
6hr Recovery	-1.94	+/- 0.6	2.11	+/- 0.71	N/D
24hr Recovery	-2.09	+/- 0.64	2.67	+/- 1.5	N/D
72hr Recovery	-1.7	+/- 0.41	-1.26	+/- 1.18	N/D
T98G, NF-κB inhibited					
0hr Spheroid	1	+/- 0.56	1	+/- 0.78	N/D
0hr Recovery	9.96	+/- 0.54	23.62	+/- 0.65	N/D
6hr Recovery	2.63	+/- 0.57	27.17	+/- 0.83	N/D
24hr Recovery	-1.98	+/- 0.47	2.48	+/- 1.19	N/D
72hr Recovery	-2.08	+/- 1.29	-1.73	+/- 1.37	N/D

Fold changes are relative to a 0hr spheroid (control) and are shown with their standard deviations (n=3). *GADD45 β* transcripts were not detected (N/D) in any sample.

Chapter 5

Concluding Remarks and Future Directions

Our laboratory has been developing processes that permit human cells to be stored at ambient conditions without media for extended periods of time. Such technologies are vital to mammalian-based biosensor development as well as for determining the inherent capabilities of human cells to exist in a quiescent state. These efforts have resulted in long-term storage of a wide variety of human cells, and such technologies are presently being evaluated in the biosensor industry.

A key aspect of this body of work is the use of multicellular aggregates (spheroids) rather than adherent monolayer cells. The work described in this thesis supports the concept that this method provides a more realistic depiction of the impact of intercellular communication on intracellular signaling. As methodologies now exist for multiplexed cytokine assays, an overall picture of these responses can be obtained relatively easily over the duration of an experiment. This research shows that signaling response networks are cytokine-profile dependent. A complete understanding of the factors controlling cell fate necessitates exploration of the synergistic relationships between cytokines and chemokines and their influence on signal transduction. This aggregate system was used for probing signal transduction networks within three different cell lines in three different cell transformation states (immortalized, carcinoma and primary).

The results presented in this thesis demonstrate that one can monitor changes in signal transduction during the process of aggregation, arrest and recovery in these different cellular transformation states. It also demonstrates that cell type, transformation state and intercellular communication must be considered when determining the “wiring diagram” of the cell in response to external stresses. This research further delineates the

utility of this multicellular aggregate system for a number of possible applications. Researchers interested in avascular tumor growth will find the transcriptional and cytokine profiling data of value for delineating the early stages of cancer growth. Scientists interested in more clearly defining the molecular aspects of contact inhibition will benefit from these data, as well as the culturing technique, as our results are very different from those obtained with confluent adherent monolayers. Finally, investigators wishing to better understand the wounding response and/or cell migration will find that our profiling data lend new insight into cell aggregation and release phenomena.

Future Directions

The work reported herein focused on the use of endogenous stress signaling utilizing multicellular aggregates as the model system. As stated repeatedly throughout this thesis, there are many discrepancies between aggregate and monolayer signal transduction pathways. These monolayer studies were performed using recombinant TNF- α stimulation on genetically modified cell lines either with knockout mutations of NF- κ B or antisense *gadd45 β* plasmids. These research groups then observed modifications on JNK signaling and apoptosis. Our results suggest that this response may be due to the genetic modification, use of exogenous TNF- α , and growth as monolayers. Which set of results is physiologically relevant? In order for the work reported within this thesis to fully address these previous results, experiments can be executed which may clarify the disagreements. Application of the genetic modifications together with the aggregate model system (endogenous stress signaling) could fully elucidate the “true” roles of these signaling pathways in apoptosis and cell survival.

Using the cell line previously described with knockout NF- κ B or a cell line with stable expression of antisense *gadd45 β* both within the multicellular aggregates system used in this report could clarify the signaling deviations observed.

Curriculum Vitae

Graham Dillon Jack
Department of Biochemistry
Virginia Tech
Blacksburg, VA 24061
e-mail: grjack@vt.edu

SCIENTIFIC TRAINING

Honors Bachelor of Science (1997-2001), University of Western Ontario
Specialist: Pharmacology and Toxicology

Master of Science (2001-2002), University of Western Ontario
Specialist: Physiology. Withdrew from Program

PhD (2002-2006), Virginia Tech, Department of Biochemistry (expected to be complete late winter 2006)

RESEARCH EXPERIENCE

Honors Research Project

Supervisor: Dr. Peter Chidiac (Assistant Professor, University of Western Ontario)
Title: *Effect of Receptor Phosphorylation on RGS GAP Activity*
Techniques Used: GTP hydrolysis assays, Western blotting, protein purifications, radioactive phosphorylation imaging, membrane purifications

Masters Research Project

Supervisor: Dr. Stephen Ferguson (Professor- Robarts Research Institute)
Title: *Beta-Arrestin Mediated Signal Termination*
Techniques Used: confocal imaging, yeast-2-hybrid, PCR, ubiquitination assays, co-immunoprecipitation assays, cloning, mammalian cell culture, bacterial cultures, transfection, transformation

Doctorate Research Project

Supervisors: Dr. Richard Helm and Dr. Malcolm Potts (Professors - Virginia Tech)
Title: *Endogenous Stress Signaling within Multicellular Aggregates*
Techniques Used: Confocal imaging, FACs analysis, three dimensional tissue culture, microarray analysis, nuclear microinjection, fluorescent microscopy, cytokine multiplex analysis, recombinant cytokine assays, RNA isolation, immunohistochemistry

AWARDS AND RECOGNITION

2006	Outstanding Graduate Student	Virginia Tech
2005	Alumni Award for Excellence	Virginia Tech
2002	Ontario Graduate Student Scholarship	Provincial Award
1999-2001	Deans List	Western Ontario
1997-1998	Entrance Scholarship	Western Ontario
1996-1997	Ontario Scholar	Provincial Award
1995-1996	Ontario Education Leadership Program	Provincial Award

PUBLICATIONS

Stroud WJ, Jiang S, **Jack G**, Storrie B. (2003) Persistence of Golgi matrix distribution exhibits the same dependence on Sar1p activity as a Golgi glycosyltransferase. *Traffic*. **4**:631-41

Jack GD, Mead EA, Garst JF, Cabrera MC, Desantis AM, Slaughter SM, Jervis J, Brooks AI, Potts M, Helm RF. (2006) Long term metabolic arrest and recovery of HEK293 spheroids involves NF-kappaB signaling and sustained JNK activation. *J Cell Physiol*. **206**: 526-36. This paper appeared in *Science* as an Editor's Choice selection (*Science* **310** [2005] 591)

POSTER PRESENTATION

Jack GD, Cabrera MC, Garst JF, Slaughter SM, Potts M, Helm RF NF- κ B and Sustained JNK Activation are Essential for Long- term Arrest and Recovery of HEK293 Multicellular Aggregates. Presented at the American Society for Cell Biology Annual Meeting, 2005.